University of Verona
Department Of Neurological and Movement Sciences

Graduate School Of Sciences Engineering Medicine

PhD program in Multimodal Imaging in Biomedicine

Cycle XXVI January 2011 – December 2013

Analysis of Diffusion Tensor Imaging for neurosurgical applications: tumor removal in eloquent areas.

PhD candidate:
Pasquale Mirtuono

Supervisor:
Andrea Sbarbati
Tutor:
Roberto Israel Foroni

Thesis submitted in 2014

Contents

Abstract

The purpose of the thesis is to investigate a clinical application of Diffusion Tensor Imaging in brain surgery.
Brain Surgery aims to maximize lesion resection while preserving surrounding vital cortical and subcortical area. MRI techniques enables neurosurgeons to define how lesions change the individual anatomy in relation to brain function mapping.
In this thesis we describe principles and methods of diffusion model and specific neuro radiological protocols for pre surgical planning (minimal risk strategy) of malignant brain tumors in eloquent area. Despite artifacts and limits, the developed framework based on DTI integrated with intra-operative localization supports neurosurgeon to analyze surgical strategies while preserving brain functions. We compare methods, procedures and different implementation of algorithms affecting the complex multi-modal processing of imaging protocol.
Clinical information (deficit quantification), and intra-operative neurophysiological stimulations with morphological characteristics of fiber bundles corrupted by tumor is widely examined.

From January 2011 to December 2013, 144 patients with lesions in eloquent areas were submitted to pre-operative DTI tractography and 94 of 144 were treated surgically.

Acknowledgments

My first sincere appreciation goes on to Prof. Andrea Sbarbati for giving me the opportunity to apply my PhD activity at Department of Neurosurgery in Verona Hospital.

I would like to express my sincere gratitude to my tutor Dr. Robert Israel Foroni, for all I have learned from him and for encouraging and helping me to shape my interest and ideas.

Besides my academic tutors, I would like to express my gratitude to Dr. Giuseppe Kenneth Ricciardi, whose expertise and understanding added considerably to my graduate experience. I appreciate his wide knowledge and skill in MRI and his assistance in developing clinical applications.

I would like to thank Dr. Giampietro Pinna and Francesco Sala for the assistance in understanding clinical, surgical and neurophysiological aspects in my research project.

Special thanks to Dr. Angelo Musumeci and Dr. Giovanniantonio Barone from Department of Neurosurgery in Verona Hospital. Their remarks and suggestions were always very useful.

Finally i would like to express gratitude to Prof. Mario Meglio for suggesting and clarifying anatomical and neurophysiological aspects related to my research activities.

I dedicate this thesis to my dad, mum, my brother and Antonella for their constant support and unconditional love.
They were always with me during the project.

1. Introduction

1.1 *Discoveries In Neuroscience*

Brain is undoubtedly the most complex biological system, since it performs an abundance of intricate tasks, such as observation, interpretation of information, reaction, planning, and display of behavior and the history of his discoveries starts a long time ago.

1.1.1 *A Short History of The Brain*

The first documented causal relationship of speeches and motor tasks with the brain were described in Edwin Smith Papyrus, an Ancient Egyptian medical text dates to 1,500 BCE. The manuscript described diagnosis and treatment of disease separately in a detailed and methodological manner [Blits 1999].
Afterward Galen of Pergamon (127-199) was the most influential scientist of ancient medicine. Central to Galen's doctrine, was his belief in the absolute need for a rigorous anatomical methodology. He claimed that only correct dissections would provide apodeictic proofs, or incontrovertible demonstrations, enabling the researcher to draw legitimate conclusions. Galen conducted many experiments that supported the theory that the brain controls all the motions of the muscles by means of the cranial and peripheral nervous systems [Jones 2010].
The use of images to document and study human anatomy began to play a role in the study of the human body.
Leonardo Da Vinci (1452-1519) performed several studies on human anatomy and function, ranging from their respective relations, to the optics of the eye. Regarding the anatomy and functions of the brain, he studied the ventricular and optical systems [Jones 2010].
Andreas Vesalius (1514-1564) focused his dissection studies on the ventricles, vessels and meninges, but did not perform accurate drawings of the gyri or sulci. He distinguished for the first time the soft tissue on the cortex of the brain from the hard white substance in its interior.
Marcello Malpighi (1628-1694), the founder of microscopic anatomy, was the first that examine the cortex at such a small scale. The white substance was investigated using a primitive microscope and he discovered that it was composed of fibers [Jones 2010].
Extending Malpighi studies, Nicolo Steno (1638-1686), argued that, in order to discover the purpose of these fibers, their pathways should be

traced and studied.

Two centuries later (1810), Gall and Spurzheim stated that the cortex had areas with specialized functions that were "wired" by white matter. This theory revolutionized neuroscience and the paradigm of cortical specialization along with the newly included neuron theory gave place to the importance of the human brain's white matter in the functioning brain.
In 1861 Broca provided the first experimental evidence of this theory: a damage in a precise area of the cortex caused speech impediments [Jones 2010].

Joseph Jules Dejerine, Ludwing Lichtheim and Carl Wernicke produced detailed descriptions and models of the white matter structure linked with neurological disorders.
They studied classical disconnection syndromes to explain disorders of languages and reading.
Wernicke proposed a diagram of the perisylvian language network, Lichtheim designed aphasia's model to explain language disorders and Dejerine described brain anatomy in a patient with reading deficits and a lesion located between the visual verbal center and the visual areas in both hemisphere.
Hugo Liepmann, a young student of Wernicke, proposed the most original network model based on the study of praxis. He declined the existence of a specialized center for praxis and he hypothesized an anatomical left-right asymmetry to explain lateralization of it.

Figure 1.1. Leonardo da Vinci's drawings

1.1.2 *Tractography*

During the twentieth century, theories about brain function began to afford a more prominent place to white matter.

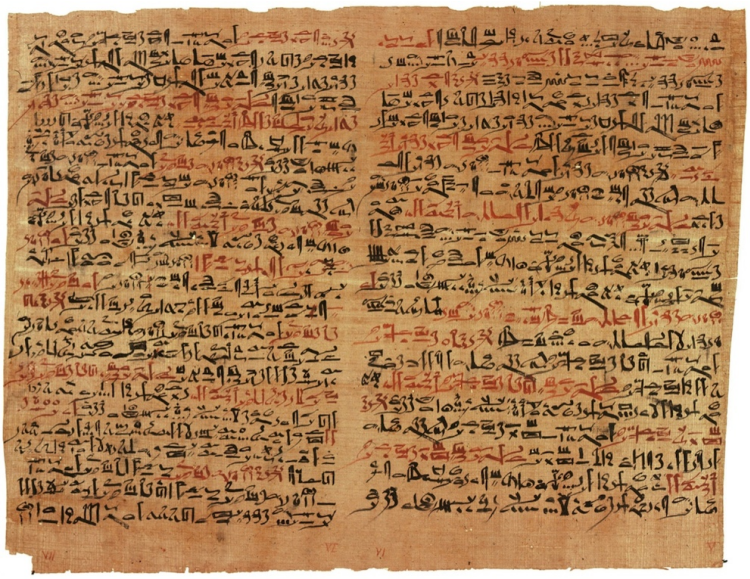

Figure 1.2. Edwin Smith Papyrus

Neuropsychological studies identify a theory about cortical functioning. Before 40's the most accepted theories about brain functions were localizationism and holistic models. Localizationists assumed that small cortical areas were fully capable to performing complex functions. In contrast, Holistic doctrine assumed that functional areas (except for cognitive functions) were fairly undifferentiated and working as an aggregate field [Catani *et al.* 2012a].
Debate started at the end of 18th century and engaged scientists from different neuroscience fields, like Franz Joseph Gall, Johannes Pukinjes, Pierre Paul Broca, Carl Wernicke, Korbinian Brodmann and Wilder Penfield [Catani *et al.* 2005, Catani *et al.* 2012a, Sala *et al.* 2002].

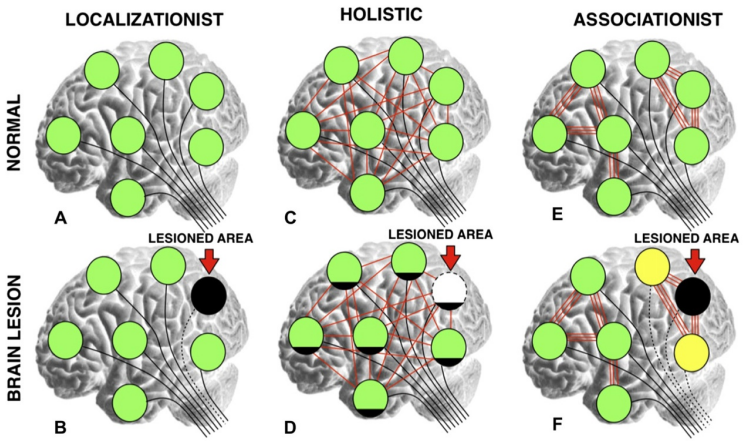

Figure 1.3. Brain Function Theories [Catani *et al.* 2012a]

In 1946 Donald Hebb proposed the first draw of associatization model of brain function based on three fundamental assumptions:

1 co-activated neurons become associated
2 associations can occur between adjacent or distant neurons.
3 If neurons become associated, they will develop into a functional unit as a cell assembly

Today the debate in brain function model is a relevant field of neuroscience. A number of modern techniques are involved in understanding brain modeling.
Tractography methods become relevant to identify anatomically network and sub-network of complex functions.
Tractography could be considered a set of techniques like neuroradiological images, dissections and microscopic analysis after specimen and preparation.

The first tractography methods were developed in vitro by dissecting tissue of the brain after death. Identification of pathways was also performed using staining methods and chemical tracing.

Klingler Fiber Dissection. In 1935 Klingler described a macroscopic technique to dissect major fiber tracts in the human brain [Agrawal *et al.* 2011 Chowdhury *et al.* 2010].
A formalin-fixed human cadaver brain was frozen down to -5 C and allowed to return to room temperature several times. The growing ice crystals separated the nerve fibers slightly from each other.

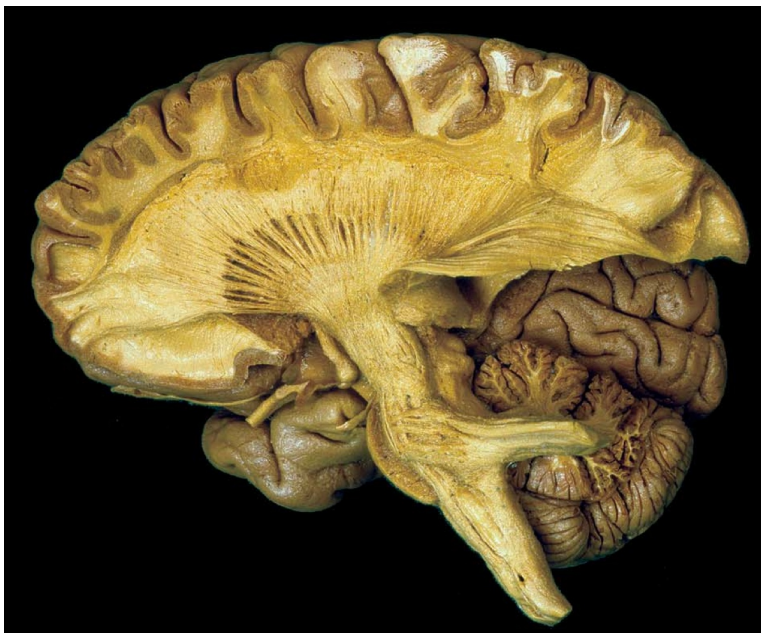

Figure 1.4. Sagittal view of Klingler's Fiber Dissection

Myelin Stains. Myelin stains defined a family of methods to visualize parts of myelin sheaths and axons. There were two mayor methods: Weigert and Luxol fast blue type [Jones 2010].
In Weigert type, developed in 1897, the sample was treated with chrome and copper solutions, which decreased the ability of the lipids to be dissolved. Afterward the tissue was stained with hematoxylin. Luxol "fast type blue stain" stained mainly the lipoprotein part of the myelin sheaths which remained stable after the dissuolution of the lipids.

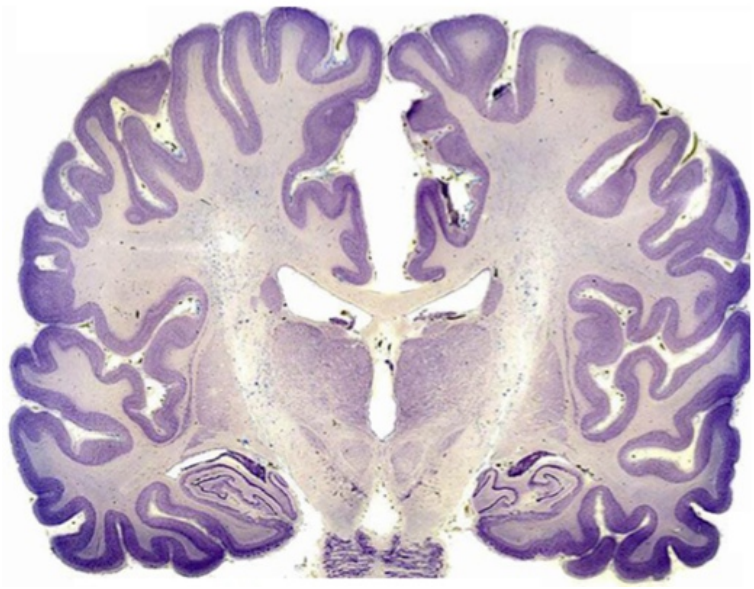

Figure 1.5. Coronal section of the brain prepared with myelin stain

Tract Tracing. Based on the increasing knowledge about brain connectivity in the 60's, tracing techniques were developed using active transport mechanism in the living cell.
The tracer was injected into a specific region of the brain and was transported via the axons into connected brain areas [Alexander *et al.* 2007, Jones 2010]. Many substances were used for tracing tracts and more recently neurotropic viruses were used to visualize interconnected circuits in the brain. The substance used depends on type of transport that was under analysis (Anterograde, Retrograde or over synapse transport). These methods were limited by very short postmortem delays for injection of the tracer. New tracking methods were described using Manganese injections and MRI detections[Jones 2010].

Imaging becomes relevant to study the brain: investigations of cortical connections were performed using tracer substances in brain tissues. The first time interval after death for injection of the tracer was the major problem related to radio-tracking methods.
New frontiers of imaging started with the development of MRI and in particular of sequence that recognize displacement of water [Alexander

et al. 2007, Jones 2010].
The first diffusion-weighted Magnetic Resonance Imaging (DWI) acquisition of biological tissue took place in 1984 by Websey, Moseley, and Ehman.
In 1985 Le Bihan and Breton were the first who performed a DWI acquisition in vivo of the human brain using a whole-body scanner.
This images change definitely the role of DWI sequences and applications that are today the most relevant tools to investigate brain connections.

1.1.3 *Tools for Brain Surgery*

Discoveries in brain function and anatomy came from research in brain's propriety and clinical applications for neurological disease.
The evolution of neurosurgery was hallmarked by development of tools, instruments and technologies introduced to help therapists and surgeons in understanding brain pathologies and possible treatments. One of the most relevant technologies introduced in brain surgery was the stereotactic procedure, that changed completely the concept of brain surgery during the last 40 years.
The complexity of brain anatomy suggested, at the end of 19th century to develop the use of guided probes.
D.N. Zernov, a Russian professor of anatomy at Moscow State University, designed a device guided by an arc-based system based on polar coordinates called "encephalometer".
Physiologist Robert H. Clarke and Victor Horsley, a physician and neurosurgeon, finally ended up a complete description of the principles in 1908 at the University College London Hospital.
These to of British scientists perfected the apparatus to study cerebellar function experimentally in monkeys.
The Horsley – Clarke device was based on the reproducibility of the relationship between landmarks on the skull and anatomical structures within the brain.
The cranial fixation points established the baseline of a three-dimensional Cartesian stereotactic coordinate system.

In 1912 Clarke suggested a first clinical application in neurosurgery: the attempt failed because of the great variability between skull landmarks and cerebral structures in the human brain [Agrawal *et al.* 2011].
Between 1947 and 1949, Ernest A. Spiegel, Henry T. Wycis, and Lars Leksell, using new intracranial anatomic landmarks discoveries, developed the first stereotactic devices for human brain surgery. Spiegel and Wycis used Cartesian coordinates and Leksell used spherical coordinates.
Jean Talaraich in Paris, aware of the work of Spiegel and Wycis, manufactured a novel stereotactic instrument [Catani and ffytche 2010].
Using collimated radiographs he demonstrated superimposition of the holes in the grid over a positive contrast ventriculogram.
In 1978 Russell Brown designed the N-Localizer, a stereotactic system guided by images from Computer Tomography or Magnetic Resonance

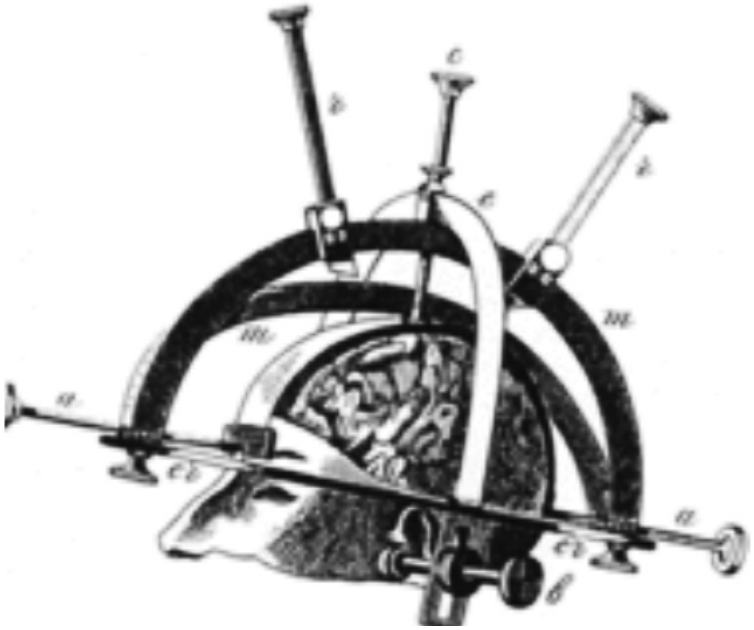

Figure 1.6. The Encephalometer

Imaging. The innovative system improved surgical precision because MRI and CT permited an accurate identification of intracranial anatomic details.

1.2 *The "Next Generation"*

1.2.1 *Computer Assisted Surgery*

Disadvantages of the stereotactic method were the need to put the patient with a frame into the CT or MR scanner and the restricted handling of the instruments in the fixed frame during surgery.

The new era of surgery guided by images was signed by the use of computer and robots. Computer assisted surgery (CAS) represents a set of concepts, methods and technology based on computer and images that help the surgeon before and during the procedure.
The most common CAS applications are image analysis and processing, patient virtualization and surgical simulation, and intra-operative navigation by images.
Medical images could be analyzed and processed to enhance descriptive and quantitative information of tissues involved surgery. In brain procedures, image processing is fundamental to identify functional areas and anatomy. Pre-surgical virtualization is one of the most important applications of CAS because help surgeons to understand relationship between pathologic and healthy tissues with a synthetic representation of patient. Trajectories can be simulated to identify a solution that minimizes the risk and maximizes the efficiency of the procedure.
The main difficulty during surgery is to identify anatomical variations

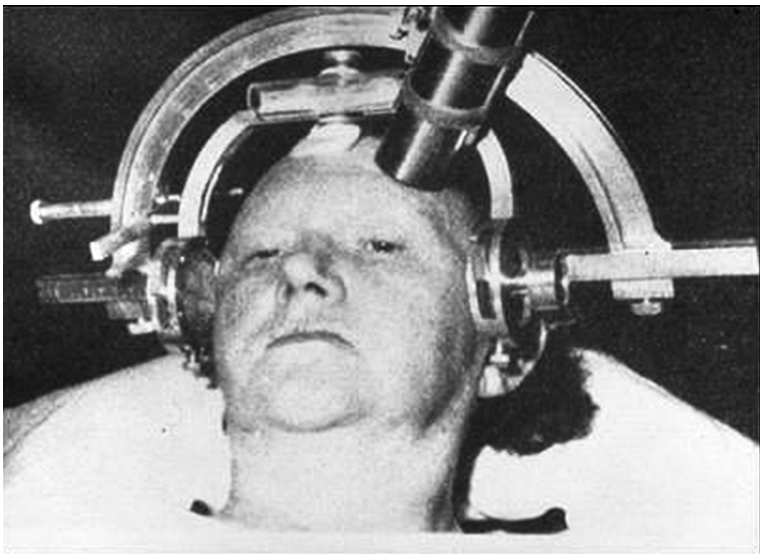

Figure 1.7. First Leksell Head-Frame

in presence of pathology [Kaneko *et al.* 2012]. The intraoperative role of computer was introduced to visualize radiological information in order to localize anatomical references [Ulmer 2010].
The development of surgical navigation systems becomes relevant in neurosurgery especially when differences between healthy and pathologic tissue are not visible. In particular, brain surgery requires a lot of landmarks because functional areas are not discernable with visible characteristics of anatomy.
This is particularly true when a lesion changes a standard localization of functions, that could introduce relevant difficulties for the surgical outcomes, in terms of deficits and completeness of lesion resection.

Figure 1.8. RoBoCast implementation in Verona

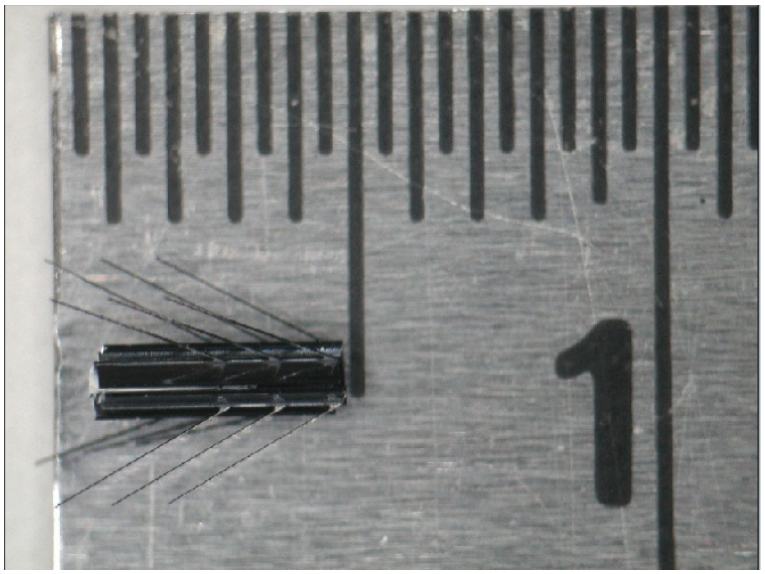

Figure 1.9. MiniRobot

1.2.2 *New Advantages In Brain Analysis*

Intraoperative Imaging. In order to seek safe and radical resection of tumors, many techniques were developed to support intraoperative evaluations. The most important approaches used tomography, magnetic resonance and ultrasound principles.
Intraoperative CT was commonly used in traumatic injuries and spine surgery. The role of CT was fundamental when geometrical characteristics had to be respected. For soft tissues, MRI-based surgical application and Ultrasound are preferred. Intraoperative MRI (iMRI) are introduced in brain surgery since 1996 [D'Andrea *et al.* 2012]. The idea was to integrate intraoperative acquisitions in order to understand brain shift and resection quality [Nimsky *et al.* 2000, Nimsky *et al.* 2001].
Today iMRI are classified by magnetic field characteristics that change uses [Prabhu *et al.* 2011]. The idea takes into account trade-off between image quality and integration with operative room [Prabhu *et al.* 2011]. Low field Magnet (LFM) produces a low quality images that are adequate to understand the progress and the quality of surgical procedures in terms of resections and brain shift quantification [Nimsky *et al.* 2001]. High field Magnet (HFM) produces good quality images (comparable with pre-operative images) but it requires more time and a compatible layout in the operative room, in terms of MR conditions (MR safe) [Fountas and Kapsalaki 2005]. HFM is more expensive and sometimes require clinical and diagnostic justifications (classical use of MRI). LFM is completely dedicated to surgical activities and could be used with MR conditional intraoperative equipment.

Alternative Imaging (Ultrasound in OR). Ultrasound is a useful imaging technique that can be applied to many clinical applications. It is based on mechanical vibration of physical medium that perturbs the

Figure 1.10. Polestar Intraoperative MRI

particles and generates regions of compression and rarefaction around them. Compared with Intraoperative MRI, ultrasound is becoming a relevant intraoperative tool that gives relevant information, with a low cost impact for hospitals and time-saving advantages for surgeons.
A milestone in ultrasound discoveries was reached in 1982 at Michigan Hospital when James E.Knake deeply studied the use of ultrasound as an intraoperative imaging in neurosurgery. Knake described their first experience as a very useful tool in detecting hemorrhage, hydrocephalus, and porencephaly in premature or other infants and could provide assistance in localization of instruments during neurosurgical procedures, identification and localization of subcortical metastatic neoplasms and information of deep lesion reguarding their solid or cystic components.

New Functional Estimation Analysis (TMS). A novel method based on cortical stimulation was developed during the last years. Transcranial Magnetic Stimulation (TMS) could identify connections between stimulated areas using the magnetic and electric propriety of the brain. The method, considered non-invasive, was based on electromagnetic induction that produces polarization's changes of the neurons. Physically a small magnetic field was rapidly changed in order to generate a magnetic flux density pulse that induced a current pulse, as explained in Maxwell and Faraday Equations.

Mathematical Model of Brain Function Network: the experience of UCLA. The Human Connectome Project (HCP) is a cooperative project sponsored by the National Institutes of Health (NIH), United States of America. Since 2009 HCP award over 50 million to understand the network map of the brain. HCP includes two consortium, one led by Washington University (WU) and University of Minnesota (UM), the second led by Harvard University (HU), Massachusetts General Hospital (MGH) and University of California Los Angeles(UCLA). HCP is

based on collaboration between the best research laboratory in medical imaging and computer science. Such as reported in HCP brochure, the project

> "aims to provide an unparalled compilation of neural data, an interface to graphically navigate this data and the opportunity to achieve never before realized conclusions about the living human brains"

Arthur W. Toga, director of Laboratory of Neuro-Imaging in UCLA, define the Connectome as

> "the complete, point-to-point spatial connectivity of neural pathways in the brain... The connectome gives rise to population-level atlases of distributed connectivity and makes it possible to assess disruptions of connectivity in clinical samples. Demographic, genomic, and cognitive/behavioral data can be superimposed on the connectome to permit inferences concerning genetic and other influences on connectedness. Information concerning connectivity is essential for understanding fundamental cognitive operations, systems-level brain activity, conditional structure-function models of brain, and debilitating brain diseases. Mapping the functional and structural connectivity of the brain using the latest neuroimaging methods must be accompanied by the tools needed to explore those data and to appreciate their richness. The expectation is that HCP will have immediate impact on the field of neuroscience and beyond; provide a framework and set of tools with enduring utility and value; and enable the broad community of investigators to generate and test new hypotheses based on the HCP data corpus and summary maps, thereby informing and advancing their own research priorities." [Toga *et al.* 2012]

Based on tractography, fMRI and multi-subject studies, the UCLA Multimodal Connectivity Database is one of the most important results of HCP. It is a web-based repository dedicated to HCP consortium studies. It is possible to analyze and navigate human brain starting from analysis of neuroimaging data. Data are organized in order to analyze and compare healthy and subjects with disease using network representation of brain connections. HCP is important because is the largest project dedicated to human brain connections that includes multiple disciplines such as Medicine, Computer Science, Biology and Physic.

1.3 *Aims of Thesis*

Inspired by projects like HCP, the purpose of the thesis is to investigate a clinical application of network representation of the brain based on various acquisitions. Therefore my aims is

- to explore concepts and methodology about medical imaging visualization and underline the relevance of visualization during surgery;
- to define and motivate a radiological protocol in order to study glioma cases which are candidate to be treated surgically;
- to describe principles and methods of diffusion model and to detail tensor modeling;
- to present a methodological framework as a guideline for DTI acquisitions and post processing elaborations.
- to compare methods, procedures and different implementation of algorithms involved in the proposed multi-modal image processing toolbox.

- to correlate clinical information (deficit quantification), and intraoperative neurophysiological stimulations with morphological characteristics of fiber bundles corrupted by tumor;
- to classify and illustrate the main limits and artifacts of diffusion imaging application in order to describe subcortical pathways;
- to present the case material of Verona Hospital in DTI application in glioma surgery.

Besides the introduction, this document is organized into the following four chapters.

State Of Art describes an historical background of Diffusion phenomena in Medical Imaging and Computer Assisted Surgery tools and applications.

Methods describes our framework into details including:

- Technical details of DTI background,
- Classification and identification of main network systems of the brain
- Model Design of surgery applications
- Pre-surgical planning such as Analysis and Visualization Data
- Intra-operative Visualization framework

Materials, **Result** and **Discussion** describe descriptive and quantitative analysis of patients studied with this application and integrations with other surgery-supporting techniques such as intraoperative neurophysiological monitoring and neuronagiation systems.

Conclusion of the thesis reports future works and reports contributions in the described application.

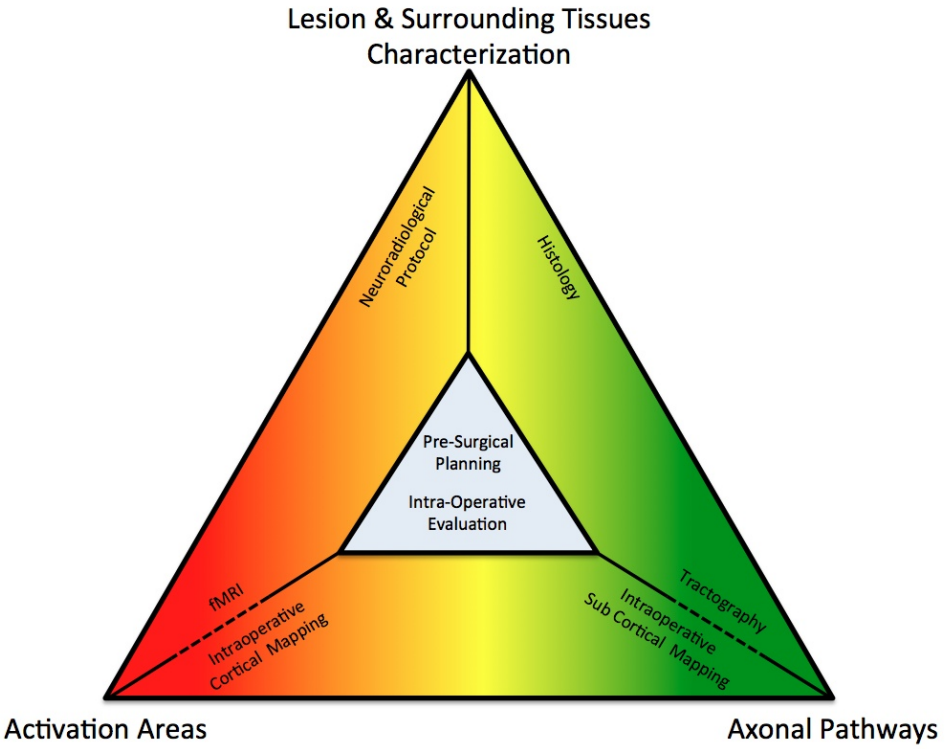

Figure 1.11. Scheme of Neurosurgical Application based on Pre-surgical and Inta-operative tools

2. State Of Art

The neural information unit of the brain is the neuron, a cell that transmits electrochemical signal. Three parts compose a neuron: body, axons and terminations.
The complex communication system based on polarization membranes produces an electrical action potential which travels along axons. Myelin covers axons and increases transmission of electrochemical signals.
Cell bodies are grey, myelin cells are white. This coloring distinguishes the two main parts of the brain: Grey and White matter.
Water is in living tissues. Inside the cell, diffusion facilitates the transport of metabolites. In neurons, water is present inside and outside the myelin's cover. Water diffusion along axons can be considered a relevant part of neuron activities.

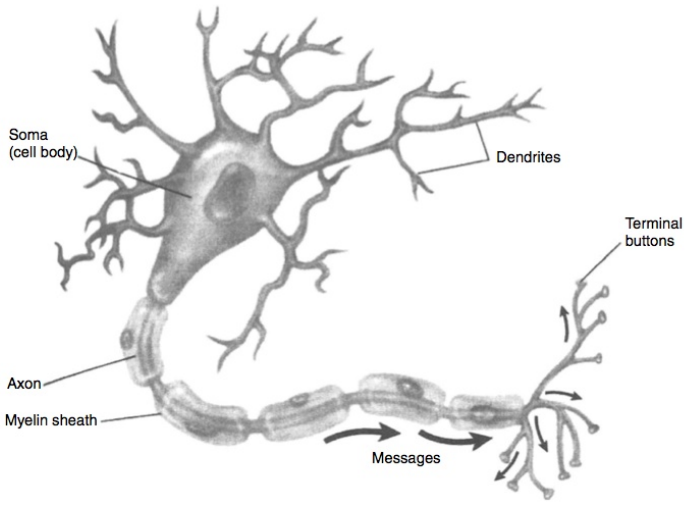

Figure 2.1. Scheme of Neuron

2.1 *Diffusion*

Diffusion is a physical phenomenon that can be observed with a simple experiment. Let us imagine a glass of water. Splashing dark ink into the glass, we can observe that the liquid first moves random in evident ink speckles. After a while, in absence of external interactions, all the

water in the glass is stained without any difference between ink and water. Diffusion is the described transport phenomenon that occurs when molecules are dissolved in a medium.

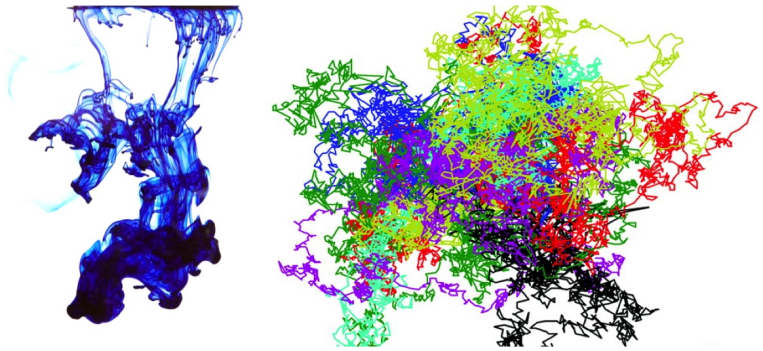

Figure 2.2. Diffusion and Brownian Motion: on the left side of the figure, dark in into water can explain diffusion of ink in a fluid. On the right site of the picture trajectory of molecules show the random pathways of free diffusion.

2.1.1 *Physic of Diffusion - Brownian Motion*

In 1827 a Scottish botanist, Robert Brown, observed a random motion of grains of pollen suspended in water. Although water appeared to be static to the naked eye, individual water molecules were constantly in motion, colliding with each other at a high speed. This phenomenon was called **Brownian motion** .

In 1855, Adolf Fick discovered a particle flux generated by a concentration gradient. Fick proposed a flux of particle equation (**first diffusion law**)

$$F = -D\frac{\partial C}{\partial x} \tag{2.1}$$

and a diffusion equation (**second diffusion law**)

$$\frac{\partial C}{\partial t} = D\frac{\partial^2 C}{\partial x^2} \tag{2.2}$$

F is the Flux, C is the concentration, D is the proportional coefficient between flux and concentration, t was time-variable, x was the displacement variable. Using a full 3-dimensional system reference a relationship between concentration and observed displacement can be redraw as

$$\frac{\partial C}{\partial t} = D\left(\frac{\partial^2 C}{\partial x^2} + \frac{\partial^2 C}{\partial y^2} + \frac{\partial^2 C}{\partial z^2}\right) = D\nabla^2 C \tag{2.3}$$

Fick's laws described the behavior of solute molecules as a consequence of a non-uniform concentration (from higher to lower). This phenomenon was called mutual diffusion and required a countercurrent of solute and solvent particles to maintain mass density.

Using a probabilistic interpretation of phenomena, molecule displacement can be described as a Gaussian distribution as

$$P(X,t) = \frac{1}{\sqrt{(4D\pi t)}} \exp\left(-\frac{X^2}{4Dt}\right) \tag{2.4}$$

In biological tissues diffusion phenomena are represented by behavior of molecular water in water, also called self-diffusion. This means that the diffusion process is not correlated by concentration gradient, but follows only thermal forces. Using the probabilistic formulation we can describe diffusion phenomena as

$$\frac{\partial P}{\partial t} = D\nabla^2 P \tag{2.5}$$

and D represent the self-diffusion coefficient. Albert Einstein demonstrated this relationship.

In 1905 Albert Einstein, using Boltzmann's thermal energy predictions, derived a rule to estimate Avogadro's number by observing how far the polled grain moved over a given time. Regarding mutual diffusion, Einstein showed that the language of the Fick's Law still applied in the cases of self-diffusion where no macroscopic gradient existed. He provided a formulation of local probability to find the molecule and he realized a correlation between thermal fluctuations and diffusion coefficient. Einstein's explanation of Brownian motion was that the Brownian particles experience a net force resulting from the exterior collisions of surrounding water molecules.

Derived from the ideal gas theory, Einstein proved that it is possible to characterize one aspect of this phenomenon. The squared displacement of the particles from their starting point over a t time, averaged over all of the sampled particles was directly proportional to the observation time:

$$\langle r^2 \rangle = 6D\tau \tag{2.6}$$

where r is the displacement variable, D a constant, and t the observation window time. Squared displacement can be obtained integrating the probabilistic interpretation of displacement molecules expressed in 2.4:

$$\langle R^2 \rangle = \int_{-\infty}^{\infty} R^2 P(\mathbf{R}, t) d\mathbf{R} = 6Dt \tag{2.7}$$

Using a time representation of displacement such as $R = r - r_0$ Einstein redefined D as

$$D = \frac{1}{6\tau} \langle \mathbf{R}^T \mathbf{R} \rangle \tag{2.8}$$

This formulation of diffusion model assumed that the medium was unrestricted and the particles therefore had equal mobility in every direction (*free diffusion*).

The diffusion of particles inside fluids depends by the characteristics of the medium. Obstacles characterize diffusion phenomena. The first classification of Diffusion is based on the presence of preferable direction of molecules in their Brownian motion; we can define:

- **Isotropic Diffusion**, when no direction is preferred by diffusion process. Ink in free water shows that the medium is isotropic. This means that no barriers obstacle the Brownian motion of particles [Beaulieu 2002].
- **Anisotropic Diffusion**, when a preferred direction is chosen by particles. This is typical in living tissues like fiber's muscles and cell's membranes. This means that obstacles characterize the medium as motion's constrictor [Beaulieu 2002].

Diffusion can be further classified into two separated classes by definition of obstacle and barrier of diffusion phenomena:

- **Restricted Diffusion** occurs when particles are in mesh by membranes and barriers obstacle the diffusion process.
- **Hindered Diffusion** occurs when particles are in mesh by surrounding object but barriers don't obstacle diffusion propagation of molecules.

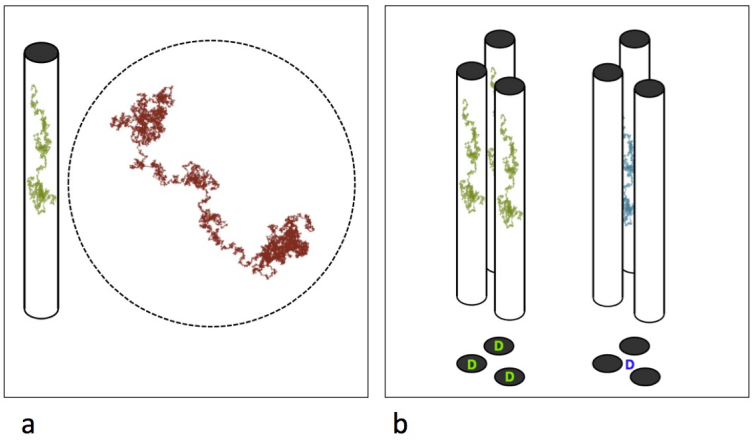

Figure 2.3. Relationship between particles and membrane characterize definition of Types of Diffusion. Picture **a** presents difference between *anisotropic* and *isotropic* diffusion (respectively left and right). Picture **b** show difference between *restricted* and hindered diffusion *respectively* left and right).

2.1.2 *Diffusion in MRI (DWI)*

Short History. During the first part of the 20th century, new discoveries in Physics changed the human history radically. At the end of 19th century classical mechanics could not explain all of the highly complex problems and the first radiation experiment opened a new

window in physics: Rutherford, Morley, Thomson, Dirac, Marie and Pierre Currie, Heisenberg, Fermi and Einstein opened a new era.
Nuclear Physics became established and a combination of glorious but sometime painful applications led to drastic changes in human technologies: the birth of the nuclear weapons and the birth of nuclear magnetic resonance. In 1946 Felix Bloch and Edward Mills Purcell simultaneously described the principles of Nuclear Magnetic Resonance (NMR) as an electromagnetic response after aligning the magnetic nucleus with a strong external magnetic field and an electromagnetic perturbation.
Otto Hahn, a German chemist, was often considered a pioneer in radioactivity the radiochemistry field.
In 1950 he described a particular characteristic of NMR spin echo: in the presence of an inhomogeneity of the magnetic field, random thermal motion of the spins would reduce the amplitude of observations. Inspired by these observations, Herman Carr and Purcell finally described advantages of the second pulse of 180 degree as a refocusing pulse in spin echo sequences.
Besides, using a small magnetic gradient and the new spin echo sequences, they observed that water diffusion can characterize NMR observations. Quantum mechanics discoveries captured the global interest of physicists.

At the end of 60's and in the first part of 70's three discoveries significantly changed the role of NMR and opened new application fields.
In 1965 a couple of American Chemists of The University of Wisconsin E.O. Stejskal and J.E. Tanner, published "Spin Echoes in the Presence of a Time-Dependent Field Gradient" the milestone of Diffusion in MR and its relative modern applications.
They defined the role of magnetic gradient field as an instrument to characterize additional proprieties of matter under NRM analysis. Few years later Paul Lauterbur changed the concept of NMR applications: until 1973 NMR has been mainly used in chemical analysis. Lauterbur produced the first acquisition of a bi-dimensional image using a particular application of NMR: *"Zeugmatography"*, the origin of *Magnetic Resonance Imaging* (MRI). Four years later Peter Mansfield developed mathematical techniques that improved magnetic imaging application. The main advantages were a shorter time of scan acquisitions (from hours to seconds) and a drastic improvement the quality of produced images.

THE JOURNAL OF CHEMICAL PHYSICS VOLUME 42, NUMBER 1 1 JANUARY 1965

Spin Diffusion Measurements: Spin Echoes in the Presence of a Time-Dependent Field Gradient*

E. O. Stejskal† and J. E. Tanner
Department of Chemistry, University of Wisconsin, Madison, Wisconsin
(Received 20 July 1964)

Figure 2.4. In 1965 Stejskal and Tanner published their result about diffusion measurement using MRI scanner and Pulsed Gradient Spin Echo sequence.

Stejskal and Tanner proposed a MR technique responsive to the

Diffusion process. In their works Stejskal and Tanner defined characteristics of diffusion sequences in MRI and a theory about physics and mathematics beyond diffusion phenomena, with the innovative concept of Apparent Diffusion Coefficient. Stejskal and Tanner MRI sequence, best-known as Pulsed Gradient Spin Echo (PGSE), was designed to measure the diffusion of water molecules in a given direction g. The sequences used two gradient pulses with an inner 180 refocusing pulse. During every application of the gradient pulse, the position of spins was assumed to remain constant. The refocusing pulse and the second gradient pulse generated phase shifts. Without diffusion phenomena, the gradient pulse can not characterize the readout signal. In presence of a displacement motion like diffusion, particles movement introduced a variation of spin position during the global alignment imposed by the first gradient pulse. This alteration, compared with a non-gradient baseline reference, produced a phase shift detectable with a radiofrequency lecture.

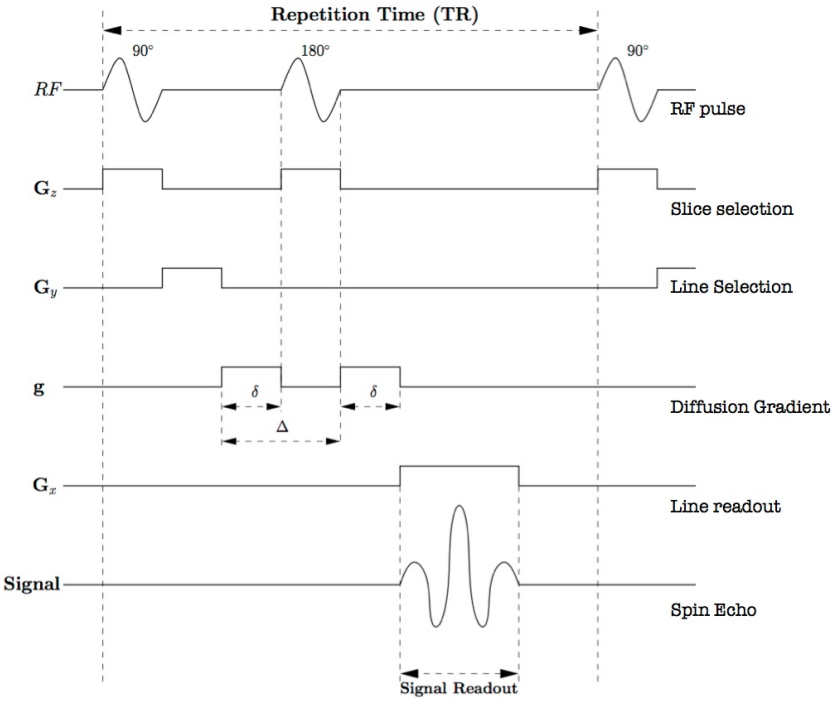

Figure 2.5. Scheme of Stejskal and Tanner imaging sequence. PGSE uses two gradient pulses of duration time δ in direction g. The sequences used two gradient pulses with an inner 180 refocusing pulse. Refocusing pulse and the second gradient pulse generated phase shifts.

The dependance of the observed echo signal intensity S on diffusion weighting is given by:

$$S = S_0 e^{-bD} \tag{2.9}$$

where the constant b is the diffusion-weighting factor, So is the signal obtained without diffusion sensitizing gradient (with $b = 0\frac{s}{mm^2}$),

and D is the water diffusion constant. The Diffusion-Weighted factor indirectly represent the observation time of diffusion phenomena. As expressed in the last formulation, the bigger is b value and smaller is the S measurement.

D can be defined as follow:

$$D = ADC = \frac{ln(\frac{S_k}{S_0})}{b} \tag{2.10}$$

A more complex formulation of diffusion MRI relationship between signal, applied gradient and diffusion characterization can be represented in this formula:

$$S_j = s_0 \exp(-bx_j^T D x_j) \tag{2.11}$$

where x_j and the transposed x_j^T are the unit vector representing the direction of the gradient j.

First Diffusion Acquisition in Living Tissues. In 1984 G. Websey, M. Moseley, and R. Ehman reported the first experiment of diffusion-weighted Imaging (DWI) in biological tissues. One year later Taylor and Bushell produced DWI images of a chicken egg. Few months later Le Bihan and Breton started a new application studying the human brain with a complete body scanner. This can be considered the milestone of DWI application for clinical purpose.
Afterwards Moseley started a fundamental set of experiments in order to obtain a measurement of anisotropy in living tissues [Basser *et al.* 1994].
Since Moseley's discoveries, diffusion studies aimed to study directional diffusion using three orthogonal orientations of the gradient pulse. Moseley showed the need to identify a more complex diffusion models using a variable geometry of gradient pulses. In these relevant discoveries of 80's and 90's, the Apparent Diffusion Coefficient calculation met the first interpretation of diffusion modeling [Basser *et al.* 1994].
The first interpretation characterized diffusion by a **Gaussian Probability Density Function** (gPDF), a diffusion descriptor based on Gaussian-shaped model in the spaces. This key point suggested future works about diffusion modeling and the meaning of measured ADC in biological tissues [Basser *et al.* 1994, Jones 2010].

Apparent Diffusion Coefficient. As explained before, the apparent faint definition of restricted and hindered diffusion has a relevant application in interpretation of diffusion proprieties in living tissues, especially in brain imaging and representations of pathways. In physics, the Apparent Diffusion Coefficient (ADC) is the observed restricted/hindered diffusion compared with free diffusion. Today the meaning of ADC as anatomical representation of barrier/obstacle of diffusion water has not yet been fully understood. ADC can represent:

- Intra-axonal restricted Diffusion

- Extra-axonal hindered Diffusion
- Both

2.2 *Mathematical Diffusion Modeling*

As explored by Moseley and Le Bihan, PDF interpretation of diffusion propagation model was described as

$$P(r|r_0,\tau) = \frac{1}{\sqrt{(4\pi\tau)^3|D|}} \exp\left(- \frac{(r-r_0)^T D^{-1}(r-r_0)}{4\tau} \right) \tag{2.12}$$

which take into account a pathway of particles that moves from r_0 to r in t time. Intrinsic diffusion in biological tissues was modeled by **tensor**, a symmetric mathematical operator defined as symmetric and positive-definite matrix, D. They coined the term of Diffusion Tensor Magnetic Resonance Imaging (DTI). D matrix can be considered as the covariance matrix that described Brownian Motion.

$$D = \begin{pmatrix} D_{xx} & D_{yx} & D_{zx} \\ D_{xy} & D_{yy} & D_{zy} \\ D_{xz} & D_{yz} & D_{zz} \end{pmatrix} \tag{2.13}$$

D is a symmetric and positively defined matrix. D requires only six coefficients to be full calculated. This means that DTI techniques require at least six DWI images and one unweighted ($b = 0\frac{s}{mm^2}$) image to solve the systems.

$$D = \begin{pmatrix} D_{xx} & D_{yy} & D_{zz} & D_{yx} & D_{zx} & D_{zy} \end{pmatrix}^T \tag{2.14}$$

The Diagonal elements of D (D_{xx} D_{yy} and D_{zz}) represent the ADC along the x, y and z axes. D_{yx} D_{zx} and D_{zy} represent correlation of diffusion along perpendicular directions.

2.2.1 *Single and Multiple main directions in Tensor Modeling*

The problem of Diffusion modeling constitutes one of the most important fields of research, because relevant artifacts depend on mathematical and hardware limitations of tensor modeling. The main limits that guided searching of new model definition concern the orthogonality of main diffusion direction in the same voxel. The calculation of ADC produces a couple of main directions that represents a couple of orthogonal anisotropy. In the single main direction tensor modeling, this case is represented as a small anisotropy.

Brain fibers present a lot of orthogonal cases. For example fiber bundles of motor cortex have a confluence point where the lateral bundle meets the medial bundle, while producing an orthogonal area. This mathematical limit introduces a strong precondition that characterizes tractography algorithms: couple of fiber populations can not be recognized.

Modeling of fiber bundles based on diffusion acquisition and analysis can be divided into two families of estimation tensor framework. Depending of diffusion modeling we can identify:

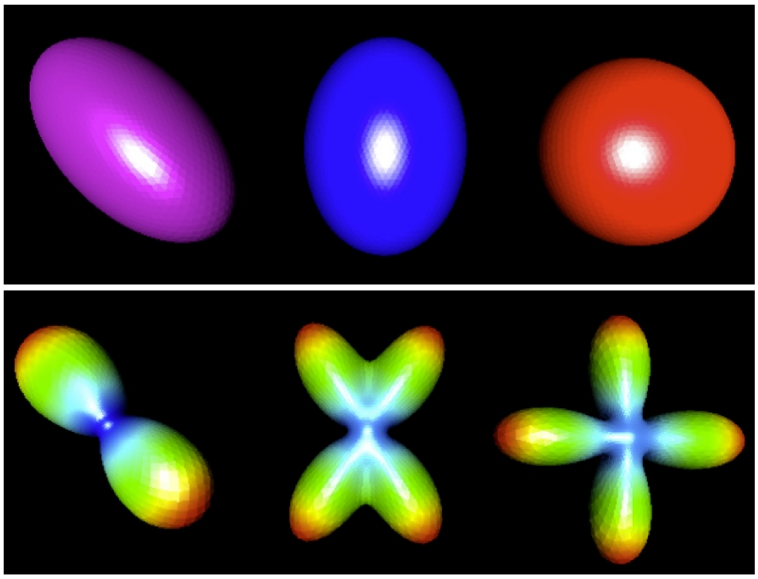

Figure 2.6. Diffusion Modeling. Using the same physic principles the choose of mathematical operator can change shape of diffusion model. First row shows diffusion modeling based on one main direction in the same voxel. Second row represents a multiple direction of diffusion interpretation based on different density function of diffusion distribution in the space.

- **single** tensor modeling method: based on probabilistic distribution function (PDF).
- **multiple** tensor modeling methods: based on orientation distribution function (ODF).

Single tensor modeling has been already explained. It is the most used method, especially in clinical applications. Multiple tensor modeling is a generalization of the single tensor approach which replaces the Gaussian model as the density diffusion model with a multiple population of molecules that stay in a single voxel [Fernandez-Miranda *et al.* 2012, Descoteaux *et al.* 2009]. Multi-tensor modeling can describe multiple behaviors of fiber bundles inside the same voxel. Mathematically, ODF is the probability of distribution as each point on the sphere corresponds to a unique orientation. Peaks of ODF provide estimation of dominant fiber orientations. Limits of multiple tensor models can be considered stability and hardware requirement. Tractography algorithms based on ODF produce additional and artificial fiber representations. Stability aspects become relevant in clinical application, especially when a bulk mass change brain structures drastically. Furthermore ODF estimation requires specific hardware and open-key sequences, not always available in clinical scanners.

2.3 *Images in Medicine*

Aims. The past decade have seen remarkable advances in medical imaging in terms of new physical applications, technologies, elabora-

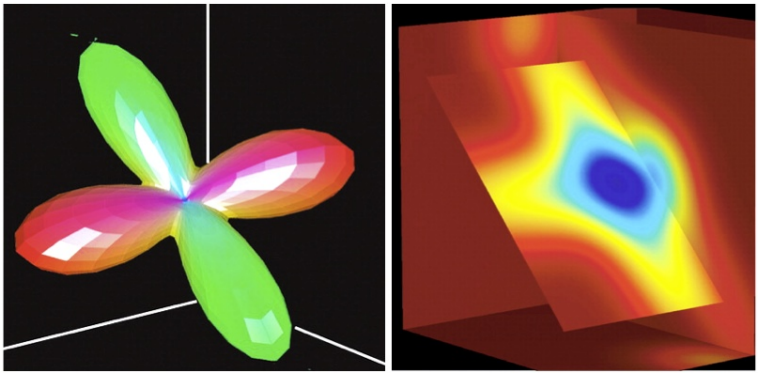

Figure 2.7. Orientation Distribution Function permits to identify two population family of fibers characterized by different orientation. Using Probability Density Function, two ortogonal distribution of fibers bundle in the same voxel appear to be confused with a planar diffusivity. Two orthogonal and high anisotropy were confused with one small anisotropy

tions and visualization. Computer tomography (CT) and his variants, Magnetic Resonance Imaging (MRI), Ultrasound (US) and Optical Imaging (OI) are widely involved in healthcare and biomedical research to study tissues from different point of view: tissue density and atomic composition, proton density, acoustic's wave and optical proprieties. Different physical approaches produce different images that allow to investigate characteristics of biological tissues from different point of views. The role of multimodal visualization, especially in medicine, is to superimpose different aspects of tissues in order to understand the composition of them. General purposes of Multimodal Imaging are detection, classification and analysis.

In neurosurgery, the aims of neuro-images are related to diagnosis and surgery. Neuroradiology protocols are designed to correlate clinical information with anatomical evidences. In presence of a pathological statement confirmed by neuro-images, the neurosurgeon can decide to perform a surgical procedures.
Surgical activities are widely guided by images. Anatomical and Functional landmark localization in neuro-images help the neurosurgeon to plan approaches and evaluate risks. This is particularly true in Glioma surgery.

Digital Medical Images and DICOM. Digital imaging was developed during the second half of 20th century in film technologies, scientific applications and military missions. British inventors H.G. Bartholomew and M.D. McFarlane produced the first digital image after the First World War [Pianykh 2011]. The *"Bertlane cable picture transmission system"* was a technique that was able to transfer images over cable line.
CT, MR and other radiological system were developed under the possibility to store digital images, but slices were almost always printed on

photographic film. The use of computers in clinical applications and network and communication developments induced a large exchange of medical data. During the 80's the need to develop a common protocol for medical data storage and transmissions emerged [Pianykh 2011]. 1983 the American College of Radiology (ACR) and the National Electrical Manufactured Association (NEMA) formed a joint committee to discuss about specifications of vendors and facilitations in picture archiving and communication systems (PACS). Two years later ARC/NEMA 1.0 was released. In 1993 the protocol name was changed in DICOM (Digital Imaging And Communications In Medicine) and finally in 1995 all the thirteen parts of the DICOM protocol were released.

The role of DICOM was fundamental, because it had set a milestone to image processing in medicine.
Digital spaces and in particular the third spatial dimensions offered new solution to understand anatomy. Visualization, manipulation and analysis of digital medical data were introduced as a new branch in Computer Sciences.

Visualization. Medical image analysis was originally involved in 2D processing. the third dimension was introduced to extend classic 2D anatomical illustrations with the use of computer graphics.
Visualization in medicine became a relevant area of scientific visualization, with the purpose to store and present 3D geometry of human body tissues. The goals of medical visualization, especially for 3D, can be:

- to **explore** data for educational purposes: VoxelMan was the first advanced anatomy education system created to show and interact with synthetic representation of human body;
- to **upgrade** diagnosis information: 3D reconstruction of pathologic variance of anatomy can help to understand shape and space relationships with surrounding tissues;
- to **create** a treatment planning: 3D scenarios can enhance the planning of surgical interventions in order to minimize risks and optimize the surgical strategy;
- to **support** intraoperative localization: Surface and Volumetric visualization can provide a visual and interactive support to the surgeons. Integration with tracers can amplify contributions in order to identification of anatomical landmarks [Kamada *et al.* 2005].

Visualization methods may be grouped into two classes: surfaces and volume rendering. Surface class includes methods where a surface of representation of elements can be generated from 3D data. Surfaces draw data using geometric elements of 3D Voxel unit. Pixel is a subset of Voxel in a plane. Surface rendering appears to be a special case of volume rendering, a visualization of 2D projection of 3D data.

Applications. The main applications of medical imaging in a patient candidate to surgery are:

- **pre-surgical** evaluation

- **intra-operative** visualization
- **post-operative** evaluation and follow up

2.3.1 *Pre-Surgical Planning Application*

The idea of pre-surgical planning is to simulate the surgical procedure using a reference model based on patient characteristics [Golby *et al.* 2011]. The set of information involved in pre-surgical planning can help the surgeon to understand and localize area not risking for patients. This is particularly relevant in brain because a minimal damage of the surrounding tissue can introduce a permanent deficit. Pre-surgical planning was introduced in the 80's, when the radiologist M. Vannier created the first computed three-dimensional reconstruction from CT images.

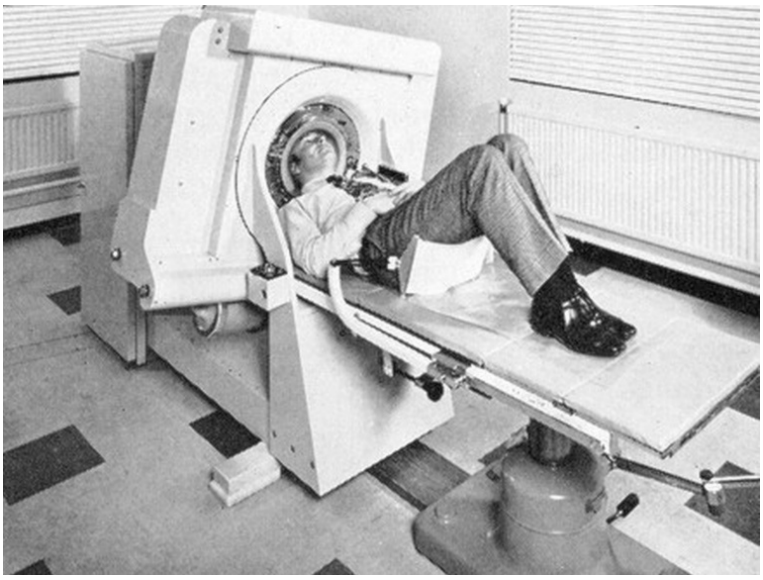

Figure 2.8. First CT Scanners: The use of CT images changes drastically clinical evaluations.

During the 90's computer sciences and technological advancements introduced relevant concepts that drastically changed pre-surgical planning evolution.
Stereolithograpic models gave a new aim to neuroradiologial images. CT acquisitions were digitalized, filtered and segmented in order to obtain automation for a 3D printer that built the model from a block of resin with a laser knife.

Sterelithograpic models were often used in neurosurgery but the mismatch in precision between planning and surgery, induced scientist to identify other solutions. Computer Graphics, such as digital representation and 3D virtualization of tissues introduced new prospectives about the role of computer technologies to support elaborations of medical data. At the end of 90's virtualization and interaction of end-user

with 3D digital medical data suggested the use of these techniques in surgery simulation.
Human tissues and surgical equipment were modeled to offer a virtualization of surgical procedures. Medical schools invested resources to create laboratories based on virtual tools to support training courses. The fast growth of computer graphic techniques and the inexpensive progression of technologies offered the possibility to virtualize medical data inside hospitals daily. Recent history showed that pre-surgical planning (as virtualization and interaction of patient data) became a pre-requisite for many surgical procedures.

Pre-surgical planning is a set of tools that analyzes and visualizes tissue information derived from different medical images. This is particularly true in neurosciences, because anatomical and functional characteristics are detectable using different sequences of MR. One of the roles of presurgical planning is to combine all of the different medical images in order to superimpose the same tissue area in all sequences. Overlay different data images required a set of processing methods that analyze images in terms of anatomical landmarks and identify spatial relationship between them. This collection of computer science algorithms is known as **Registrations**.

Registration Methods. Combining information from multiple imaging modalities, monitoring changes in features, relating digital represented images to the physical reality and relating the individual anatomy to a standardized atlas represent potential applications for registration methodologies. The main idea of registration is to establish a spatial relationship between different spaces represented by images as a mathematical transformation. Registration methods and algorithms work on pixel and voxel units. The **pixel** is the picture element that stores a specified area of images. It can contain a level of grey, a combination of colors or an unspecified type of data. The Pixel is defined in **2D space** such as a plane (slices) and can indirectly represents images in the 3D spaces. 2D slices can be stacked together to form a 3D volume. Units are called the **Voxel**. The pixel and the voxel have specific dimensional characteristics such as dimension and spatial position. Space orientation is defined in the structures that define the collection of pixels and voxels and his acceptance is relevant if defined in a world system. Medical images are organized in pixels or voxels that digitalize tissue proprieties.

Transformations define types of registrations classified by the spatial modification involved. The dimension of Transformations describes the type of displacement described:

- **Type1**: 2D images are overlapped up to 2D image.
- **Type2**: 3D volumes are overlapped up to 3D volume
- **Type3**: 2D images are overlapped up to 3D volume and viceversa.

The number of degree of transformations defines the type of spatial variation permitted such as:

- **Translation**: 3 Degrees of freedom; it defines the vector that identifies a displacement of all pixel/voxel of the image in the space;
- **Rotation**: 3 Degrees of freedom; it defines the spatial rotation of images along world axes;
- **Linear Warping** (affine): it can shrink the whole image along 3 world axes direction;
- **Total Warping** (for example voxel-by-voxel deformation vector): for each pixel or voxel it defines a vector that moves every element to another place a world coordinate system.

The characterization of registration and transformation type depends on applications that these methods require.

Other particular registration methods can be implemented in order to map a 3D shape into 2D or 3D image representations. This kind of methodology is useful when miscellaneous data types are involved in a multimodality scenario. The typical application is the surface recognition of the skin in the intraoperative calibration of the NeuroNavigation System [González-Darder *et al.* 2010, Chen *et al.* 2007].

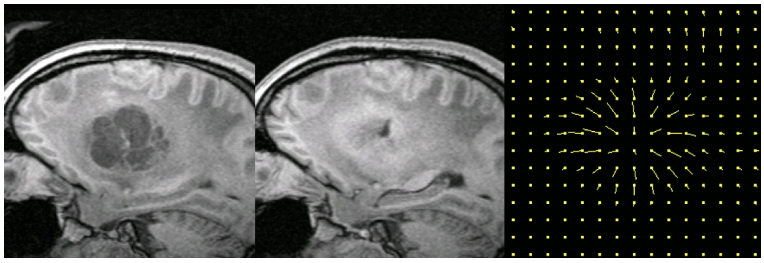

Figure 2.9. Tumor growing and displacement evaluation using Deformable Registration. Third image shows tensor field that represent the displacement information between two images.

2.3.2 *Intraoperative Application*

Computer Assisted Surgery and NeuroNavigation Systems
One of the most important applications that meets computer sciences, robots, medicine, neuroradiology and technologies is Computer Assisted Surgery (CAS).
CAS originated in 1986 when D.W. Roberst designed the first frameless integration with CT images and microscope. Few months later, E. Watanabe defined the term of “neuronavitator” for the first time as

> "... an adjunct for computed tomography (CT)-guided stereotaxic or open neurosurgery. It is composed of a multijoint three-dimensional digitizer (sensor arm) and a microcomputer, which indicates the place of the sensor arm tip on preoperative CT images... ... At surgery, after fixing the patient head and the sensor arm, sampling of the standard points was done to translate the position of the tip of the sensor arm onto the CT images displayed on a computer screen. In this way positional data from conventional preoperative CT scan can be directly transferred into the surgical field. This system has the unique feature of introducing CT-guided stereotaxis into conventional open neurosurgery."

Figure 2.10. NeuroNavigation Systems: Stereo camera trace object in the real scene. Workstation produces a virtual representation of patient and marked tools.

Today navigation systems can be defined as a selective intraoperative tool for localization of anatomical structures guided by radiological images acquired before surgery. The first and most used applications of navigation systems concerns surgery of central nervous system. The NeuroNavigation system is the common term used to identify this kind of technologies [González-Darder *et al.* 2010].

A NeuroNavigation Systems is composed of:

- **Detector**: using specific physical principles, the detector is the main view-point. His role is to identify the position of markers in the space.
- **Marker-Tool**: object with a specific shapes that can be easily tracked in the space.
- **Workstation**: calculates the position of markers in the space and projects 3D models of markers in the spaces.
- **Screen**: visualizes workstation 3D scenarios.

The main classification of NeuroNavigation systems concern the physical principle used to localize markers in the spaces. The most famous and used tracking systems are:

- **Passive optical tracking**: stereo-camera with an infrared system detector flashes infrared lights and optical markers reflect its.
- **Active optical tracking**: stereo-camera detect LED flashes from the observed scenarios. LED lights are fixed on the markers.
- **Electro-Magnetic tracking**: a low-frequency magnetic field is superimposed over the surgery site(under operating table). The position of a tracking probe is determined by analyzing the effect of its ferromagnetic parts on the magnetic field. The first presentation of this kind of system by Kato in 1991 reported an appreciable accuracy between 2 an 4 millimeters.

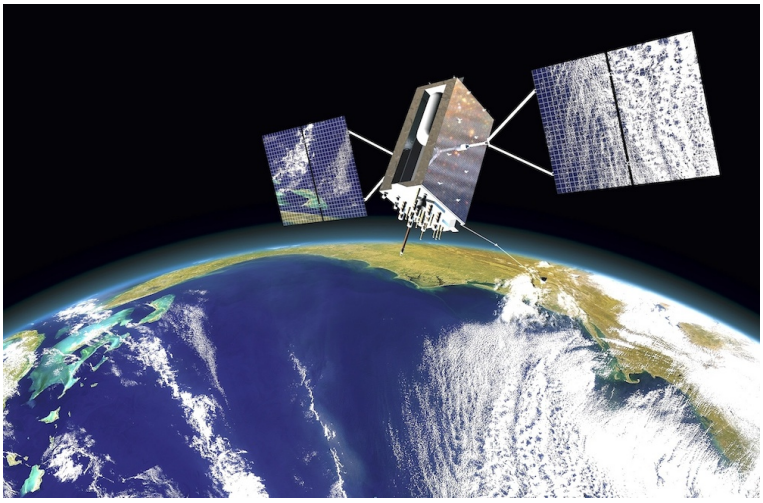

Figure 2.11. Similarity to Global Positioning System (GPS): Neuronavigation System can be presented as GPS where radiological images are the maps of the world and the stereo-camera or the magnetic field is the satellite.

2.4 *Intra-Operative Neurophysiological Techniques*

Penfield and Boldrey (1937) published their first article in Brain describing mapping of eloquent cortices by intraoperative electrical stimulation in awake patients. To follow, this technique was used by many neurosurgeons as a tool to neurophysiologically identify the functional anatomy of the cerebral cortex and the subcortical part of the CT. The **Penfield's method** has become very popular among neurosurgeons also thanks to its extensive use by Dr. Ojemann and colleagues, aiming to map language during awake craniotomy. This tremendous amount of work made Penfield's technique, in the 1980s and 1990s, a standard method for cortical mapping within the neurosurgical community [Sala 2010].

The Penfield's technique consists of electrical stimuli delivered through

a bipolar hand held probe, at a rate of 50-60 Hz and sustained for 3–4 s or longer. During electrical stimulation of the motor cortex, Dr. Penfield could rely only on visual observation of different movements of limbs and orofacial muscles [Sala 2010]. Interestingly, since then, most neurosurgeons and neurophysiologists followed this same method.
It was only a decade ago that Dr. Yingling and colleagues supplemented the original Penfield's technique with simultaneous recordings of motor evoked potential (MEPs) from the limb and facial muscles, thus improving the sensitivity of the original method. In 1993 **Taniguchi** introduced a new method for mapping and monitoring the motor cortex [Sala 2010].
They used a short train of high frequency (250-500 Hz) electrical stimuli consisting of 3–5 stimuli of 0.5 ms duration, with interstimulus interval of 2-4 ms (short train technique). This method was initially introduced to allow (MEPs) monitoring in patients under general anesthesia, but it was soon adopted by different authors to combine MEPs monitoring with cortical and subcortical mapping of motor pathways.

Rather recently comparison of efficacy of those 2 basic techniques for mapping and monitoring of the eloquent cortices and corticospinal tract has been published by Szelenyi [Sala 2010]. In conclusion of their study authors claimed that monopolar subcortical stimulation of corticospinal tract using a short train of stimuli is the most effective technique.
After this paper this technique become a standard for intraoperative identification of the corticospinal tract and intraoperative continuous monitoring of the its functional integrity [Sala *et al.* 2007b,Sala *et al.* 2000,Sala *et al.* 2007a,Sala *et al.* 2002,Sala *et al.* 2006,Sala 2010].

3. Methods

3.1 *Data Acquisition (DWI)*

Sequences
The estimation of white matter fibers is characterized by the type of diffusion modeling. The most common diffusion model applied to clinical study is the *tensor* model.
The tensor model is calculated using the probability density function based on Gaussian interpretation of diffusion characteristics. An acquisition protocol can be designed in order to calculate the apparent diffusion coefficient D matrix, as discussed before.
A DTI reconstruction is based on n-volumes of DWI characterized by different gradient properties (orientation) and fixed b-values. One or more B_0 volumes are acquired as a non-gradient-application reference. The collection of planes that describe the orientation of gradients is called a *gradient table*. The size of the gradient table and the b-value depend on applied protocols that can be customized in order:

- to **optimize time** of total acquisition: the number of applied gradients significantly influences the required acquisition time; more gradients can be interpreted as a better angular definition of diffusion characteristics. Today this assumption is not completely proved. A large gradient table can be used when the patient is cooperative. When patient is not cooperative it is better to perform a fast acquisition using a small gradient table;
- to **optimize signal-to-noise ratio** (SNR): b-values describe the time-window of observations. A small window (low b-value) gives a short observation time in order to calculate anisotropies. A large window (high b-value) can offer additional information about anisotropic paths. Calculation of D-matrix depends indirectly by the b-value. This means that b-value is conditioning measurement of S and the associated calculation of D.

Modern diffusion models are based on multi-b-values in the same sequences. MRI scanner proprieties can be optimized in order to obtain long-b-values. This significantly change SNR and can offer a more specific model of diffusion phenomena. In clinical applications, this type of diffusion sequences are infrequent. Other more specific physical parameters are not discussed in this document.

3.2 *Pre-Processing elaboration (Artifacts Removal)*

fMRI and DTI are considered 4D images because 3D volumes are acquired along a fourth dimension: time in fMRI and orientation gradient in DTI. 2D (typical MRI artifacts and related to acquisition proprieties) and 4D artifacts occur during acquisition time and post processing elaboration. 2D artifacts of DTI are slice motions and eddy currents. 4D artifacts are volume motions.

MRI Artifacts
MRI artifacts can reduce the quality of images drastically. A wide variety of artifacts is encountered in MR images [Baselice *et al.* 2010]. A first classification identifies three classes of artifacts:

- Patient-Related MR artifacts (physiological)
- Signal Processing-dependent artifacts
- Hardware Related Artifacts

Physiological Artifacts (PA) can be considered all kinds of motion that introduce inconsistences in phase and amplitude of the signal [Jenkinson 2003]. PA derive from involuntary movements of the body (like respiration or cardiac motion), small movements of the body or flow. Blurring and Ghosting are two subclasses of PA.
Blurring is a blur effect related to a lack of coherent phase among the population of moving spins at the time of echo formations.
Ghosting is a replication of a part of images and it is caused by motion during the acquisition time.
Signal Processing-dependent Artifacts (SPDA) occurred when the sample signal was mapped incorrectly to the image matrix. Typical SPDA are Chemical Shift, Wrap Around and the Ringing Artifacts (Gibbs phenomenon).
Hardware Related Artifacts (HRA) are linked to failures in terms of electronic and magnetic properties. The most important HRA are related to inhomogeneity (Gradient Field Artifacts, Radio Frequency Noise and Inhomogeneity) and in presence of physical phenomena that disturb acquisitions (Eddy Currents) [Bodammer *et al.* 2004].

4D Motion Correction (Philips MRI Console)
To reliably estimate diffusion tensor measures, such as fractional anisotropy and fiber orientation, a large number of diffusion-encoded images are needed. Longer acquisition times increase the chances of subject motion adversely affecting the estimation of these measures. The typical solution of 4D motion is to co-register all DWI volumes using a B_0 volume as reference. This step was performed in the Philips MRI console. A variant of this approach adjusts the B-matrix in order to re-orient gradient information in coherence with co-registration transformations. Different studies show that the re-orientation of B-Matrix can increase the quality of Tractography algorithms, especially for deterministic approaches.

Eddy Current Correction (FSL / ECC Module)
In echo-planar images, which are usually used to acquire diffusion tensor images, eddy currents produce significant distortions in the phase-encoding direction induced when strong gradient pulses are switched rapidly: low bandwidth and large changes in diffusion gradients occur during DTI acquisitions. When the gradient pulses switch, the time-varying magnetic field produces a current induction (eddy) in conducting surfaces of the scanner. Eddy currents persist after the primary gradient is switched off. Eddy current introduced two types of artifacts. The first type is a DWI image distortion caused by a wrong phase detection.
The second type is a mis-registration between voxels part of DWI volumes, that cause a miscalculation of D matrix and associated eigenvector/eigenvalue.
Eddy current can be reduced effectively in three ways:

1 Selecting the appropriate pulse sequences (such as a dual spin-echo sequence) or gradient waveforms (such as bipolar gradients)
2 Correcting the k-space data by calibrating eddy current artifacts in k-space and
3 Implementing post-acquisition image processing in order to co-register the DW images to reference images.

The third method is the most used, because it can be applied without changing MRI sequence proprieties. This solution is often used in clinical applications especially when end users could not customize MRI sequences. An eddy current occurs when a gradient pulse is applied. This means that eddy artifacts don't characterize the reference DTI volume B_0. The post-acquisition methods apply a multi-volumes registration that uses a B_0 volume as reference. A common implementation of Eddy Current correction is included into FSL packages. It only requires a NIFTI conversion of DTI volumes and can perform a re-calculation of diffusion gradient matrix.

3.3 *Diffusion Processing*

Tensor estimation
Diffusion MRI data contain a high number of information because the diffusion tensor field contains three degrees of freedom for the position in the space and six degrees of freedom that characterize diffusion information properties. The major difficulties in order to understand diffusion proprieties regard analysis and visualization of this complex type of data. Several approaches have been implemented to visualize WM fiber tracts using DTI data [O'Donnell and Westin 2011]. The most common used regard the construction of 2D maps or 3D glyphs (geometrical models as ellipsoids or cylinders). The tensor D is defined as a matrix with 6 unique components:

$$D = \begin{pmatrix} D_{xx} & D_{yy} & D_{zz} & D_{yx} & D_{zx} & D_{zy} \end{pmatrix}^T \tag{3.1}$$

$$D = \begin{pmatrix} D_{xx} & D_{yx} & D_{zx} \\ D_{xy} & D_{yy} & D_{zy} \\ D_{xz} & D_{yz} & D_{zz} \end{pmatrix} \tag{3.2}$$

Main diffusion directions in every voxel can be calculated by diagonalization of the D matrix. D mathematical proprieties (symmetric and positively defined) require only six coefficients to be full calculated. This means that DTI techniques require at least six DWI images and one unweighted ($b = 0 \frac{s}{mm^2}$) image to solve the systems. An eigenvector e of the tensor D and its corresponding eigenvalue λ imply that the inner product of the original tensor and the eigenvector results in a vector that is a scalar multiple of the original eigenvector:

$$Dx = \lambda_i \text{ and } x \neq 0 \tag{3.3}$$

The association between ei and respective λ i eigenvalue represents the solution of the D matrix. Rewriting the equation as

$$(D - \lambda_i I)x = 0 \tag{3.4}$$

we can observe that D- λ i I is singular and its determinant is zero. This implies that eigenvalues are the solution of the systems

$$|D - \lambda_i I|x = 0 \tag{3.5}$$

and the system can be solved by eigenvalues λ i as

$$(D - \lambda_i I)e_i = 0 \tag{3.6}$$

Eigenvectors and Eigenvalues pair together represents information described by the original tensor D. The diffusion tensor matrix and its eigenvalues may be used to express diffusion anisotropy present in the tissue of interest [O'Donnell and Westin 2011]. The eigenvector corresponding to the largest eigenvalue identify the direction of the largest diffusion coefficient and the smallest couple of eigenvalue-vector points to the smallest diffusion coefficient direction. Eigenvalues and eigenvectors are the base of DTI representation strategies.

2D maps

The most common method to visualize eigenvectors into a volumetric map is to codify the direction of the major eigenvector with a RGB color combination. Three-color scales refer to three intensities of diffusion along the three-coded direction. RGB color components are defined as the absolute value of the x,y,z components of e1 and multiplied with an anisotropy measure (FA) In particular:

- intensity of **red** identifies the first component of eigenvector and codifies the *right-left direction*,
- intensity of **green** identifies the second component of eigenvector and codifies the *anterior-posterior direction*,
- intensity of **blue** identifies the third component of eigenvector and codifies the *superior-inferior direction*.

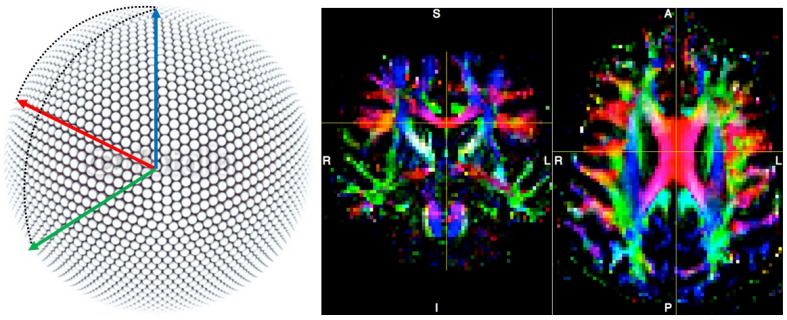

Figure 3.1. In FA-colormaps colors identify main direction of tensors. Red, Green and Blue are the main axes; sloped directions are calculated using color-projection in the sphere.

Colored maps are considered very helpful in many applications because they collapse the anisotropy measurement and his principal direction in a single visualization [Sedrak *et al.* 2011].
These can be useful to identify specific WM tracks and visualize their rough trajectories, especially during the Region of Interest drawing process. Other scalar diffusion maps and his relative measurement can be derived from the eigenvector and eigenvalue representations. The most common studied indices in diffusion MRI are fractional anisotropy (FA), mean diffusivity (MD), longitudinal diffusivity (landa parallel) and radial(or transversal) (landa perpendicular) diffusivity. All of these scalar representations are a particular combination of Diffusion Coefficient eigenvalues:

$$Trace = \lambda_1 + \lambda_2 + \lambda_3 \tag{3.7}$$

$$MD = \langle\lambda\rangle = \frac{\lambda_1 + \lambda_2 + \lambda_3}{3} \tag{3.8}$$

$$FA = \sqrt{\frac{3}{2}} \frac{\sqrt{(\lambda_1 - \langle\lambda\rangle)^2 + (\lambda_2 - \langle\lambda\rangle)^2 + (\lambda_3 - \langle\lambda\rangle)^2}}{\sqrt{{\lambda_1}^2 + {\lambda_2}^2 + {\lambda_3}^2}} \tag{3.9}$$

$$RA = \frac{\sqrt{6}}{2} \frac{\sqrt{(\lambda_1 - \langle\lambda\rangle)^2 + (\lambda_2 - \langle\lambda\rangle)^2 + (\lambda_3 - \langle\lambda\rangle)^2}}{\lambda_1 + \lambda_2 + \lambda_3} \tag{3.10}$$

$$VR = \frac{\lambda_1 \lambda_2 \lambda_3}{\langle\lambda\rangle^3} \tag{3.11}$$

$$Cl = \frac{\lambda_1 - \lambda_2}{\lambda_1 + \lambda_2 + \lambda_3} \tag{3.12}$$

$$Cp = \frac{2(\lambda_3 - \lambda_3)}{\lambda_1 + \lambda_2 + \lambda_3} \tag{3.13}$$

$$Cs = \frac{3\lambda_3}{\lambda_1 + \lambda_2 + \lambda_3} \tag{3.14}$$

These diffusion descriptors emphasize different diffusion properties stored in tensor data with peculiar response curves and noise characterization.

Trace can be seen as orientational diffusivity or diffusion magnitude. *Mean Diffusivity* (MD) characterizes the overall mean-squared displacement of the molecules. *Fractional Anisotrophy* measures differences from isotropic case (sphere). *Relative Anisotrophy* (RA) shows ratio of magnitudes of anistropic and isotropic parts of the tensor. *Volume Ratio* (VR) represents volume correlation between ellipsoid and sphere. *Linear Coefficient* (Cl), *Planar Coefficient* (Cp) and *Spherical Coefficient* (Cs) describe diffusion white matter proprieties such as organization of fibers and isotropic's area (like CSF or peritumoral edema areas) [Stadlbauer *et al.* 2011,Stadlbauer *et al.* 2007].
Many other descriptions were introduced during the last 10 years. In general, optical metric depends on the precise nature of application itself and a characterization of variability of diffusion metrics becomes relevant in statistical analysis of groups.

3D ellipsoid
The *Ellipsoid* is a spatial object that can be defined as a warped sphere with a particular orientation in the space. The ellipsoid definition requires a 3 axis dimension and its relative orientation in the space. Every axis orientation required a vector that defines the 3 components for each axis. The scalar value defines the length of 3 axis. The 3 vectors must me orthogonal, the 3 scalar associate values must be non-zero.

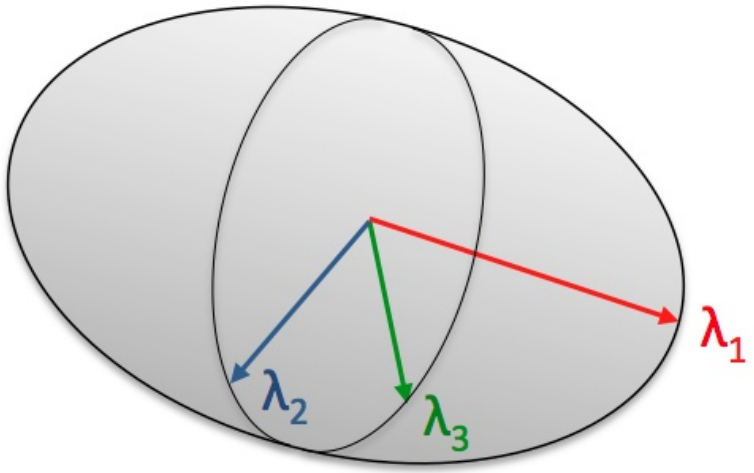

Figure 3.2. 3D ellipsoid represent the shape of diffusion modeling based on one main direction. Three axes are constructed using eigenvalues as shape proprieties and eigenvectors as shape orientations.

The relationship between axises lengths defines 3 kinds of ellipsoid:

- **scalen** ellipsoid when a>b>c
- **oblate** and prolate ellipsoids when two axes have the same dimension
- **sphere** when all axes have the same dimension

This interpretation can help to understand diffusion's results in DTI

analysis and visualization data. In fact the ellipsoid shape represent the probabilistic isosurface of molecular diffusion at a given time constant.

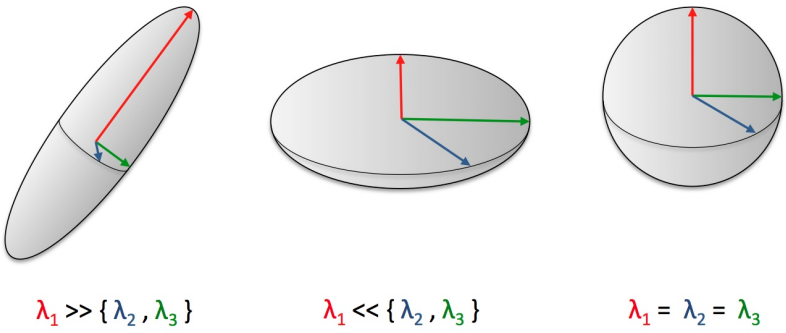

Figure 3.3. 3D ellipsoid configurations: shape of ellipsoid is defined by eigenvalues. *Scalen* shape of ellipsoid represents anisotropic condition of diffusion, *oblate* represent a typical case of crossing fibers configuration and *sphere* represents isotropic diffusivity.

3.4 *Tractography*

Tractography can be considered a large class of algorithms that generate a bundle interpretation of Diffusion Processes in the brain [Soares *et al.* 2013]. This means that tractography is an interpretation of anatomy with a different grade of accuracy based on diffusion data elaborations. Fibers are obtained by following the paths of particles dropped in a vector field [Soares *et al.* 2013]. The strategy used to approximate these paths constitutes the main difference between the methods analyzed. White matter tractography algorithms can be classified into deterministic and non-deterministic. The first only considers the main eigenvector direction in order to reconstruct the tract; the second class introduces the concept of perturbation in order to modify the vector direction at each location. We discusse only the probabilistic approaches, a subset of non-deterministic algorithms.

The *deterministic approach* produces a streamline that represents the main direction of diffusion for each voxel. This approach works well for many fiber bundles and can help to understand many configurations of lesion-pathways. The limit concerns the interpretation of voxels with low anisotropy[Soares *et al.* 2013].
The FA interpretation is correct when voxels describe a region without any particular diffusion direction (ventricles). When a region is involved in fiber crossing, FA is around zero and the algorithm produces a wrong reconstruction (i.e. lateral portions of the corticospinal and corticobulbar tracts).

The *probabilistic approach* aims to address this criticism by considering multiple pathways moving from the seed point and from each point along the reconstructed trajectories: the method accounts for

the uncertainty in the estimation of fiber direction. Behind the probabilistic algorithm there are many of pre-processing steps, such as co-registration, white-matter extraction and statistical model estimation. This mean that it is very slow and non-interactive[Behrens *et al.* 2007, Behrens *et al.* 2003].

Despite differences between strategies and algorithm implementation, the tractography procedure is based in the solving pathway equation:

$$p = \int_0^m e_1(D(x_n))dx \tag{3.15}$$

where x_0 and x_m are the Region of Interest at 0 time and m time (respectively seed point and termination point). Common steps between different approaches are required to solve the pathway equation:

- **Definition Of Seeds**: the tracking process requires a starting point; this is typically known as seed region, a collection of voxel defined in derived tensor map. Drawing seed region requires anatomical knowledge of fiber bundles and their localization. Alternative approaches can used label definition of the brain from external sources: using digital label atlas and *parcellation* method, it is possible to automatically set seeds. This method can be imprecise and computationally expensive.
- Selection of an **integration strategy**: different integration methods can be applied in order to calculate pathways. The difference between them consists in the methodology of calculating the propagation direction and the step size. The most applied strategies are the Euler integration method, Runge-Kutta, Fiber Assignment by Continuous Tracking (FACT) [Mori *et al.* 2002] and other alternative interpolation methods (Interpolated Streamline).
- Definition of **stopping criteria**. As required for seed definition, stopping criteria determine when the tracking process has to finish. Stopping criteria can be defined as a combination of limits imposed by used definition that interrupts calculation of fiber tracts. Common stopping criteria are FA threshold, Angle Threshold, maximal length of fiber and number of iterations.

Deterministic Tractography

Deterministic algorithms use a linear propagation approach. Fiber trajectories are generated in a stepwise fashion deriving the direction of each step from the local diffusion tensor. Approaches of deterministic category are the following:

- **Streamline** approaches generate fibers following the direction of faster diffusion (often main eigenvector). The propagation direction is described by a linear propagation of diffusion measurements. The main drawback appeared in areas where diffusion propagation was not linear, such as planar regions, since the trace of the fiber can not be determined in order to partial volume effects, such as crossing, kissing, and branching [Tournier *et al.* 2008]. FACT (Fiber Assignment by Continuous Tracking) algorithm altered the propagation direction at the voxel boundary interfaces. FACT algorithm used variable step sizes,

depending upon the length of the trajectory needed to pass through a voxel. An alternative procedure described uses a constant step size (CSS) approach or estimates the continuous tensor field and dynamically varies the step size as a function of the tract curvature. For all approaches, the step size must be small relative to the curvature of the trajectory.

- The **tensor deflection** approach (TEND) was proposed in order to improve propagation in regions with low anisotropy, such as crossing fiber regions, where the direction of fastest diffusivity is not well defined [Tournier *et al.* 2008]. The idea is to use the entire D to deflect the incoming vector direction and to obtain a smoother tract reconstruction result.
- The **tensorline propagation** method incorporates information about the voxel orientation, as well as the anisotropic classification of the local tensor given anisotropic indices. Tensorline propagation direction is a combination of the previous direction (main eigenvector) and the tensor deflection direction.

Diffusion Toolkit and *Trackvis* is a famous couple of packages dedicated to diffusion tractography. The Diffusion Toolkit implements the most relevant deterministic algorithms such as the FACT, 2-order Runge Kutta, Interpolated Streamline and Tensorline.
The Trackvis is the extraction software that calculates a sub-set of fiber bundle using ROI approaches.
The Camino (UCL Microstructure Imaging Group) implements streamline algorithm based on single tensor modeling and Q-Ball tractography based on multi-tensor modeling of diffusion phenomena.
ExploreDTI is a novel platform to test many implementation of tractography; two deterministic algorithms are developed: streamline DTI and streamline constrained spherical deconvolution (CSD).

Probabilistic Tractography

Probabilistic fiber tractography algorithms aim to overcome bugs of deterministic approaches by adding some random issues. Probabilistic fiber tracking can be considered a simulation protocol that describes random walk of particles through a set of voxels guided by tensor rules[Ciccarelli *et al.* 2006]. For each seed points, probability algorithms trace different paths and calculate the spatial probability distribution of connectivity [Friman *et al.* 2006]. Final tracking is the spectrum of possible paths[Behrens *et al.* 2007, Behrens *et al.* 2003].
Since last decade, more than one probabilistic implementation was developed .
In 2003 T.E.J. Behrens designed a novel interpretation of probabilistic fiber tracking [[Behrens *et al.* 2007, Behrens *et al.* 2003]] based on

- the estimation of **local** probability density function;
- the sampling of **data model** based on Markov Chain Monte Carlo techniques [Parker and Alexander 2003, Parker and Alexander 2005];
- the estimation of **spatial** probability density function for each voxel A and every other point in the data field;

- the estimation of **global connectivity estimation** based on spatial probability density function;
- using a special case of maximum likelihood strategy, the optimization of **parameter** that characterizes the global connectivity and the local estimation parameters;
- the determination of **global pathways** that follow the estimation of local probability density function.

Behrens formulation is implemented in the FMRIB Diffusion Toolbox (FDT), a software tool for probabilistic analysis of diffusion-weighted images implemented in the FSL package. FDT includes a set of procedures that completes the probabilistic workflow:

- **Eddy Current Correction Toolbox** corrects DWI volumes affected by distrortion,
- **Bedpostx Toolbox** calculates local PDF supervised by the global connectivity estimation,
- **Probtrackx Tractography Toolbox** calculates spatial pdf between voxels.

ExploreDTI implements two probabilistic approaches based on wild-bootstrap model-based resampling. Difference between algorithms depends on sample proprieties.

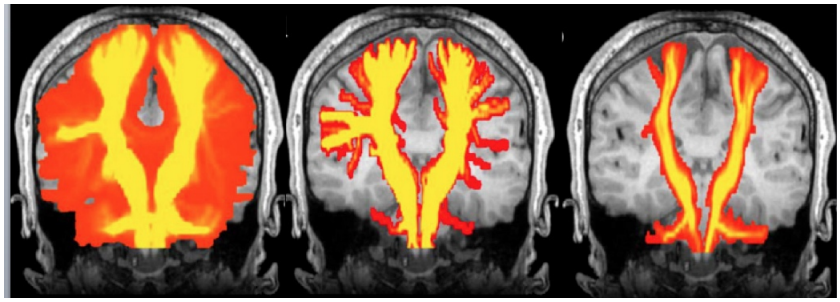

Figure 3.4. Probabilistic Tractography describes random walk of particles through a set of voxels and guided by tensor's rules. In Yellow it shows higher probability of fiber connection between two ROIs. Changing parameters of global connectivity the probabilistic distribution changes.

Extraction Protocol Based on Region Of Interest

Tractography algorithms performe a global connectivity estimation of the brain tissues. A second step called *"extraction"* interacts with the global model of white matter fibers while computing a subset of fibers of the brain. Extraction step casts fibers from defined regions. Regions can be drawn into 2D maps of diffusion tensor imaging (like FA, color-FA, mean diffusivity, ADC, etc).

Region of Interest (ROI) is a portion of the image that itemizes a focusing analysis.
The shape of the ROI can either correspond to an anatomical structure depending on the aims of the selection. An alternative sub-selection

method can be defined using an automated labeling segmentation of the brain (parcellation) [Zhang *et al.* 2010, Wang *et al.* 2011, Liberman *et al.* 2013, Huang *et al.* 2005].
Based on deformable registration, global model of pathways can be sub-selected using a set of label defined by parcellation algorithm. Parcellation algorithm defines a deformable transformation of a labeled atlas between the atlas and a 2D map of tractography. Advantages of parcellation method concerns the independence of user by knowledge of anatomical landmarks. Disadvantages derives by the presence of unlabeled tissues (tumor) that introduces errors in transformation model. This explains why neurosurgical application based on tumor resection are developed using manual drawing of ROI.
The ROI drawing requires a strong knowledge of fiber anatomy as 3D shapes and slice representations. The main difficulties occurred when brain anatomy is distorted and common landmarks are unrecognizable.

ROI Strategies
Anatomical ROI defines a collection of voxels that are necessary to identify fiber bundles.
Strategies change depending on anatomical characteristics of fibers. Extraction of fiber bundle is supported by three or more type of ROI in order to help ROI policing [Liu 2011]. Standard classification of ROI includes

1 **Seed ROI** is the set of voxel necessary in the first step of extraction methods;
2 **Waypoint ROI** is the set of voxel that forces generated path to pass by itself;
3 **Exclusion ROI** is the set of voxel that forces generated path to avoid by itself.

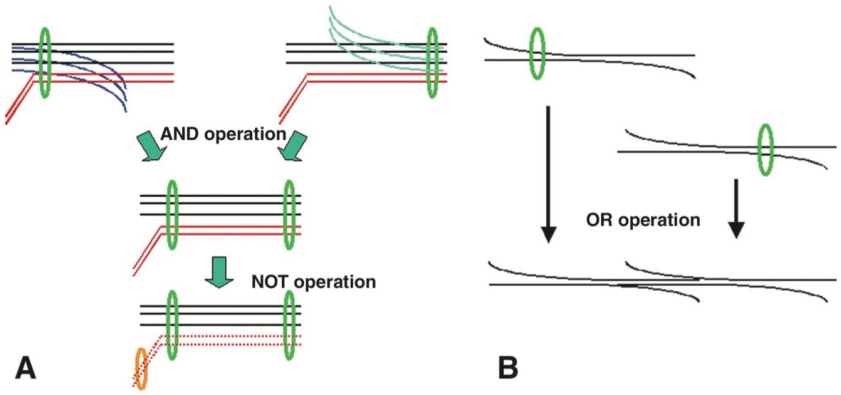

Figure 3.5. Classification of ROI type [Wakana *et al.* 2004]

Alternative extraction method defines a logician nomenclatures of ROI; it introduces a logician behavior of the ROI in extraction algorithm:

- **AND ROI** is a set of voxel that defines the logician conjunction with

other ROI. Without additional ROI, conjunction takes into account the whole set of voxel included in the DTI study.
- **NOT ROI** defines the exclusion logician operator. It excludes voxel from extraction analysis.
- **OR ROI** defines the disjunction operator. It produces an extraction that includes a non-specific conjunction between ROI definitions.

Artifacts and tractography algorithms can change ROI policing.

3.5 *Pathways*

Three distinctive groups of fibers entering and leaving regions in cerebral hemispheres can be defined :
association, commissural and *projection* pathways [Catani and Schotten 2008, Jones 2010].
Association pathways connect cortical regions in the same hemisphere with an anterior-posterior direction (both directions). Two different types of associational pathways can be defined in terms of shape and length[Jacobson and Marcus 2011]. Short fibers connect the nearest regions in a U-Shape configuration. Other fibers run all along the brain, from the parietal lobe to the frontal lobe.
Associational pathways are involved in higher cognitive function such as language, visuo-spatial processing, memory and emotions. The most important are Arcuate Fasciculus, Cingulum, Uncinate Fasciculus and Inferior Front Occipital Fasciculus.
Commissural fibers interconnect areas in the opposite hemispheres. The most important commissural fiber bundles are the corpus callosum, the anterior commissure and the hippocampal commissure. Commissural fibers play a significant role in the functional integration of motor, perceptual and cognitive function. They allow learning process and they are involved in all kinds of higher tasks that require a bi-lateral employment of functional areas.
Projection Pathways connect the cortex to subcortical structures such as deep cerebral nuclei, brainstem nuclei and spinal cord. Sensory and motor information travels through a projection system of fiber that functionally connects the central and the peripheral nervous system. The most important projections are the corticospinal tract and the corticobulbar tract.

3.5.1 *Association Pathways*

Arcuate Fasciculus
The arcuate fasciculus is a lateral associative bundle that connects the perisylvian cortex of the frontal, parietal, and temporal lobes [Baars and Gage 2013]. The arcuate fasciculus can be divided in three parts:

- long segment involved in the direct connection between Broca and Wernicke areas [Catani and Mesulam 2008];
- anterior segment (front-parietal direction) that connect Broca and Geschwind areas [Catani and Mesulam 2008];

- posterior segment (parietal-temporal direction) that connect Geschwind and Wernicke areas [Catani and Mesulam 2008].

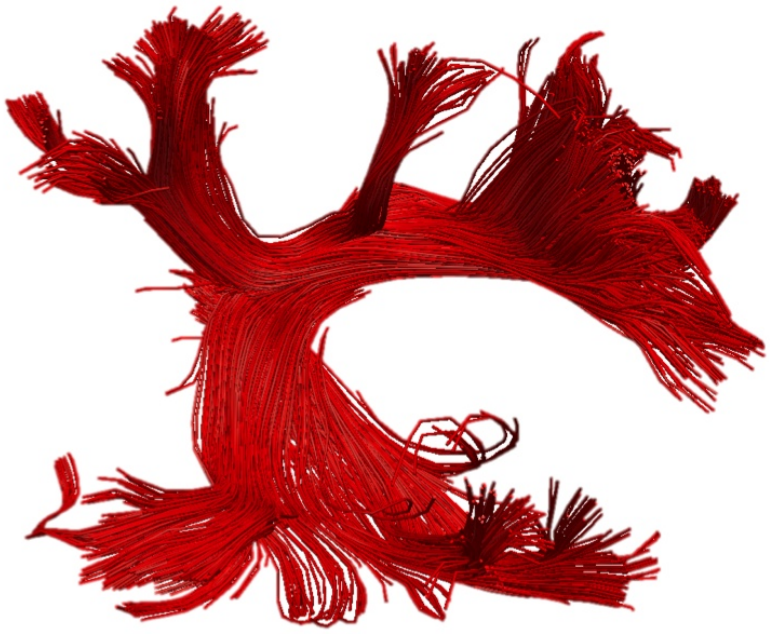

Figure 3.6. Reconstruction of Arcuate Fasciculus using deterministic implementation of DTI.

The anterior and posterior segments lie more lateral than the long fibers. The arcuate fasciculus of the left hemisphere is involved in *language* and *praxis* [Catani *et al.* 2005, Hayashi *et al.* 2012]. The arcuate fasciculus of the right hemisphere is involved in *visuo-spatial processing* and in some aspects of language, such as *prosody* and *semantics* [Mandonnet *et al.* 2007, Pulvermüller 1999]. The organization of the languages network is not completely known [Catani *et al.* 2005].
Long segments are possibly involved in rapid answer, anterior and posterior segments are possibly involved in high level and complex speech tasks.
The Broca area is possibly involved in phonologic speech tasks, the Wernicke area in sensitive component of languages as understanding, the Geschwind area as an integration and buffer area, in a global control of coherence of language tasks, from speech productions to understanding [Henry *et al.* 2004].

Uncinate Fasciculus
The uncinate fasciculus(UNC) is a ventral associative bundle that connects the anterior temporal lobe with the medial and lateral or bitofrontal cortex.
This fasciculus is considered to belong to the limbic system but its functions are poorly understood. It is possible that the UNC is involved

in emotion processing, memory and language functions. The UNC can be divided into a temporal, insular and frontal portion. It originates from the anterior three temporal convolutions anterior to the temporal horn and the cortical nuclei of amygdala.
All the fibers joint together into the anterior temporal stem and form a solid fiber tract while running toward the limen insulae [Kier *et al.* 2004].
The UNC travels in the extreme and external capsule along the lateral, and ventral circumference of the putamen, towards the retro-orbital cortex and gyrus rectus.

Figure 3.7. Reconstruction of Uncinate Fasciculus using deterministic implementation of DTI.

Inferior-Fronto Occipital Fasciculus
The inferior longitudinal fasciculus(IFOF) runs medially through the temporal lobe and connect the frontal lobe with the middle occipital pole inferiorly [Catani *et al.* 2003]. At the junction of the frontal and temporal lobes, the fasciculus narrows in its cross section as it passes through the anterior floor of the external capsule [Martino *et al.* 2010]. The functions of the IFOF are poorly understood; its involvement was often incorrectly attributed to the uncinate fasciculus [Catani *et al.* 2012b]. Very likely it participates to reading, attention and visual processing. The UNC and the IFOF have a role in extratemporal lesions triggering temporal-lobe syndromes, such as visual hallucinations. In some patients, lesions of the IFOF in association with several other tracts contribute to produce global aphasia [Pulvermüller 1999].

3.5.2 *Projection Pathways*

Corticospinal Fasciculus
The motor pathways can be divided into two group of tracts: corticospinal-tract(CST) and corticobulbar-tract(CBT). This definition reflects anatomical differences in terms of terminations. At the brainstem, the CST follows the spinal cord, the CBT synapses the lower motor neurons of the cranial nerves. For technical reasons (crossing fibers), DTI considers and reconstructs only the CST [Zolal *et al.* 2012, Nimsky *et al.* 2006].

Figure 3.8. Inferior Front Occipital Fasciculus reconstruction using deterministic implementation of DTI.

The CST is one of the most important pathways involved in motor functions in the human brain. Cortical areas generate signals that descend along the CST that transmits signals through the spinal cord to the extremities (such as hand and foot).
On cortical areas, the Left CST passes signals to the right side of the body and the right CST to the left side of the body. The two pathways decussate inferiorly to the brainstem.
The control of motor functions can be represented as the **Cortical Homunculus**, a pictorial map representation of body parts in the cortex. The homunculus was designed to localize and represent relationships between controlled body part and their cortical spatial employment.

The homunculus permits a partial classification of motor task in a sagittal plane of the brain. Another CST classification follows a surface classification of cortex area involved in motor tasks:

- **Primary Motor Cortex** (M1 and Area 4 in Brodmann Classification) is a region of cortex that contains specialized neurons called giant pyramidal Betz cells. These neurons are the largest in the central nervous systems and send their axons along spinal cord. They connect directly to their target muscle through anterior horn cells. The boundaries that define M1 are:
  - Anterior: precentral sulcus;
  - Posterior: central sulcus;
  - Medial: the midline;
- **Somatosensory Cortex** (S1) is the first structure of the parietal lobe after central sulcus. It is identified with the postcentral gyrus and it is representative of the main sensory receptive area of the body. As M1, S1 can be represented as a Cortex Homunculus.
- **Premotor Area** (Area 6 in Brodmann Classification) is the anterior M1 cortex area and its function is not completely understood. It is knows that it plays a relevant role in planning and spatial guidance of movements using abstract rules to perform motor tasks. Cells contained in F5 are a transition between giant Betz cells (five layers) and prefrontal cells (six layers). Premotor areas can be classified into two regions: premotor dorsal-caudal area and premotor ventral caudal area.

Classifications and identification of a finest functional mapping are currently a research area.

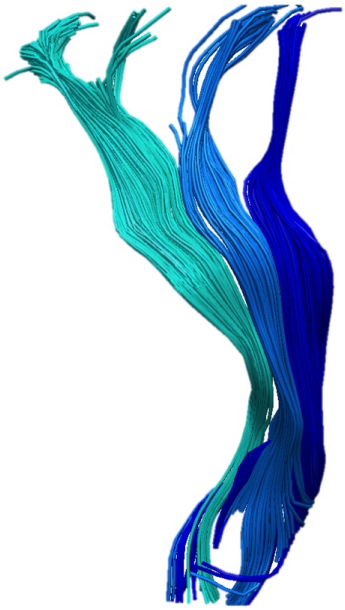

Figure 3.9. Reconstruction of Corticospinal-Tract using deterministic implementation of DTI: three color underlines anatomical subset of fibers characterized by different cortical seeding ROIs.

From the fifth layer of cortex areas,the CST descends along the internal capsule, passes through the peduncle and pons and medulla oblongata. At this level the decussation of pyramids occurs. Understanding the anatomical composition of the CST permits to define certain Regions Of Interest. The standard drawing is based on a couple of regions: the first one is placed in a specific cortical area (M1, S1 or premotor area) [Bello *et al.* 2008, Kim *et al.* 2008, Qazi *et al.* 2009, Seo and Jang 2013]. The second one is placed on the pons level. Anterior or posterior parts of pons can help to enhance specific motor or sensitive functions.

Optic Radiation

The *Visual System* is a part of the central nervous system involved in all visual processes. Photoreceptors, nerves, fiber bundles and visual cortex compose it [Ebeling and Reulen 1988]. Photoreceptors capture light signals and transmit them to the optical nerve. In the optic chiasm, portion of signals crosses over to the opposite side of the brain. The Optic tract, composed of retinal ganglion cell, connects the chiasm to the lateral geniculate nucleus (LGN). The LGN is connected to the primary visual motor cortex (occipital region) via optic radiation (OR) [Catani *et al.* 2003]. Visual information flows through cortical stratified areas. These secondary visual regions process visual primitives elaborated from primal visual motor cortex [Maruyama *et al.* 2007, Jenkins *et al.*

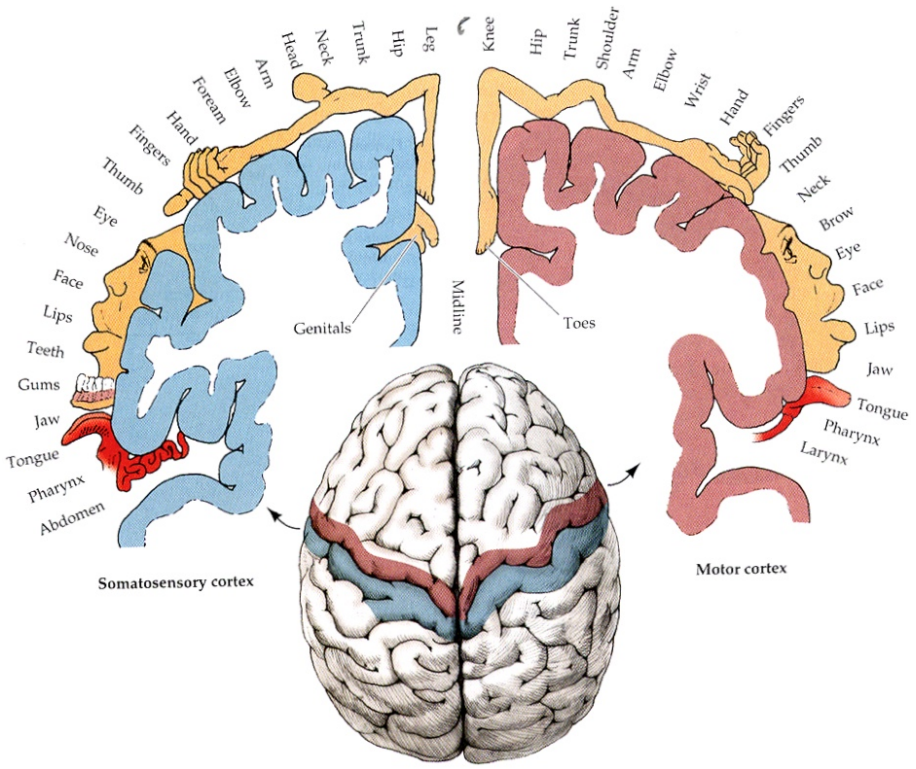

Figure 3.10. Cortical Homunculus: a pictorial representation of *primary motor cortex* (pre-central gyrus) and *primary somatosensory cortex* (post-central gyrus). It visualize relationship of motor and sensitive task with the amount cortical area involved for a specific task.

2010a]. The Optic Radiation is the most studied part of Visual System [Sherbondy *et al.* 2008, Rocca *et al.* 2008]. The OR requires two ROIs: one is placed in the axial section of the **Lateral Geniculate Nucleus** (LGN); the second ROI is chosen to cover an area defined in a coronal section of the occipital lobe from the **Calcarine Fissure** to the **Cerebellum**, near the brain midline.
The OR is often confused with the IFOF, because they run below the under posterior horn of the ventricle [Winston *et al.* 2011, Tao *et al.* 2009]. In axial projection, from posterior to anterior direction at thalamic level, the OR curves to generate Meyer's Loop, an anatomical structure very difficult to reproduce with DTI techniques due to the wide angle of the tract in this region.

3.6 *Reconstruction Parameters and Guidelines for Algorithm Use*

Anatomical knowledge can help to understand how to use the wide set of parameters and possibilities in DTI processing.
The goal of the DTI algorithm is generally an anatomically correct interpretation of tensor data. This means that in Tractography the main problem derives from interpretation of FA values in order to understand the shapes of fiber bundles.

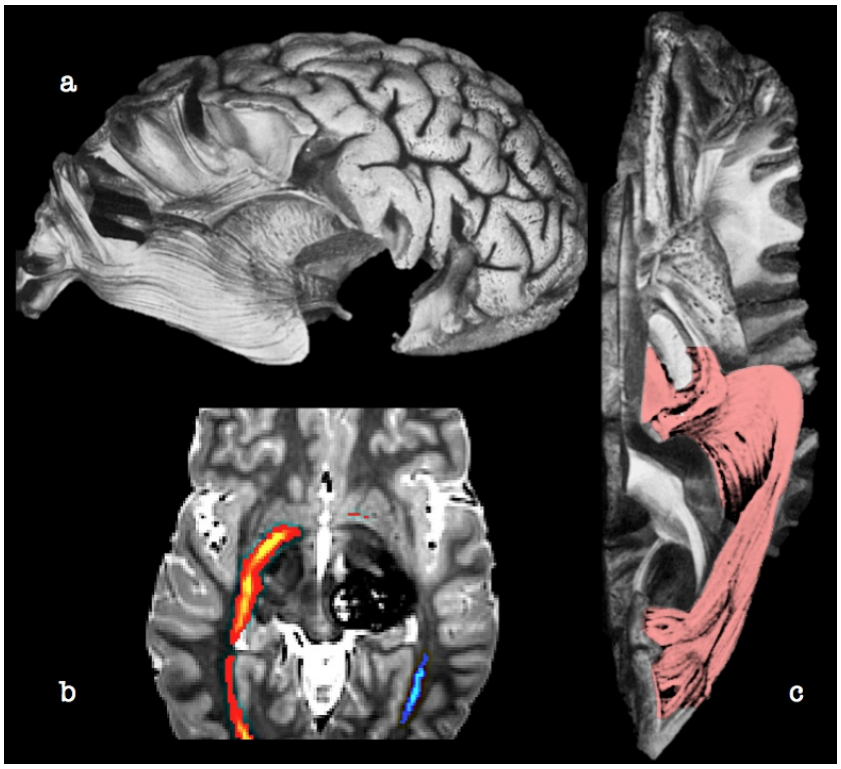

Figure 3.11. Optic Radiation: **a** and **c** show anatomical fiber dissection of visual pathways [Catani *et al.* 2003]. Figure **b** represents probabilistic reconstruction of optic radiation: in red/yellow the healthy-side of the brain; in cyanic/blue the reconstruction of optic radiation interrupted by Cavernous Malformation .

The governance of DTI framework is first based on the reconstruction approach chosen. As it is known, deterministic approaches are preferred in order to take advantages of high interactive ROI drawing. This is very important when anatomical overlapping of tumor and landmarks is not easily identified. Anyway, probabilistic approaches offer methods to identify a huge variety of FA interpretation pathways (useful especially in cases of Crossing Fibers artifacts).

Using a fiber bundle classification we define this collection of strategies and parameters in fiber bundle reconstruction:

- Intermingling Pathways that include
  - **CST Approach 1**: when required information of the motor pathways is located in medial portion of the cortex, a deterministic approach is preferred. the angle threshold is 30 degrees, and FA-values are chosen using an automatic detector of boundaries (background noise and maximum FA in the images). Depending on MRI scan, seed point can change in bulb.
  - **CST Approach 2**: if one of the most lateral information of CST it is required, we use th probabilistic approach. Angle threshold can be over 40 degrees.

  - **OR Approach 1**: the probabilistic approach is the only possible method to identify Meyer's loop. The high angle involved in OR and the presence of surrounding bundles suggest to use a strong probabilistic method. The curvature threshold is set up to 55 degrees [Wu *et al.* 2012 , Fernandez-Miranda *et al.* 2012, Stieglitz *et al.* 2011]. Other parameters like number of threshold, minimum and maximum number of steps and step length depend on cases.
  - **OR Approach 2**: a deterministic approach should be considered in order to define an approximation of OR path. From Geniculate Body to Calcarine Fissure, it is possible to reconstruct a fiber bundle that doesn't represent Meyer's loop correctly; OR representation is linear, parallel and medial relative by to IFOF. This approach should be used for the tractography surrounding the visual cortex.

- Unmix and cross-free fiber pathways

  - **ARC**: the deterministic approach is preferred. The angle threshold is 45 degrees, and FA-values are chosen using an automatic detector of boundaries (background noise and maximum FA in the images).
  - **IFOF**: the deterministic approach is preferred. The angle threshold is 35 degrees, and FA-values are chosen using an automatic detector of boundaries (background noise and maximum FA in the images).
  - **UNC**: the deterministic approach is preferred. The angle threshold is 45 degrees, and FA-values are chosen using an automatic detector of boundaries (background noise and maximum FA in the images).

Configuration Fibers

Has explained in capitol 2, different configurations of fibers arise in human brain[Jacobson and Marcus 2011]. Canonical classification of fiber pattern identify three main configurations:

- **Parallel**: fibers are approximately straight and parallel. High anisotropic diffusion along the fiber direction is represented by scalen ellipsoid.
- **Fanning / Bending**: fibers present a variable orientation that can be represented as a small anisotropic diffusion along principal fiber direction. Tensor model represent entirely PDF as an ellipsoid with poor scalen characteristics.
- **Crossing/Kissing**: Crossing fibers arise when two population of fiber are represented in the same voxel. PDF show clearly the two main directions but the tensor model collapse in a disk representation [Qazi *et al.* 2009, Schultz and Seidel 2008].

Crossing/Kissing fiber configuration shows the main limits of diffusion modeling based on a single tensor combined with deterministic algorithm tractography [Dargi *et al.* 2007].
Based on single tensor diffusion model, crossing and kissing fiber configuration can be presented well using probabilistic approaches.
Novel approaches based on multi-tensor modeling are designed in order to identify a bigger set of fiber configurations.

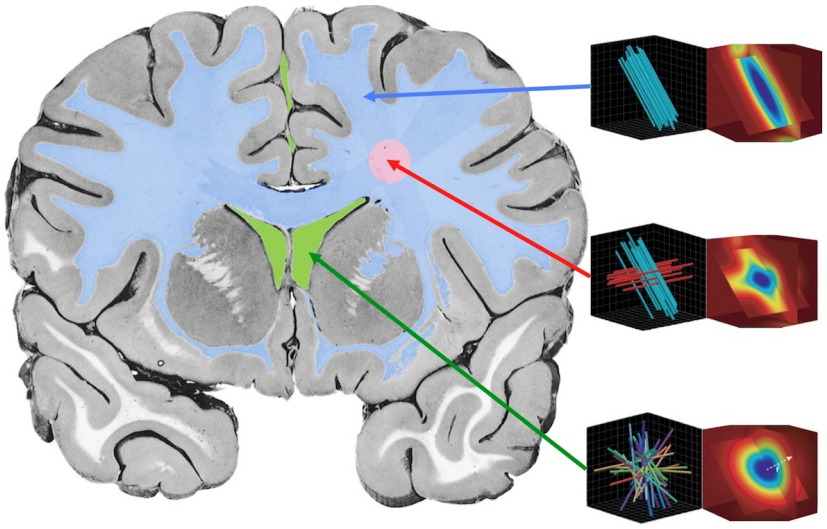

Figure 3.12. Fiber's configuration of the Brain

3.7 *Digital Tractography Interpretation*

Interaction of fiber tracts in presence of neoplasms
The aim of surgical treatment of neoplasm (i.e. gliomas) is to maximize the extent of pathological tissue resection while minimizing post-operative deficits related to the damage of eloquent functional areas.
Damage of cortical areas, subcortical structures (such as neural pathways) and the vascular system can introduce a post-operative neurological deficit [Castellano *et al.* 2012, Bello *et al.* 2008].
DTI is today the unique technique that gives an idea about WM structures and about the relation between cortical areas connected [Catani *et al.* 2002]. Altered states of WM might be expected to influence characteristics of anisotropy such as the scalar value and the space orientation of tensors. Displacement and attenuation are the common characteristics that can describe the relation between the tumor and the WM structures using DTI techniques. Jellison describes [Jellison *et al.* 2004] a potential classification of relationship between pathological masses and fiber bundle in series of 20 patients with brain tumor. He describes four possible pattern:

- Pattern 1, **Deviation**: normal or a slightly decreased FA, combined with consistent displacement caused by the bulk mass of tumor. The registered status of deficit in a specific function can be partially or totally retrieved after decompression of fiber bundles caused by a strong deviation.
- Pattern 2, **Infiltration**:a high decrease in FA calculation and a normal location. The infiltrated bundle presents *"normal"* hues in a FA-color map.
- Pattern 3, **Edematous**: a high decrease of FA and a normal localization with abnormal hues in FA-color map. Sometime deficits related to the

tumor-surrounding fiber bundle are not registered before DTI.
- Pattern 4, **Destruction**: isotropic diffusion in the course of fiber bundles. The deficits can be considered persistent after surgery.

Quantification methods universally confirmed and accepted do not exist at the present time.
This is caused by the incomplete understanding of Gliomas, by the gross detection of diffusion properties and by the short story of in-vivo tractography techniques in clinical cases [Kinoshita *et al.* 2005 ,S Pujol 2009 ,Tournier *et al.* 2008].

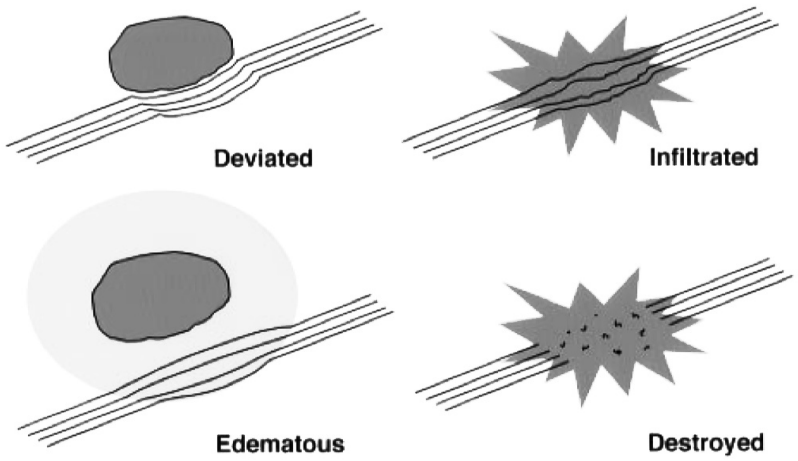

Figure 3.13. Tumor to Fiber Configurations[Jellison *et al.* 2004]: Jellison's drawing shows the four patterns described in his paper. This classification is up-to-date.

Alternative Evaluation Methods

Like Jellison's Patterns, many methods are developed to identify the state of fibers, based on their representation in diffusion maps or their reconstructions.
Classic methods based on diffusions maps try to investigate the relationship of a particular statement with a specific representation of WM proprieties such as Fractional Anisotropy, Mean diffusivity, Radial Diffusivity and other derived measurements.
The geometrical reconstruction of the WM fiber bundle based on tractography methods is conditioned by reconstruction factors involved in pipelines. The reliability to virtual reconstruction is not commonly accepted as a basis of quantitative methods. However, it is to possible give some visual information based on virtualization of fiber bundles. For example a gross-symmetric tract like CST, IFOF, UNC, OR can be bilaterally reconstructed. Equate morphological characteristics such as fiber counts, average angles can be useful as a comparison method.
Using the pathways definition, spectral representation and analysis of shapes reconstruction or a FA measurements can be offer a set of quantitative descriptors of diffusion phenomena in the brain.

3.8 *Pre-Operative Multimodal Visualization*

3.8.1 *PreSurgical Brain Tumor MRI Protocol*

Imaging plays a central role in diagnosis, characterization, surveillance and therapeutic monitoring of brain tumors and MRI is actually considered the most informative technique [Upadhyay and Waldman 2011]. Weighted images of MRI are commonly used to classify brain masses and this initial classification can drastically change treatments [Upadhyay and Waldman 2011]. Intracranial metastases and glioblastomas are the two most common brain neoplasms in adults. In patients with multiple lesions, diagnosis of brain metastases is usually uncomplicated. However, in cases presenting with unknown primary malignancies differentiation may be difficult [Lee *et al.* 2013].

Convectional MRI sequences have a limited ability to differentiate between these two types of lesions, because their neuroimaging appearance is often similar. Conventionally, T1 weighted, T2 weighted and gadolin-enhancement are considered enough to evaluate the type of lesion and to propose a rough classification in order to identify the surgical strategy. The histological response after surgery is considered relevant for designing a therapeutic treatment after surgery.

For example, depending on the type of the lesion, a classification of perituroral edema can sugest different neurosurgical strategies:

- In glioma, *peritumoural edema* is better referred to as infiltrative edema. As reported by Jellison, glioma growth is correlated to the enlargement of lesion through surrounding tissues. These assumptions change depending on glioma grade. Low-grade gliomas are described as infiltrative lesions; high-grade glioma present expansive characteristics.
- In non-infiltrative primary tumors, such as metastasis and meningiomas, *peritumoural edema* is synonymous with vasogenic edema, which increases extracellular water from the leakage of plasma fluid. Metastatic tumors tend to grow in an expansible manner, and typically displace the surrounding brain tissue.

Many new studies demonstrate that in infiltrative tumors the extent of resection can influence timing of relapse [Gerstner *et al.* 2010]. Recently, *Fluid Attenuated Inversion Recovery* (FLAIR) acquisitions are often included in the pre-surgical study in order to use a correct classification of brain tumor and to understand its infiltrative characteristics [Artzi *et al.* 2013, Pichler *et al.* 2013].
Infiltrative characteristics can also change interpretation of relationship between fiber bundle and tumors and this characterization can change surgical approaches and the interpretation of post-operative deficits [Gerstner *et al.* 2010].

The *Blood oxygen-level dependent* (BOLD) method is used in fMRI to observe activated areas in the brain at any given time [Tomycz and Friedlander 2011]. The BOLD sequence is commonly used as a noninvasive technique to identify the site of the primary motor areas preoperatively. [Ulmer 2010]
fMRI is used increasingly by neurosurgeons to introduce functional landmark in their surgical planning in order to maximize tumor resection and preserve eloquent areas [Smith *et al.* 2007]. However fMRI can provide any type of information about subcortical pathways of functional signals [Smith *et al.* 2007].

Neurosurgical applications require a strict MRI protocol [Upadhyay and Waldman 2011] that includes information about:

- tumor classification in order to identify future progress of disease (T1 weighted, T2 weighted, and gadolinium enhancement);
- infiltration characteristics in order to understand the resection limits (FLAIR);
- eloquent area surrounding tumor in order to identify cortical no-way areas (fMRI activation areas);
- subcortical pathways in order to identify subcortical no-way areas (DTI and tractography pathway definition).

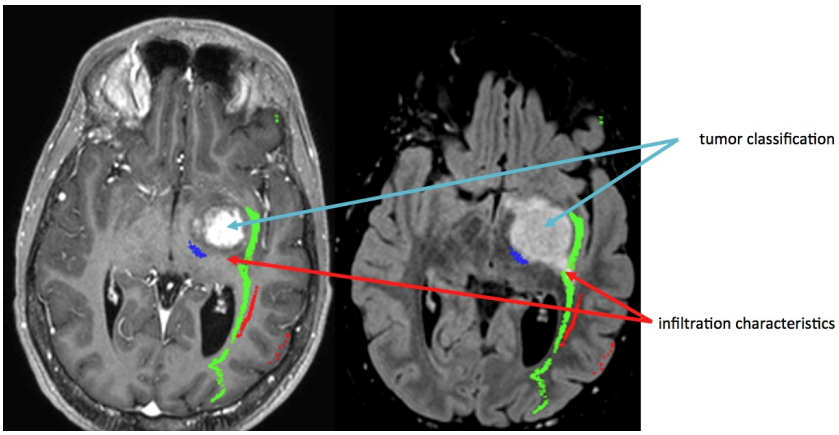

Figure 3.14. PreSurgical Brain Tumor MRI Protocol - Part 1: Tumor Classification and Infiltration Characteristics. Left and Right images show the ability to differentiate tissue's proprieties. FLAIR highlights infiltration characteristics of Gliomas [Pichler *et al.* 2013].

3.8.2 *Multimodal Visualization Packages (Slicer 3D)*

Pre-surgical virtualization is one of the most important applications of CAS, because it helps surgeons to understand the relationship between pathologic and healthy tissues with a virtual representation of the patient. Using MRI data it is possible to combine different diagnostic information in one integrated tool that overlaps tissue properties and spatial information. Applied to surgery, virtualization becomes

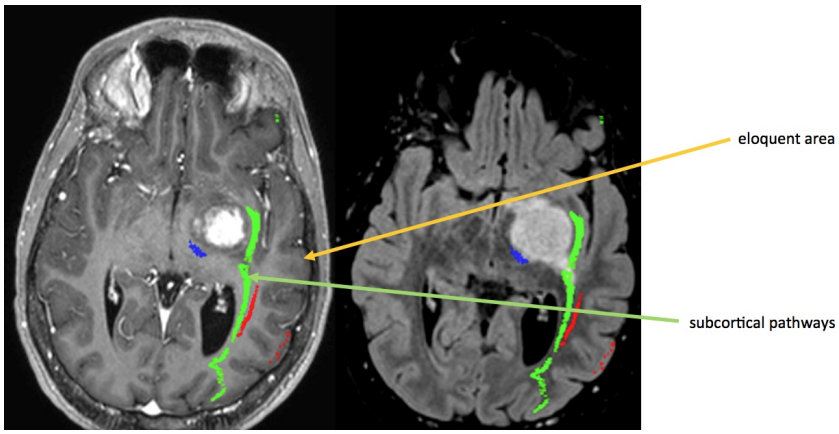

Figure 3.15. PreSurgical Brain Tumor MRI Protocol - Part 2: White-Matter Pathways and fMRI activation areas. DTI and fMRI play a central role in identification of eloquent areas and valuable subcortical structures involved in complex functional tasks.

planning and can help to identify the best surgical strategy for surgical treatment. Pre-surgical planning requires two main fundamentals:

- Visualization Toolkit: a collection of virtualization methods that permit to explore digital data using 2D and 3D views.
- Images Toolkit: a collection of image processing implementations needed to elaborate digital data.

Slicer 3D is a free open source package that includes a strong visualization core and a set of easy-to-use image analysis toolbox. Slicer3D is based on the most famous cross-platform packages dedicated to medical image elaboration and visualization: **Insight Segmentation and Registration Toolkit** (ITK) and **Visualization Toolkit** (VTK).
ITK and VTK are implemented in order to be included in the most used programming languages such as C++, Python (as a scripting code) and Java. Python implementation substitutes the older TCL/TK scripting languages.

The history of ITK and VTK is strictly connected with the most important American human body atlas such as the **Visible Human Project** (U.S. National Library of Medicine). ITK was implemented as an open resource algorithms in order to process medical images with the most innovative computer science approaches.
Registration and Segmentation algorithms are included in order to offer a powerful set of toolboxs to manipulate CT and MRI data. In 1993 VTK was created as a framework library dedicated to 3D Graphics methods. The aim of VTK developer was to create an object oriented approach to computer graphics simultaneously with the first implementation of Open Graphic Library (OpenGL, a Silicon Group product).
Few years later VTK become a reference in medical imaging implementation and this offered new scenarios to his development.

Pre-surgical planning software are now implemented into the most important navigation systems such as iPlan and TraumaCad in BrainLab Products and StealthViz for Medtronic. The major limit of these commercial solutions is compatibility with heterogenic systems. Other visualization toolboxes are designed as 2D DICOM viewer and PACS retriever and receiver client application.
3D visualization and image processing modules are limited (Osirix by Apple and Carestream by Kodak).

Slicer3D includes different features such as:

- A Robust DICOM and biomedical file-support reader;
- 4 miscellaneous window viewers (3 as 2D planes, 1 as 3D scenarios);
- A Set of Registration and Segmentation toolbox;
- Miscellaneous type of Data (2D slices, 3D volume, 3D surfaces, 3D objects, 2D label map).

Slicer3D can import or export:

- DICOM series
- Nifti files
- Analyze+Header files
- 3D object DATA (vtk files, pial files,...)

The Registration Toolbox includes:

- editor of transformation
- Fast Rigid Registration algorithm implementation
- Fast Affine Registration algorithm implementation
- Fast Non-Rigid BSpline Registration algorithm implementation
- Automated Registration
- Linear Registration algorithm implementation
- Atlas Creator
- Set of Brains Parcellation toolbox (Warping Deformation, Resample and Fitting module)
- Registration Based by Fiducial Points
- Multi-Resolution Affine Registration
- Surface Registration algorithm implementation

The Segmentation Toolbox includes:

- Fast Marching Segmentation
- Mesh Contours Segmentation
- Threshold Segmentation
- Robust Statistic Segmentation methods
- Region Growing algorithm implementation

The most important surface modules are:

- Grayscale model maker
- Surface Connectivity
- PolyData to model Converter

The Filtering Section of Slicer3D Toolbox includes:

- Skeleton Extractor
- Histogram Matching
- MRI bias Field Correction
- Resample Scalar Volume
- Threshold Filters
- Arithmetic, De-noising and Morphology toolboxes

3.8.3 *Data Descriptions*

Data analysis is the process of inspecting, modeling and processing data in order to discovery useful information. In computer sciences identification and understanding of types of data have a practical and theoretical relevance as feasibility studies and implementations. Multimodal medical imaging applications include different types of data that can be alternatively classified by dimensionality.

2D images: it is a collection of pixels or voxels that storage a level of grey. As explained before, pixels and voxels have typical space properties like dimension, origin, orientation and index (required for unique identification).
2D images can be presented as a plane or a slice that shows a particular section of medical data. Conventionally radiologic planes are axial, sagittal and coronal.
2D sequence of images (series): a set of 2D images defines a series. A series is composed by index-linked 2D images characterized by spatial orientation and inter-slices spaces. A series can be considered an anisotropic projection of a 3D volume in 2D planes.
3D volumes (isotropic 2D sequence of images): it is a particular case of a series of images described by isotropic projection of a 3D volume in 2D planes. A voxel unit can be considered a cube.
3D geometry is an object described by surfaces. Surface is a manifold described by geometrical 3D elements. The most common 3D elements are 2D or 3D shapes like polygons or meshes.
6D tensor: it's part of 3x3 matrix that represents the six coefficients needed to define a D matrix in DTI. The other three elements can be derived.

Image Registration Algorithms
Image registration is the process of transforming images acquired at different time points, or with different modalities into the same coordinate system. It is an essential part of any neurosurgical planning and navigation system, because it facilitates combining images with important complementary information to improve clues for critical surgical decisions. The main idea of registration is to establish a spatial relationship between different spaces represented by images as a mathematical transformation.
Image registration algorithms are based on similarity measurements between reference image and moving image. Registration is considered an optimization problem, with the goal of finding a spatial mapping

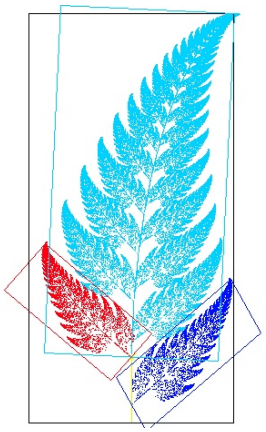

Figure 3.16. Example of Affine Transformations: leaf was repeated using affine transformation and red or blue shape.

that will bring the moving image into alignment with the reference image (also called fixed).

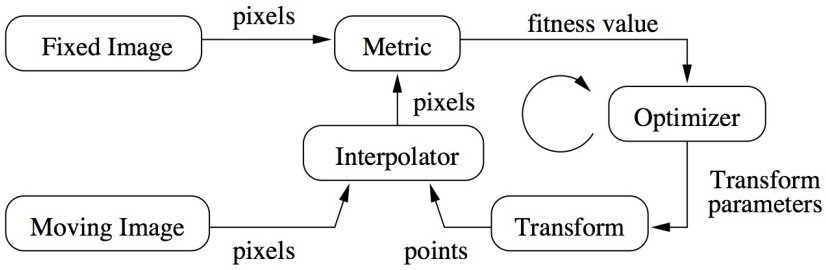

Figure 3.17. Registration Framework in ITK software guide: fixed and moving images were placed in the same spatial spaces using comparison's methods based on pixel values.

Transformation represents the spatial mapping between images. **Interpolator** is a mathematical operator used to evaluate intensities between fixed and moving images.
Metric component calculates measurements of difference between images.
Metric is a quantitative criterion, to be improved into the searching space by **optimizer** that guides the best parameters of the final transformations.

Transformations define the classification type of registrations. Dimension of Transformations describe the type of displacement described:

- Type1: *2D image* are overlapped up to a 2D image.
- Type2: *3D volume* are overlapped up to a 3D volume
- Type3: *2D image* are overlapped up to a 3D volume and viceversa.

Registration types represent different types of spatial operator. The most important are:

- *Translation*: three Degree of freedoms; it defines the vector that identifies a displacement of all pixels/voxels in the image in the space.
- *Rotation*: three Degree of freedoms; it defines the spatial rotation of images along world's axes.
- *Linear Deformation* (affine): can shrink the whole images along three world axes direction (4x4 matrix).
- *Total Deformation* (for example voxel-by-voxel deformation vector): defines a vector that moves every element in another place in world coordinate system for each pixel or voxel.

Depending on the application, registration algorithms are applied in order to calculate the best spatial operator required to superimpose images. The types of data involved in pre-surgical planning show that a volume-to-volume registration is required. According to analysis of geometrical MRI proprieties, it is well know that different sequences can present geometrical distortions dependent upon protocol-sequence specifications:

- Diffusion 2D-maps are calculated from different DWI volumes. This means that any kind of DWI geometrical proprieties are transferred to diffusion maps. As it well knows, different artifacts, such as Eddy Currents, motions and ghosting, often warp Spin Echo sequences [Wang *et al.* 2012].
- T1w, T2w and FLAIR can be affected by geometrical distortions caused by chemical shift [Wang *et al.* 2012].

In neurosurgery applications, especially when NeuroNavigation systems are engaged, T1w, T2w or FLAIR are usually chosen and considered reliable as anatomical reference. This means that one of these sequences can be used as reference of a multi-modal imaging application, like pre-surgical planning.
By choosing T1w as global reference image, all of the other images are co-registered. Typically, high-resolution images require a linear transformation that performs rotations and translations of moving images. Otherwise, diffusion maps require a combination of rigid transformations (translation and rotation) and warping transformations (affine map). A warping transformation applied to maps of diffusion properties can be considered limited by applications. A warping transformation of diffusion maps must be mirrored in tensor space and in geometrical fiber spaces. Mirroring deformable transformation introduces approximations and artifacts derived by

- mismatch between resolution of reference and moving images
- difficulties to identify a proper mapper between imaging and alternative domains interpolators.

3.8.4 *Voxelization Algorithm*

Voxelization Algorithm (VOXA) is a python script implemented using ITK and VTK packages that convert a 3D geometry into 3D raster image. Based on image registration VOXA calculates the intersection between

3D geometry and target volumes. Voxel values are changed by crossing of 3D data.
VOXA is designed to break the limitation of medical image viewers that use slice visualization of exams. Medical systems are not designed to import 3D models.

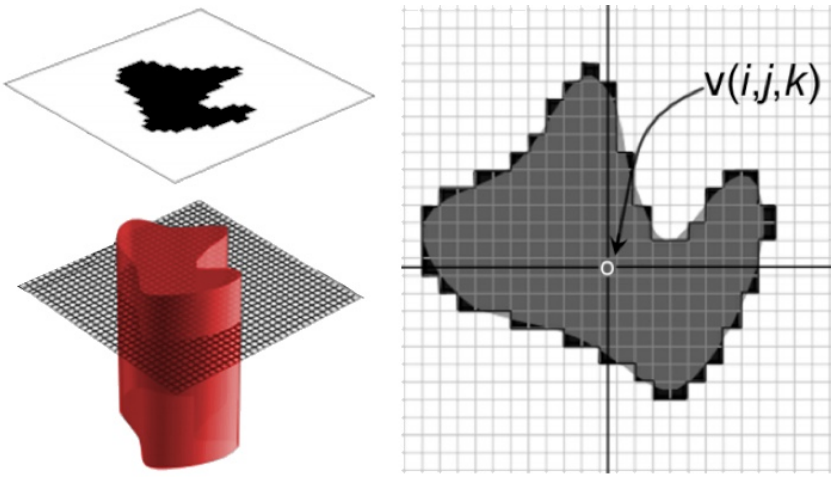

Figure 3.18. VOXA Algorithm converts 3D geometry into 3D raster images. This is one possible solution to integrate fiber bundles in Neuronavigation Systems.

VOXA is useful in all kind of applications that use 3D geometry in pre-operative and intra-operative visualization visualization on classic medical viewer systems during surgery. All of the commercial NeuroNavigation Systems accept only series of DICOM slices as navigation maps. VOXA is able to create raster images of DTI fiber bundles over structural MRI exams such as T1w or FLAIR. Applied to the fiber bundle voxelization, VOXA requires a strict pre-processing.
At first, linear registration transformation is calculated between reference series (commonly T1) and moving images that represent the fiber bundle coordinate system. The best solution tested is the use of FA-maps as moving images, because the fractional anisotropy representation is a good skeleton of WM, well represented in T1. The obtained linear transformation (LTRF) between T1 and FA-map (or DTI) space properties is used to move all 3D geometry in the same space of T1. Harden-Command include LTRF in 3D geometry properties: this mean that fiber bundle are now automatically in the same space of T1.

VOXA is now applied in order to intersect the fiber bundle 3D geometry in the referred T1 voxels.

3.9 *Intraoperative Integration*

3.9.1 *NeuroNavigation System*

The main localization methods commonly used for tracking are based on optic and electro-magnetic detection. Optical navigation systems

are widely used with passive and active landmarks. Common setup of NeuroNavigation Systems is composed by:

- Mayfield head holder, a skull clamp engaged by adjustable and inflexible arm to the surgical table
- Detectable System References engaged with the surgical table
- Detectable Surgical Tools

The Mayfield head holder clamps spatial relationship between head of the patient and system reference.
A 3D representation(3D virtual spaces) of the patience generates from MR or CT images. A 3D virtualization of detectable objects is included in 3D scenario in order to interact with the virtual spaces of the head of the patient. The navigation of virtual head is performed using both 2D view and 3D view.
In 2D view images are presented by set of slices.
In 3D view radiological images are projected in a 3D spaces using 3D surfaces and 3D meshes.

Standard procedure based on optical systems can be summarized as follow:

- head of the patient and system references are engaged to the surgical table;
- using MRI/CT images, 3D reconstruction of skin surfaces is calculated by NeuroNavigation workstation;
- calibration procedure estimates relationship "3D virtual" and "in the real world" head using a common system reference and a pre-calibrated tool. Calibrated tool collects and shapes a cloud of point touched in the skin.
- Fitting procedures calculate Euclidean distance between head-model and point-model.

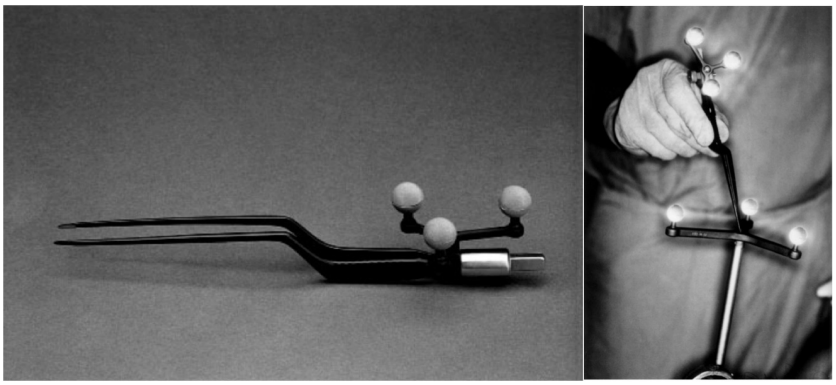

Figure 3.19. Equipment in Optical Neuronavigation Systems: tool presented in left part of the picture is an bipolar stimulation equipped by passive optical marker. On the right side of the picture a typical step of pre-calibration procedure.

During navigation, calibrated tool is visible by NeuroNavigation camera. Its model is represented in 3D model and is virtualized in the

same position in respect to the real space. Virtual distance between tool-model and head-model can be updated in real time. NeuroNavigation system supports multiple images of the patient. Results obtained by pre-surgical planning can be integrated intra-operatively using co-registration toolbox implemented in NeuroNavigation systems [Nimsky *et al.* 2001]. Using MR images, T1-weighted images are used as the reference of the navigation (fixed images). Extracted subcortical pathways (DTI) and activation areas (fMRI) can be integrated as moving images in intraoperative visualization setup.

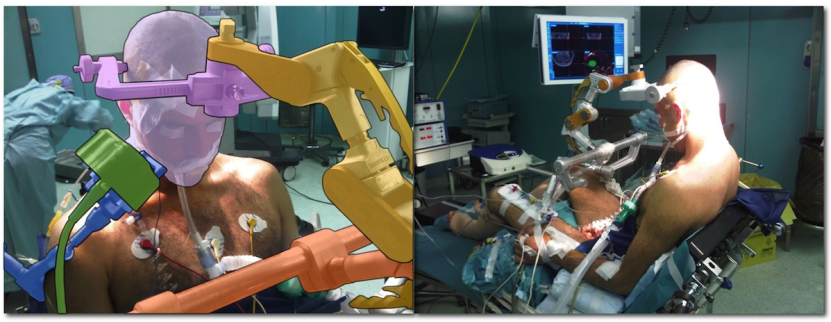

Figure 3.20. Example of posterior approach surgery assisted by *magnetic* Neuronavigation Systems.

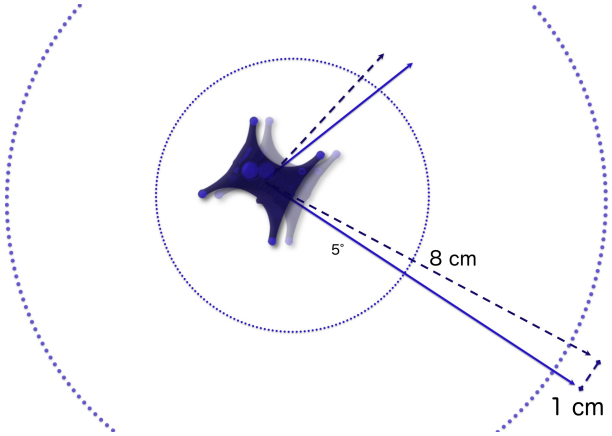

Figure 3.21. Example of error propagation caused by rotation of system reference: considering 8 cm of radius, 5 degree of rotation in the origin produces 1 cm of inaccuracy.

NeuroNavigation system has different type of measurement errors. Optical or Magnetic detections are characterized by sub-millimeter errors. Additional error can derived during engaging procedures of references, co-registration algorithms and 3D modeling of the head of the patients.

3.9.2 *Neuro-Physiological Monitoring*

In 1937 Penfield and Boldrey established a milestone in intraoperative neurophysiology by publishing the first description of eloquent areas mapping using electrical stimulation in awake patients. This technique was used by many neurosurgeons as a tool to identify the functional anatomy of the cerebral cortex and the subcortical part of the CT.
The Penfield's method has become very popular among neurosurgeons also thanks to its extensive use by Dr. Ojemann and colleagues, aiming to map language during awake craniotomy [Deletis and Sala 2001, Deletis and Sala 2008]. This tremendous amount of work made Penfield's technique – in the 1980s and 1990s – a standard method for cortical mapping within the neurosurgical community.
The original Penfield's Method consists of single electrical stimuli delivered through a bipolar hand held probe, at a rate of 50– 60 Hz and sustained for 3-4 sec or longer. During electrical stimulation of the motor cortex, Penfield could rely only on visual observation of different movements of face muscles.
The Taniguchi's method is based on short train of 3-5 stimuli (0.5 ms duration) separate by interstimulus interval of 2–4 ms. This method is today used both motor evoked potential monitoring and cortical-subcortical mapping of motor pathways.
The issue of subcortical mapping has emerged recently thanks also to the advent of diffusion tractography and functional localization in brain tumor surgery [Bertani *et al.* 2009]. What matters to the neurosurgeon when removing pathological tissue at the subcortical level is to know how far run the from white matter tracts, in order to avoid permanent deficits.
Today neurosurgeon use different types of subcortical stimulation in order to identify fiber bundles intraoperatively [Bello *et al.* 2008]. The most popular methods applied in neurosurgery introduce a variability regarding stimuli (single stimuli vs. short train) and stimulator (bipolar vs. monopolar).

4. Materials

4.1 *Subjects*

From January 2011 to December 2013, 144 patients with lesions in eloquent areas were submitted to pre-operative DTI tractography (49 in the last 10 months). Sample were described in table 4.1. Biopsy and histology confirmed final diagnosis as described in table 4.2 and detailed in 4.3 with the definitive World Health Organization (WHO) classification of brain tumor.

Total Cases	144
average Age	48
minimal Age	4
Maximal Age	78
Male	79 (54.9 %)
Female	65 (45.1 %)

Table 4.1. Subject's characteristics

Confimed Diagnosis	#	Percentage
Gliomas	110	(76.4 %)
Metastasis	7	(4.9 %)
Cavernous Malformation	6	(4.1 %)
Other	21	(14.6 %)

Table 4.2. Diagnostic Pathology: Distributions

WHO Grading Scale		Percentage
High Grade (Class III and IV)	74	(67.2 %)
Low Grade (Class I and II)	36	(32.8 %)

Table 4.3. Subset of WHO Glioma Grading

94 of 144 were treated surgically.
81 of 94 were monitored using Neurophysiological monitoring (NM)

and in 70 of 94 cases surgery integrated NeuroNavigation Systems (NS).
59 of 94 used both NM and NS.
4 cases were studied with intraoperative navigated ultrasound.

4.2 *Brain Tumor Protocol Definition*

Neurosurgical MRI protocol designed for brain tumor surgery could be offer information about tumor classification (T1w, T2), infiltration characteristics (FLAIR), eloquent area (fMRI activation areas) and subcortical pathways (DTI). **T1 weighted** images, acquired with Spin-Lattice relaxation mechanism, show in dark Cerebrospinal Fluid (CSF), edema and necrosis. Bright pixel values show fat and using Gadolinium contrast blood, vessels and tumor. Blends of Gray define Gray (GM) and White Matter (WM).
T2 weighted images, acquired with Spin-Spin relaxation time mechanism, show in black, air, calcium and flow. Dark values show GM and WM. Bright on T2 show CSF, blood, edema and lesions.
FLAIR performed by special inversion recovery sequences expresses similar tissue's proprieties of T2 weighted with the suppression of CFS signal using long T1. GM and WM become similar and edema contrasts surrounding lesion.
DTI sequences acquires the brain from cerebellum to the highest point of the cortex in inferior-superior direction and whole brain in the other two directions.
Depending on MRI scan (Siemens and Philips) two type of protocols identify the number of volumes used in DTI study:

- in Philips scanner we defined *DTI medium*, 16 applied gradient volumes and 1 B_0 volume. B-Value was $800\frac{s}{mm^2}$. *DTI high* was a 32 volumes acquisition using $800\frac{s}{mm^2}$ B-value and 1 additional $B_0 = 0\frac{s}{mm^2}$ volume. Voxel dimension was 1.7mm x 1.7mm x 2 mm.
- In Siemens scanner two sequences were commonly used: a short time sequence defined acquisition of 18 total volumes with 3 B_0 and 15 diffusion volumes; a long time sequence defined acquisition of 33 volumes with 30 gradient volumes and 3 B_0 volumes. B-Value was $800\frac{s}{mm^2}$. Voxel size was 2mm x 2mm x 2mm.

Recently 3.0 T Philips scanner implemented new sequence based on 64 gradient volumes and 1 B_0 as reference volume.
fMRI acquisition protocol used BOLD sequences. Motor task paradigm was designed as a block Rest-Activation model with 10 cycles. Vocal command guided motor task execution. Rest and activation cycles were intervals of 10 seconds.
Motor paradigms were finger tapping for hand task, and dorsiflexion for foot.
Characteristics of MRI acquisitions were presented in 4.4 4.5 4.6 4.7 and 4.8 tables.

Scanner	144 Total Acquistion	Percentage
Philips	80	(55.6 %)
Siemens	42	(29.2 %)
both	22	(15.3 %)

Table 4.4. MRI scanners

	102 Philip Acquistion	Percentage
1.5 T	26	(25.5 %)
3.0 T	51	(50.0 %)
both	25	(24.5 %)

Table 4.5. Philips MRI scanners

Gradients	Philips 1.5 Acquistion (26+25 = 51)	Percentage
16	29	(56.9 %)
32	2	(3.9 %)
64	0	(0.0 %)
16 & 32	20	(39.2 %)
16, 32 & 64	0	(0.0 %)

Table 4.6. Size Of Gradient Table in Philips Scanner 1.5 T

Gradients	Philips 3.0 Acquistion (51+25 = 76)	Percentage
16	3	(3.9 %)
32	13	(17.1 %)
64	2	(2.6 %)
16 & 32	54	(71.1 %)
16, 32 & 64	4	(5.3 %)

Table 4.7. Size Of Gradient Table in Philips Scanner 3.0 T

Gradients	64 Siemens Acquistion (42+22)	Percentage
30	42	(65.6 %)
15	13	(20.3 %)
30 & 15	9	(14.1 %)

Table 4.8. Size Of Gradient Table in Siemens Scanner 3.0 T

4.3 *Processing DWI data*

DTI pre-processing protocol was performed on DWI data from Philips scanner. Moving artifact was corrected by multi-volume registration on Philips Workstation. Eddy Current correction (ECC) was performed using the FSL toolbox. No re-orientation of gradient was applied.
Partial DTI pre-processing protocol was applied to DWI data from Siemens scanner. ECC was performed using FSL implementations. Deterministic algorithm was applied in all cases. Depending on difficulties to reconstruct fiber bundles, probabilistic approach was additionally performed.
In this set of cases two common application required probabilistic approaches:

- tumor in eloquent area and out of reach by crossing fibers
- peritumoral edema characterized by incorrect tensor estimation in many voxels
- peritumoral edema characterized by low ratio between anisotropic and isotropic areas.

Diffusion Toolkit (DTK) and ExploreDTI performed deterministic tractography. FSL (probtractx) and Explore DTI performed probabilistic approaches.
Interpolated Streamline was the most used implementation of Deterministic tractography. Alternative algorithms were tested due to identify the best methodological framework. Numerical algorithm comparison wasn't performed. The major hindrance was the variability of data (type of lesion, size and perilesional characteristics and sites).
In 13 of 144 cases we weren't able to reconstruct fiber bundles. Reconstruction process failed depending on different hang-ups :

- in 6 cases extensive peritumoral edema conditioned diffusion tensor estimation; anisotropic tissues like fiber bundle were "drenched" and anisotropic components were blanked by more extensive isotropic characteristics.
- in 3 cases extreme warping lesions changed drastically shape of fiber bundles. Stopping criteria were broadened but the free-gaining of threshold introduced more artifacts than informative representation of fibers.
- in 4 cases a combination of factors like patient motion and inhomogeneity of static magnetic field introduces extreme warped DWI images that influenced drastically diffusion tensor processing.

The global brain tractography was submitted to the fiber extraction process. Neuroradiologist supervised cases and listed a set of requesting pathways.
Inclusion criteria depended on tumor's adjacencies: surrounding pathways and cortical areas were considered. Fiber extraction based on ROI techniques required anatomical knowledge required to decode anatomical variances of brain. Additional differences were introduced

by tumor growing. Contralateral reconstruction was often taken into account due to clarify both aspects.

Each single DTI case was composite by extraction of fiber bundles and 2D maps. Deterministic tractography produced a tube's 3D geometry that represented fibers.
Probabilistic tractography produced a cloud of voxels as a representation of the path's probability between seed and termination ROI.
Voxel could contain a decimal value from 0 to 1 (0 no probability, 1 maximal connection probability).
Whole DTI process (tensor estimation and fiber extraction) produced a set of different type of data: geometries and volumes. VTK format was used as geometry file for fiber bundle. NIFTI file format was used to archive volumes such as probabilistic process and extraction of pathways and diffusion process maps such as FA, color FA, DW, ADC and Bo maps.

4.4 *Pre-Surgical Planning*

Pre-surgical planning protocol was applied to 144 patients. DTI output files were imported with the standard input *file importer*. Anatomical images were loaded using a *DICOM importer*. fMRI outputs were stored in NIFTI files and were imported in slicer3D using standard input file importer.
After data-loading slicer3D produced an xml-style scheme called *Scenario*.
Multimodal visualization of medical data needed a fixed image as the reference for all data. Rigid registration module calculate spatial relationship between additional anatomical data, DTI and fMRI data (moving images) and T1w (fixed images).
Spatial relationship is a 4x4 transformation matrix.

Four registration processes were launched sequentially:

- T1 as fixed images and T2 as moving images: **T2rT1.trf** stored transformation matrix between T1 and T2.
- T1 as fixed images and FLAIR as moving images: **FLAIRrT1.trf** stored transformation matrix between T1 and FLAIR.
- T1 as fixed images and FA-map as moving images: **DTIrT1.trf** stored transformation matrix between T1 and DTI's data. DTIrT1.trf was applied to fiber's geometries.
- *(optional)* T1 as fixed images and fMRI activation area as moving images: fMRIrT1.trf stored transformation matrix between T1 and fMRI's activation areas.

Using a blending tool, each calculated transformation was supervised. Visual and qualitative methods were applied due to appreciate the registration's output. Anatomical correspondences between reference and fixed images were taken into account in order to evaluate registration's re-processing.

Ventricle's shape, skin's surface and white matter and grey-matter were chosen as comparable landmarks. Considering restrained deformations, anatomical correspondences between 2D DTI's map and T1 were focused into the middle of the images. Brain's middle space was located in the much stable area of magnetic field.

Scenario of slicer3D was submitted to the neurosurgical team. Scenario integrated 2D and 3D views of medical images. Visualization was performed by three orthogonal and canonical planes and one 3D window. Orthogonal plane visualized slices of volume and raster images of 3D geometry like fiber bundle. 3D window implemented a computer graphics scene that integrated planes of anatomical images (T1, T2, FLAIR) and 3D geometry (fiber bundle).
Neurosurgeons interacted with Scenario using 2D and 3D navigation tools.
2D tools achieved user to visualize planes following canonical visualization's direction (axial plane moved in superior-inferior direction, sagittal plane in left-right direction, coronal plane in posterior-anterior plane).
3D tools achieved user to select visible objects, to change surface proprieties (color, light reflection, alpha-color) and to navigate 3D scene (rotation, translation and zoom).
Using 3D scenario neurosurgeon could better identify a set of information helpful in order to optimize **surgical approaches** and **trajectories** and to plan subcortical stimulation area.

4.5 *Intraoperative Monitoring*

The issue of subcortical mapping has emerged recently thanks also to the advent of diffusion tractography and functional localization in brain tumor surgery. What matters to the neurosurgeon when removing unhealthy tissue at the subcortical level is to know how far white matter tracts are, in order to avoid permanent deficits. Actually neurosurgeon use different type of subcortical stimulation due to identify fiber bundle intraoperative. The most popular methods applied in neurosurgery introduce variability about *stimuli* (single stimuli vs. short train) and *stimulator* (bipolar vs. monopolar). Today comparison between bipolar vs. monopolar stimulation is on debate and stimulation parameters introduces new variables. Depending on neurosurgeon, neurophysiological technologist and Institute association, different methods can be applied.

In Verona Institute, depending on the type of the surgery, two methodologies were commonly used:

- In **awake surgery** Penfield's Method permitted to identify functional area involved in language tasks. Bipolar probe introduced temporary aphasia on Broca's area (speech arrest or not).
- In **asleep surgery** cortical and subcortical mapping were used to localize motor pathways[Berman *et al.* 2004, Berman *et al.* 2007]. Short

train of stimuli was supplied by monopolar probe eliciting (MEP) from target muscle.

59 of surgical cases used a combination of Neurophysiological monitoring (NM) NeuroNavigation Systems (NS).
In 49 cases MEP signals were measured in target muscle. In 39 of them, MEPS were under 10 mA.

4.6 *Diffusion Weighted Imaging in the follow up*

In Verona Hospital, post-operative imaging could be classified into two main classes by postponed acquisition after surgery.
Early post-operative CT images were acquired few hours after surgery in order to identify hemorrhages.
Late post operative MR images were acquired 30 days after surgery in order to identify residual tumor that help multi-disciplinary neuro-oncological team to define treatments after surgery.
In a set of cases we performed an early MRI acquisition that included the DTI protocol.
In 3 of 94 cases, early post-operative DTI artifacts were introduced by the transitive ischemia and edema's areas.
In 21 of 94 cases late post-operative DTI was performed in order to evaluate the state of surrounding fiber bundles in surgical areas. 13 of 21 cases comparison between pre and post operative DTI showed a retrofit of fibers in changing of shape and size.
The *qualitative* analysis of reshaping was performed using the contro-lateral comparison before and after surgery.
A *quantitative* analysis was difficult caused by different pre-configuration of fiber bundles and surrounding tissues (edema, shape and compression).

Table 4.9. List of 144 patients with lesions in eloquent areas they were submitted to pre-operative DTI tractography

ID	Surgery	Awake	INM	Diagn	Site	Hemisphere	F1	F2	F3	F4	F5	AGE	SEX
1	y		y	Meta.	Post-rolandic	L	CST					52	F
2	y		n	G (IV)	Temporale	L		ARC	IF			65	M
3	n		n	G (IV)	T.I.	L	CST					70	M
4	y		n	G (IV)	T.I.	L		ARC	IF			73	M
5	n		n	G (IV)	Insulare	L	CST					63	M
6	n		n	Cav.	Insulare	L		ARC	IF			22	F
7	y		y	G (IV)	Parietal	L	CST					38	F
8	y		y	Astr.	Parietal	L	CST					37	M
9	y	A	y	Astr.	Temporale	L		ARC				27	M
10	y		y	Glioma	Tronco alto	R	CST					45	M
11	y		y	G (IV)	Fronto-T.I.	L	CST					63	M
12	y		n	G (IV)	Temporale	L		ARC				39	M
13	y		y	Cav.	Parietal	R	CST					38	F
14	y	A	y	G (IV)	F.I.T.	L	CST	ARC				67	M
15	y		y	G (IV)	Rolandic	R	CST					65	M
16	y	A	y	G (IV)	Temporale	L	CST	ARC	IF			58	M
17	y		y	Meta.	Pre-rolandic	R	CST					61	M
18	y		y	Astr.	Pre-rolandic	R	CST					58	M
19	y		y	Glioma	Pre-rolandic	L	CST					49	M
20	y		y	Meta.	Pre-rolandic	R	CST					73	M
21	y		y	Glioma	Pre-rolandic	R	CST					47	F
22	y		y	G (IV)	Pre-rolandic	L	CST	ARC				56	F
23	y		y	G (IV)	Temporale	L	CST	ARC				55	M

continued on the next page

ID	Surgery	Awake	INM	Diagn	Site	Hemisphere	F1	F2	F3	F4	F5	AGE	SEX
24	y		y	G (IV)	Pre-rolandic	L	CST					69	F
25	y		y	G (IV)	Frontale-Broca	L	CST	ARC				56	M
26	y		y	Astr.	Pre-rolandic	R	CST					40	M
27	y	A	y	Other	Temporo-Uncale	L		ARC	IF			41	M
28	n		n	Glioma	Pre-rolandic	R	CST					57	F
29	y		y	G (IV)	Rolandic	R	CST					49	F
30	y	A	y	G (IV)	Temporale	L		ARC	IF			66	M
31	y		y	G (IV)	Rolandic	L	CST					51	M
32	y		n	G (IV)	Temporo-Uncale	L		ARC		UNC		41	M
33	y		y	Other	Cisterne	L	CST					65	M
34	y		y	G (IV)	Rolandic	L	CST					66	M
35	y		y	G (IV)	Temporale	R	CST					58	F
36	y	A	y	G (IV)	Temporale	L		ARC	IF			61	M
37	n		n	G (IV)	Frontal	R	CST					67	M
38	n		n	G (IV)	Rolandic	L	CST					39	F
39	y		y	Astr.	Rolandic	R	CST					31	F
40	y		y	Astr.	T.I.	L	CST	ARC		UNC		51	M
41	n		n	G (IV)	Rolandic	R	CST					66	M
42	y	A	y	G (IV)	Temporale	L		ARC	IF			59	M
43	y	A	y	G (IV)	Rolandic	L	CST	ARC				50	M
44	y		y	Cav.	Ponts	R	CST					38	F
45	y		n	Astr.	Temporale	L		ARC				56	M
46	y		n	G (IV)	Temporale	L		ARC	IF			78	M
47	n		n	G (IV)	Talamico	L	CST					39	F
48	y		y	G (IV)	Temporale	R	CST					73	F

continued on the next page

ID	Surgery	Awake	INM	Diagn	Site	Hemisphere	F1	F2	F3	F4	F5	AGE	SEX
49	y	A	y	Astr.	Frontale	L	CST	ARC				38	F
50	y		n	G (IV)	Temporale	L		ARC				71	M
51	y		y	Cav.	Temporale	L	CST					36	M
52	y		y	G (IV)	Temporale	L	CST	ARC				61	F
53	y		y	Glioma	Rolandic	L	CST					31	M
54	y		y	Other	Intraventr.	R	CST					35	M
55	y		y	Glioma	Post-rolandic	R	CST					10	F
56	y		y	G (IV)	Frontale	L	CST	ARC				51	M
57	y	A	y	G (IV)	Temporale	L	CST	ARC				46	M
58	y		y	G (IV)	Temporale	L	CST	ARC				51	M
59	y		n	G (IV)	Temporale	L		ARC				61	F
60	y		y	G (IV)	Rolandic	L	CST					43	F
61	y	A	y	Glioma	Fronto-T.I.	L			IF	UNC		43	M
62	y	A	y	Astr.	Temporale	L		ARC	IF			41	M
63	n		n	G (IV)	Intraventr.	R	CST					62	M
64	y		y	Cav.	Ponts	R	CST					42	F
65	n		n	G (IV)	Rolandic	R	CST					39	F
66	y		y	G (IV)	Fronto-T.I.	L		ARC	IF			26	F
67	y		y	G (IV)	Fronto-T.I.	L	CST	ARC				53	M
68	y		y	Astr.	Fronto-T.I.	L	CST	ARC				60	M
69	n		n	G (IV)	Talamo	L	CST					63	M
70	y		y	G (IV)	Rolandic	R	CST					59	F
71	y		y	G (IV)	Rolandic	R	CST					51	F
72	y		y	G (IV)	Rolandic	L	CST	ARC				43	M
73	y		y	G (IV)	Rolandic	L	CST					66	F

continued on the next page

ID	Surgery	Awake	INM	Diagn	Site	Hemisphere	F1	F2	F3	F4	F5	AGE	SEX
74	n		n	G (IV)	Rolandic	R	CST					42	M
75	y		n	G (IV)	Temporale	L			IF	UNC		54	M
76	y		y	G (IV)	F.I.T.	L	CST	ARC		UNC		69	M
77	y	A	y	G (IV)	F.I.T.	L	CST	ARC	IF			62	M
78	y		y	G (IV)	F.I.T.	L	CST	ARC				54	M
79	y		y	G (IV)	Rolandic	R	CST					37	F
80	y		y	Astr.	Rolandic	R	CST					7	F
81	y		y	G (IV)	Temporale	L		ARC	IF			46	M
82	n		n	Meta.	Talamico	R	CST					52	F
83	y		y	Astr.	Frontale	L	CST					41	M
84	y		y	Meta.	Rolandic	R	CST					43	F
85	y		y	Cav.	Talamico	L	CST	ARC	IF		OR	14	M
86	y		y	Other	Tronco alto	R	CST					56	F
87	y		y	G (IV)	Temporale	L	CST	ARC	IF	UNC		55	F
88	y		n	G (IV)	Temporale	L		ARC	IF			61	M
89	n		n	Other	Tronco alto	L	CST					62	F
90	y		y	Glioma	Temporale	L	CST	ARC	IF	UNC		53	F
91	y		y	Glioma	Talamo	L	CST		IF	UNC		58	M
92	y		y	Glioma	Rolandic	R	CST					63	M
93	n		n	Cav.	Rolandic	R	CST					39	M
94	y		y	Astr.	F.I.T.	L	CST	ARC	IF			42	M
95	y		y	Cav.	T.I.	L	CST	ARC	IF			30	M
96	n		n	Glioma	Talamo	L	CST					23	F
97	n		n	Glioma	T.I.	R	CST					43	M
98	n		n	G (IV)	P.S.T.	R	CST					52	F

continued on the next page

ID	Surgery	Awake	INM	Diagn	Site	Hemisphere	F1	F2	F3	F4	F5	AGE	SEX
99	n		n	Meta.	Rolandic	R	CST					75	M
100	y		y	Meta.	Rolandic	L	CST					65	F
101	n		n	G (IV)	Rolandic	R	CST					59	F
102	n		n	G (IV)	F.I.T.	L	CST	ARC	IF			53	M
103	n		n	Glioma	F.I.T.	L	CST	ARC	IF			62	F
104	y		y	Astr.	Rolandic	R	CST					49	M
105	y		n	Glioma	Temporale	L			IF			4	F
106	n		n	G (IV)	Rolandic	R	CST					29	M
107	y		n	Cav.	Temporale	R			IF			44	M
108	y		y	Glioma	Rolandic	L	CST	ARC				34	F
109	y	A	y	Astr.	T.I.	L		ARC				41	F
110	n		n	G (IV)	T.I.	L	CST	ARC	IF			65	M
111	y		n	G (IV)	Temporale	L		ARC	IF		OR	62	M
112	y		y	Other	Temporale	L	CST	ARC	IF			23	M
113	y		y	G (IV)	Temporale	R	CST		IF			75	F
114	n		n	Glioma	Rolandic	L	CST					24	M
115	y		y	Astr.	F.I.T.	L	CST	ARC				33	F
116	y		y	Cav.	Rolandic	L	CST					44	F
117	y		y	G (IV)	F.I.T.	L	CST	ARC	IF			67	M
118	n		n	Glioma	Rolandic	R	CST					50	F
119	n		n	Glioma	Rolandic	R	CST					28	M
120	n		n	Glioma	Rolandic	L	CST	ARC				77	F
121	n		n	Glioma	Rolandic	L	CST					65	M
122	n		n	Other	Rolandic	R	CST					56	F
123	y		y	Glioma	F.I.T.	L	CST	ARC				50	M

continued on the next page

ID	Surgery	Awake	INM	Diagn	Site	Hemisphere	F1	F2	F3	F4	F5	AGE	SEX
124	n		n	Cav.	Rolandic	L	CST					38	F
125	y		y	G (IV)	F.I.T.	L	CST	ARC				21	F
126	n		n	Glioma	Temporale	R			IF		OR	30	M
127	n		n	Other	Rolandic	R	CST					50	M
128	n		n	Other	Rolandic	R	CST					50	M
129	n		n	Other	Rolandic	L	CST					50	M
130	n		n	Other	Rolandic	R	CST					50	M
131	n		n	Other	Rolandic	L	CST					50	M
132	n		n	Other	Rolandic	R	CST					50	F
133	n		n	Other	Rolandic	L	CST					50	F
134	n		n	Other	Rolandic	R	CST					30	M
135	n		n	G (IV)	Temporale	L		ARC				59	F
136	n		n	G (IV)	Rolandic	R	CST					50	F
137	n		n	Other	Temporale	L	CST	ARC				28	M
138	n		n	G (IV)	Rolandic	L	CST					50	F
139	n		n	Other	Rolandic	R	CST					41	M
140	n		n	Glioma	Temporale	L	CST	ARC				56	M
141	n		n	Glioma	Temporale	L		ARC				72	M
142	n		n	Glioma	Temporale	L	CST	ARC				31	M
143	n		n	Other	Temporale	R			IF	UNC		38	M
144	n		n	Glioma	Rolandic	R	CST					57	M

5. Results

As discussed before, 144 patients with lesions in eloquent areas were submitted to pre-operative DTI tractography. 94 of 144 were treated surgically. 50 of 144 were elaborated in order to perform clinical evaluations.
We would present five particular cases that show differences between uses of pre-surgical planning.

5.1 *CASE 1*

Surgical Case
Patient: Female 43 years old;
Diagnosis: Glioblastoma (WHO: IV grade, confirmed by histology);
Location: Right Hemisphere, motor area;
Brain Tumor MRI Protocol: T1w, FLAIR, DTI_{high} 32 gradient, 1 B_0 volume and DTI_{medium} 16 gradient, 1 B_0 volume;
MRI scanner: Philips Achieva 3.0 T.
DTI: reconstruction of Cortico-Spinal Tract; **DTI Algorithm**: Interpolated Streamline, the angle threshold is 35 degree;
Intra-operative Technologies: Optical Neuronavigation System, Neuro-Physiological Monitoring and Neuro-Physiological subcortical stimulation;
Figure 5.1

5.2 *CASE 2*

Non-Surgical Case
Patient: Female, 57 years old;
Diagnosis: Glioblastoma (WHO: IV grade);
Location: Right Hemisphere, motor area;
Brain Tumor MRI Protocol: T1w, FLAIR, DTI_{high} 32 gradient, 1 B_0 volume and DTI_{medium} 16 gradient, 1 B_0 volume;
MRI scanner: Philips Achieva 3.0 T.
DTI: reconstruction of Cortico-Spinal Tract;
DTI Algorithm: Interpolated Streamline, the angle threshold is 35 degree;
Neurosurgical Consideration: in this cases surgical treatment of lesion was considered too risky compared to benefits.
Figure 5.2

5.3 *CASE 3*

Surgical Case
Patient: Male, 63 years old;
Diagnosis: Cavernous Malformation ;
Location: Right Hemisphere, temporo-parietal region;
Brain Tumor MRI Protocol: T1w, T2w, FLAIR, DTI_{high} 32 gradient, 1 B_0 volume and DTI_{medium} 16 gradient, 1 B_0 volume;
MRI scanner: Philips Achieva 3.0 T.
DTI: reconstruction of Inferior Front Occipital Fasciculus;
DTI Algorithm: Interpolated Streamline, the angle threshold is 35 degree;
Intra-operative Technologies: Optical Neuronavigation System integrated with Ultrasound Images;
Figure 5.3

5.4 *CASE 4*

Surgical Case
Patient: Male 66 years old;
Diagnosis: Glioblastoma (WHO: IV grade, confirmed by histology);
Location: Right Hemisphere, motor area;
Brain Tumor MRI Protocol: T1w, FLAIR, DTI_{high} 32 gradient, 1 B_0 volume and DTI_{medium} 16 gradient, 1 B_0 volume;
MRI scanner: Philips Achieva 3.0 T.
DTI: reconstruction of Cortico-Spinal Tract;
DTI Algorithm: Interpolated Streamline, the angle threshold is 35 degree;
Intra-operative Technologies: Optical Neuronavigation System, Neuro-Physiological Monitoring and Neuro-Physiological subcortical stimulation;
Figure 5.4

5.5 *CASE 5*

Surgical Case
Patient: Male 66 years old;
Diagnosis: Glioblastoma (WHO: IV grade, confirmed by histology);
Location: Left Hemisphere, temporal area, posterior segment of arcuate fasciculus (parietal-temporal direction) that connect Geschwind and Wernicke areas);
Brain Tumor MRI Protocol: T1w, FLAIR, DTI_{high} 32 gradient, 1 B_0 volume;
MRI scanner: Philips Achieva 3.0 T.
DTI: reconstruction of Arcuate Fascicolus, Inferior front Occipital Fasciculus and Cortico-Spinal Tract;
DTI Algorithm: Interpolated Streamline, the angle threshold is 40 degree;
Intra-operative Technologies: Optical Neuronavigation System, Neuro-Physiological Monitoring and Neuro-Physiological subcortical stimula-

tion;
Clinical Information: the patient presented slight signs of conductive aphasia.
Figure 5.5

5.6 *Illustrations*

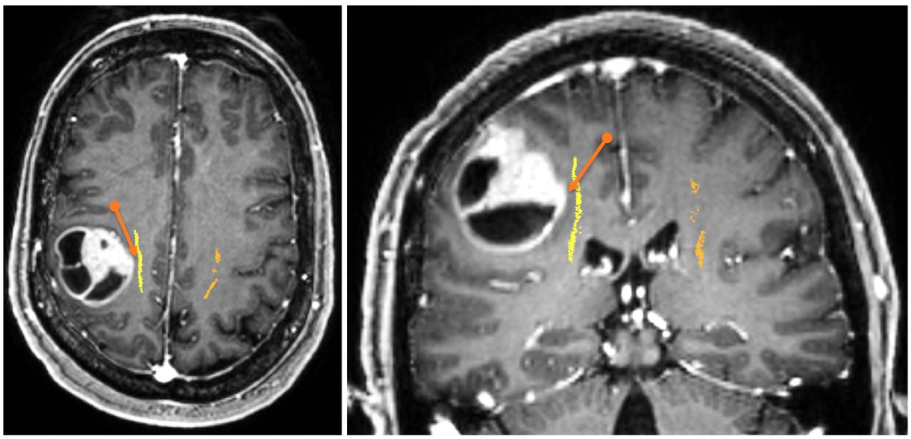

Figure 5.1. CASE 1: surgical case with intraoperative neuromonitoring and intraoperative neuronavigation system. This patient, who presented with slight hemiparesis, had subcortical glioblastoma that was attached to the CST. After a gross complete removal of the lesion the patient developed significant hemiparesis the following day. The patient returned to pre-surgical condition within the 7th day after surgery. Orange arrows show location of MEPs (3mA in LABP).

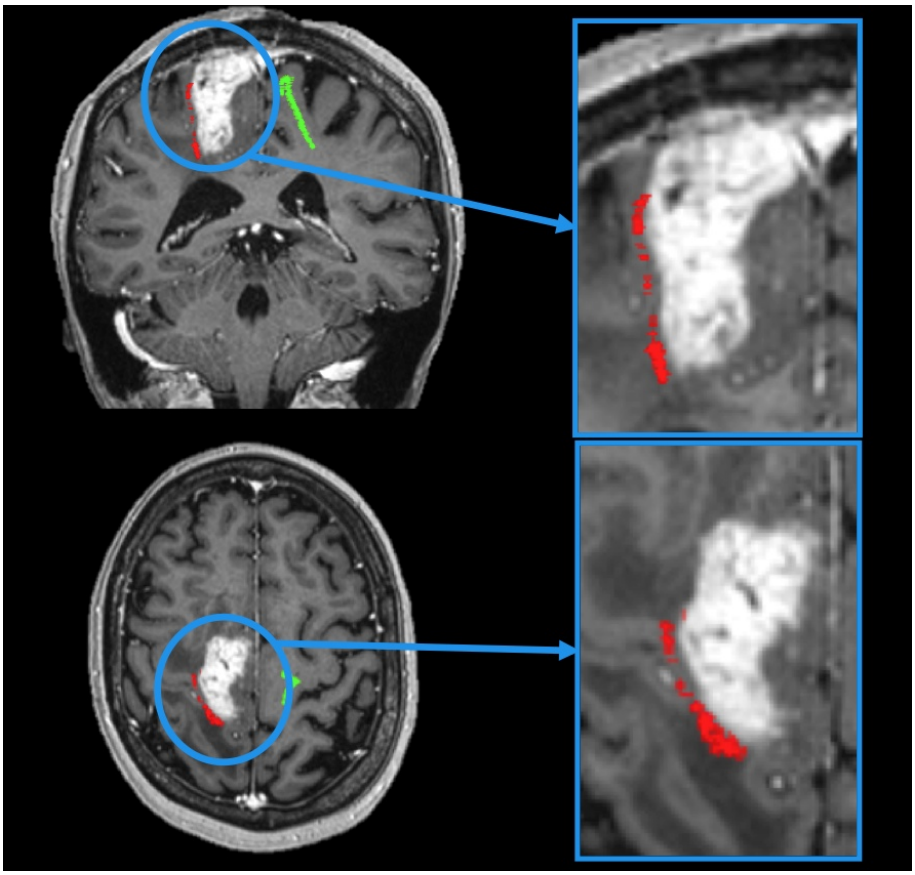

Figure 5.2. CASE 2: non-surgical case. In this cases surgical treatment of lesion was considered too risky compared to benefits. In fact, although the lesion could be easily approached from the vertex, DTI elaboration showed the CST nearly in contact with it along an extensive portion of its surface,making the risk a clinical worsening very high.

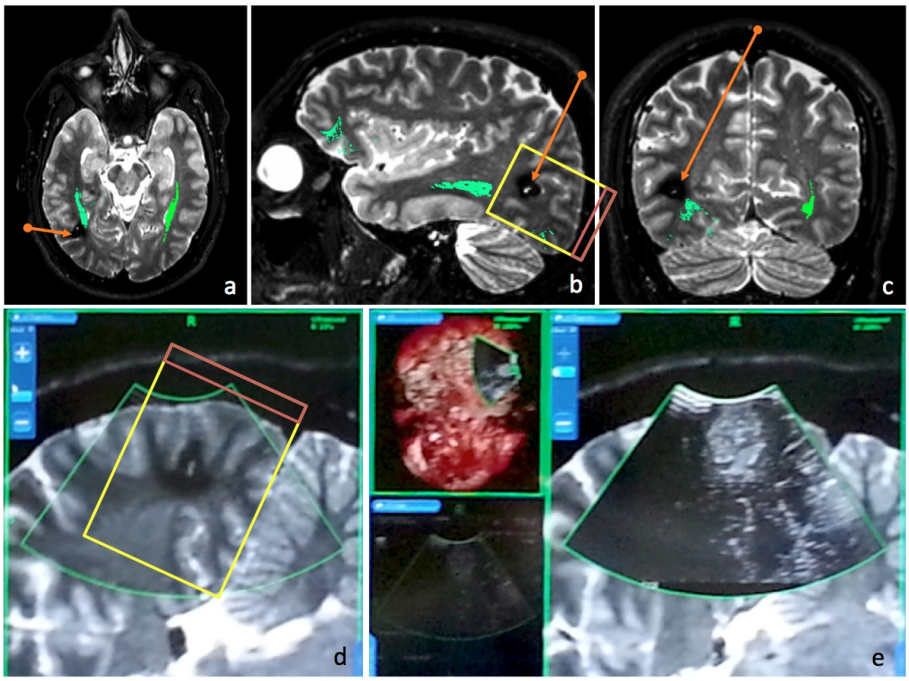

Figure 5.3. CASE 3: surgical case that integrates intraoperative ultrasound images and pre-operative MR-images using neuronavigation system. (**a**), (**b**) and (**c**) show presurgical planning based on IFOF reconstruction and T2w. (**d**) shows intraoperative localization supported by neuronavigation system over MR images. (**e**) shows the same localized area of **d** superimposed to Ultrasound Images.

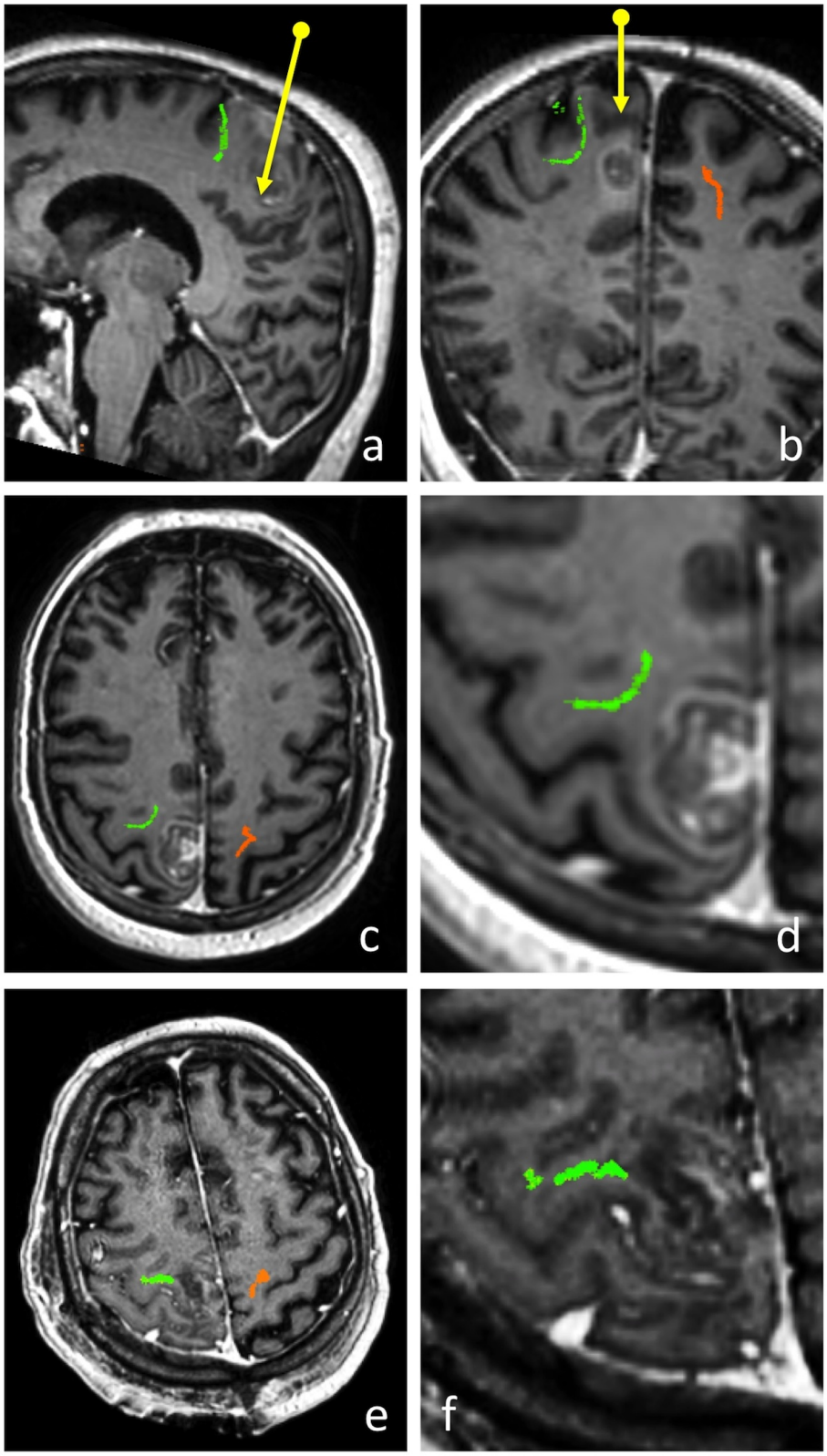

Figure 5.4. CASE 4: surgical case based on pre and post operative DTI.(**a**) and (**b**) show pre-surgical reconstruction of CST. The yellow arrow shows surgical trajectory. (**c**) and (**d**) detail axial view of CST and lesion before surgery. (**e**) and (**f**) detail axial view of CST and lesion after surgery. The patient had positive Neuro-Physiological monitoring and stimulation scores (MEPs: 5mA in LALL an LT

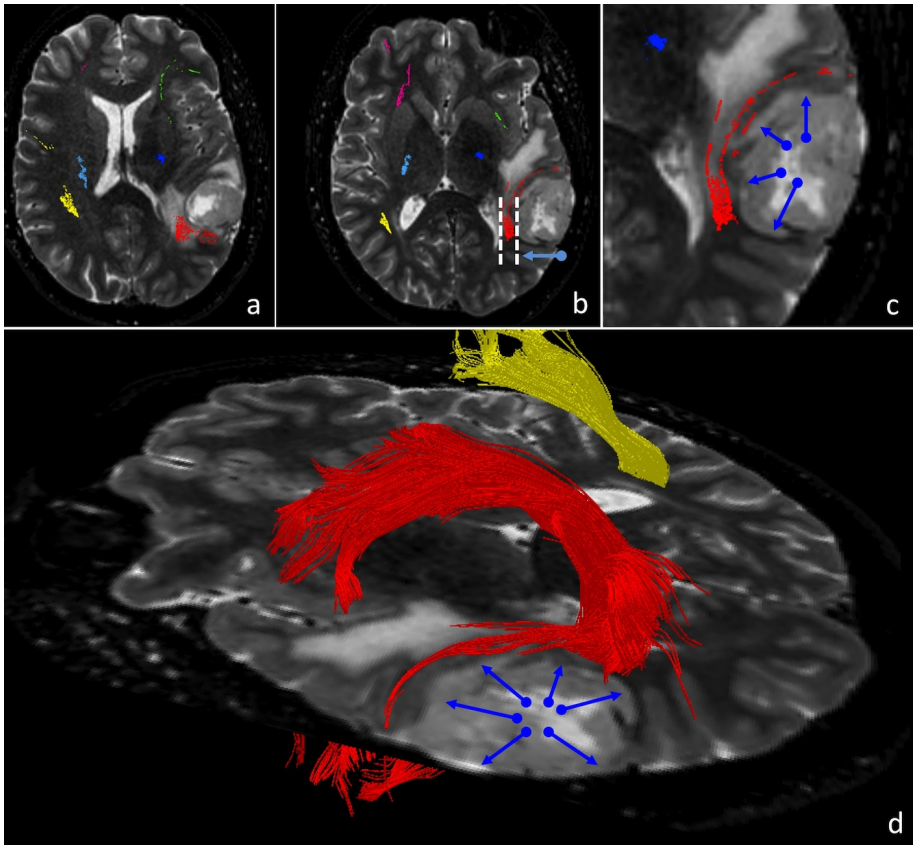

Figure 5.5. CASE 5: surgical case with intraoperative neuromonitoring and intraoperative neuronavigation system (Arcuate Fasciculus). ARC reconstruction shows a displacement highlighted by blue arrows (**c** and (**d**). A gross total removal was performed with no worsening of deficits after surgery. The patient end up scoring better at BADA test within 10 days after surgery, than he had before surgery.

6. Discussion

We have designed and implemented a clinical application grounded in advanced techniques of MRI images. Based on a specific neuroradiological protocol, we have performed a pre-surgical planning in 144 patient affected by brain lesions.
We have implemented an intraoperative methodology due to integrate pre-surgical information in operative room.
We have integrated our results with intraoperative neurophysiological stimulations.
We have performed early and later neuroradiological acquisitions and DTI elaborations due to evaluate state of subcortical pathways around lesion.

Results of the thesis could be discussed in four main categories: the role of *protocols*, the importance of *visualization*, *limits* of techniques, *quantification* and evaluation of quality and identification of future developments.

Protocol is important when different methodologies requires to be joined in one optimal and multimodal vision.
Two kind of protocols have been defined: neuroradiological protocol and processing protocol.
Patient landmarks grounded in neuroradiological protocol need to underline relevant aspects for a neurosurgical treatment of gliomas.
Processing protocol defines a set of steps required to contain artifacts and methodological errors.
Neuroradiological and Processing protocols have been designed to be flexible and compatible with the patient's management. Both protocols are independent by scanner's acquisitions and elaboration as much as possible. Scanner's independence derives by the possibility to use one of three scanners sited in Verona's Hospital.
Sequence's independence is a requirement because it was not finally demonstrated that an higher number of gradients links with a better tractography reconstructions.
In our cases we have observed that a better MR signal could be preferred to the higher angular definitions of diffusion processes.
In surgical cases especially when warped anatomy could introduce artifacts short b-value ($b = 800 \frac{s}{mm^2}$) favorites reconstructions of tracts.

Furthermore, independent processing permits us to change framework's steps in order to test the best set of tools involved in our elaborations such as diffusion estimation, tractograpic reconstructions, image registration and artifact's removal.

Visualization covers a central role in neurosurgical applications.
The main idea has been developed such as a virtualization toolbox that permitted visualization of landmarks in three main stages:

- pre-operative planning that shows anatomical and functional characteristics of brain tissues,
- intra-operative visualization supported by intra-operative localization of subcortical eligible areas for intra-operative stimulation and
- post-operative evaluations based on images and clinical notices (deficits).

Compatibility between these stages permit to identify effects of surgery in connection with deficits and their anatomical correspondences.

Well-known uncertainties of diffusion technologies characterize complexity of applications in neurosurgery.
First, subcortical pathways extraction has been conditioned by strong assumptions like modeling of diffusion proprieties, physics of diffusion phenomena and MRI proprieties to detect phenomena.
Second, in tumor studies subcortical pathways could be affected by "surrounding" artifacts like edema that could meddled in the diffusion analysis, from acquisition to elaborations.
Finally, intra-operative localization systems based on virtualization of brain tissues have been biased by the lack of brain shift modeling.
This framework grounded in renewabilities, supports changes by novel and reliable methods in neurosurgical application.

Quantifications could be considered one of the most important field of research in diffusion analysis.
Analysis of diffusion data has been developed by processing diffusion outputs like 2D volumes and 3D Geometry.
Quantification in diffusion analysis was relevant in presence of a multi-subject experiments when anatomy wasn't drastically warped by pathology.
Pattern Recognition approaches could be applied in order to identify small alteration of MR signals.
In presence of tumor that drastically distort anatomy quantification analysis was difficult because it was challenging to identify comparable patterns.
Furthermore it has been performing a qualitative analysis of contro-lateral reconstruction due to identify displacements and compressions.
Reshaping observation of fiber bundles after surgery could help to identify glioma's behavior without guarantee of clinical follow up.
This is caused by unknown modeling of glioma's characteristics.

7. Conclusion

The complex communication system of the brain can be studied with Diffusion Tensor Imaging, a capable MRI method that characterizes the diffusion behavior of water in a tissue. DTI has become a relevant field of research since it provides visual information of white matter fiber paths.
Today the DTI and the standard anatomical MR images occur in pre-surgical evaluation in order to plan surgical treatment. The aim of tractography is to obtain a white matter pathways map based on the anatomical changes in patient. Despite the potential of in-vivo tractography, there are still many factors that make its application difficult, especially in daily clinical practice.

DT-tractography is limited by **technical and methodological** factors that can not permit to distinguish anatomical specificities of the detailled function of brain.
For example motor representation of pathways based on DTI can not be considered huge and specific like motor and sensitive homunculus representations.
Beside, DT-tractography helps to understand the essential shape (skeleton) of subcortical pathways; this information is useful to plan surgical treatment, especially when tumor growing significantly changes relation between healthy and pathological tissues. Bulk masses can displace fiber bundle without clues about the shape and the site.
Information about fiber bundle can be useful to plan surgical strategies and in particular the entering point, the surgical trajectory and no-way areas.
In this thesis we have focused our interest in single tensor modeling in order to be compatible with MRI scanner sequences. Compared with other MRI sequences, DWI and DTI imaging are conditioned by low Signal to Noise Ratio (SNR).
This means that artifacts characterize reconstructions based on diffusion MRI sensitization. Despite the anatomical reliability of probabilistic approaches, especially in presence of complex fiber configurations, we widely use deterministic algorithms. **Probabilistic approaches** are limited by processing requirements and field of application. In presence of big tumor bulk we observed that probabilistic approach trends to introduced errors in diffusion estimations. The **Interpolated Streamline** is generally preferred to other deterministic algorithms because its

estimation and reconstruction are less susceptible to local abnormalities derived from diffusion tensor calculation.
Some artifacts can be corrected applying software correction (multi volumes registration, eddy current correction).
Despite corrections, sophisticated post-processing algorithm applied to low SNR images can produce unrealistic representation of pathways.
The interpolator in streamline model of tensors reconstructs pathways considering that local variation of tensor depend on surrounding anisotropic tensors. The streamline interpolator highlights the *global behavior of fiber shape* and de-emphasize the local differences in anatomy.
In presence of big tumor bulk, approaches based on tensor interpolation are able to obtain a realistic skeleton of fiber shape. In presence of small and infiltrative tumor, approaches based on sophisticated analysis of tensors are helpful in order to obtain specific information of *local differences in anatomy*.
DTI application in neurosurgery focuses to obtain a realistic information about anatomical landmarks involved in brain functionalities. Interaction between tumor and fiber bundle characterizes the choice of the algorithm.
Global and local requirements of DTI reconstructions depend on relationship between lesion and pathways, type of lesion and surrounding tissue characteristics.

Today, **quality evaluation** in DTI reconstruction is not standardize. Quantification of fibers characteristics are conditioned by different factors (acquisition and elaboration factors).
In this thesis we evaluate quality of reconstruction by superimposing anatomical pathways to high resolution images of the brain. Comparison between healthy and pathological hemisphere highlights displacements and distortions.
In some cases hypothesis of *neuroplasticity* are supported by deficit evaluation (especially when lesion is a low grade glioma and it sites in motor areas) [Jenkins *et al.* 2010b, Jenkins *et al.* 2010a, Sokki *et al.* 2012].
Anyway DTI is a essential tool in pre-surgical planning applications despite artifacts and uncertainty about workflow processing.
Anatomical considerations extracted by analysis of DT-images help to understand correlation between deficits before and after surgery. DTI introduces a set of anatomical landmarks that help neurosurgeon pre and intra-operatively. Despite the capability to detect small anatomical differences in pathways configurations, DTI can show and explain how brain tumor can warp and can change anatomy.

The role of **pre-surgical planning** is to superimpose multimodal medical images of the same tissues in order to upgrade diagnosis information and to obtain relevant references for surgery. In this thesis we have focused our interest in acquisition and elaboration protocol definitions in order to reduce practical difficulties in a daily clinical application. We have introduced an easy-to-use pre-surgical DTI visualization integrated with standard anatomical MR sequences.

Information about subcortical pathways meet additional information about tumor classification, infiltration characteristics and in some cases eloquent cortical areas in order to help neurosurgeon to plan a surgery. Based on rigid registration we superimpose different tissue information from MR-images. We combined volumes and geometries with an useful 3D and 2D visualizations.

Based on **Neuronavigation System** requirement, we have implemented a fiber bundle wrapper that exports the pre-surgical scenario into an intra-operative visualization tool.
Pre-surgical scenario can be interactive by the use of neuronavigation system. Localization tool permits to identify tissues during the surgery and test its functionality with a neuro-physiological monitoring and stimulation. Interaction between these technologies helps neurosurgeon investigate feedback intra-operatively. DTI validation is performed by the intra-operative localization of fiber bundel and the intra-operative subcortical stimulation (neuro-physiological techniques).

Despite the integration between pre and intra-operative analysis of WM pathways, virtualization and neuronavigation of patient data can be inaccurately. **Brain shift** is the main factor that reduce inaccuracy during a brain surgery. In a few cases we proposed an intra-operative estimation of brain shift based on **ultrasound images**. Supported by probe-localizer we integrate the neuronavigation system with ultrasound images and we navigated US images superimposed on pre-surgical images of the patient. We try to localize low grade gliomas, metastasis and cavernous malformations but the use was the discouraged by inexperience in reading US images.

Finally we have proposed the use of additional DTI acquisition in the **post-operative** evaluation in order to study changes of fiber bundles.
The post-operative DTI is performed in two modalities after surgery: early post-operative DTI were acquired few hours after surgery and late post operative DTI were acquired 30 days after surgery.
The early post-operative DTI is often conditioned by the transitive ischemia and huge edema's areas.
The later post-operative DTI helps neurosurgeon to evaluate the state of surrounding fiber bundles in surgical areas. Comparison between pre and later post-operative DTI showed a retrofit of fibers in changing of shape and size.

Our aim has been accomplished by the develop of a framework composed by **MR-images processing toolboxes** that support neurosurgeon to analyse surgical strategies. Today DTI is considered an useful set of techniques that can be integrated in neurosurgical application.

7.1 *The Future*

Our future work will be focused on the newer diffusion models that beat the limitations of tensor-based tractographic models. The main advanced factors will permit to acquire data with more resolution, to reduce image acquisition time, to reduce noise and distortion effects, to improve data visualization and to validate digital fiber bundle extractions.

The aim of future work in tractography is to obtain a white matter pathways map of the patient that details global and local differences with an high corresponde of reconstructed pathways with specific function of the brain.
Future developments will take into account DWI spatial resolution super-sampling and high-angular resolution descriptors of fiber configurations [Manjón *et al.* 2010]. The multi-tensor modeling can be calculated using a complex estimation of additional eigenvectors derived from D-matrix solution problem. The multi-tensor estimation can be supported by calculation of D-matrix using a multi-b-value sequence.
Multi-eigenvalue estimation of diffusion modeling can discern complex fiber configuration (such as crossing and kissing fibers).

Diffusion Spectrum Imaging (DSI) allows to calculate an high angular measurements of the diffusion probability density function. The main advantages of DSI is that it can resolve complex intra-voxel distribution of fiber orientation [Takahashi *et al.* 2010].
Today the main disadvantages of DSI is given by the acquisition requirement which is incompatible with neurosurgical application.
Q-ball imaging (Q-ball) is based on high angular resolution diffusion imaging (HARDI). Q-ball can resolve intra-voxel distribution of fiber orientation but anatomical accuracy is not guaranteed and it requires validations [Berman *et al.* 2008, Descoteaux *et al.* 2009,Fernandez-Miranda *et al.* 2012, Schultz and Seidel 2008, Tournier *et al.* 2004, Tournier *et al.* 2008].
Finally, Spherical Deconvolution (SD) is to assume that white matter share identical diffusion characteristics. The diffusion weighted signal attenuation measured can be expressed as the convolution over the sphere of a response function with a specific orientation distribution function [Tournier *et al.* 2004, Tournier *et al.* 2008]. Today the main disadvantages of SD is given by its susceptibility to noise which often introduces peaks in orientation distribution function.

Despite the anatomical quality of fiber definitions, clinical application of these novel techniques are not spread. Additional future development of my thesis can be the development of physical and software phantom. Phantoms can help to identify recurring artifacts caused by software hardware settings. Furthermore phantoms can help to tune parameters during fiber reconstruction and can help to understand limits of different algorithm implementations in order to identify the

preferable field of application in the huge set of diffusion techniques.

Finally a future development of my thesis can be focused on intra-operative quantification of shift based on Ultrasound Images. As discussed before, the main limitation of intra-operative application of US depends on inexperience in reading US images. Automatic segmentation of brain tissues based on US images can help to guide the steering of US in finding helpful anatomical landmarks intra-operatively.

List of Tables

List of Figures

Bibliography

Agrawal, Abhishek, Josef P Kapfhammer, Annetrudi Kress, Hermann Wichers, Aman Deep, William Feindel, Volker K H Sonntag, Robert F Spetzler, and Mark C Preul

2011 'Josef Klingler's models of white matter tracts: influences on neuroanatomy, neurosurgery, and neuroimaging', *Neurosurgery*, 69, 2 (Aug. 2011), PMID: 21368687, 238–252; discussion 252–254, ISSN: 1524-4040, DOI: 10.1227/NEU.0b013e318214ab79.

Alexander, Andrew L, Jee Eun Lee, Mariana Lazar, and Aaron S Field

2007 'Diffusion tensor imaging of the brain', *Neurotherapeutics: the journal of the American Society for Experimental NeuroTherapeutics*, 4, 3 (July 2007), PMID: 17599699 PMCID: PMC2041910, pp. 316–329, ISSN: 1933-7213, DOI: 10.1016/j.nurt.2007.05.011.

Artzi, Moran, Orna Aizenstein, Tali Jonas-Kimchi, Vicki Myers, Hen Hallevi, and Dafna Ben Bashat

2013 'FLAIR lesion segmentation: application in patients with brain tumors and acute ischemic stroke', *European journal of radiology*, 82, 9 (Sept. 2013), PMID: 23796882, pp. 1512–1518, ISSN: 1872-7727, DOI: 10.1016/j.ejrad.2013.05.029.

Baars, Bernard J. and Nicole M. Gage

2013 *Fundamentals of Cognitive Neuroscience: A Beginner's Guide*, Academic Press, 475 pp., ISBN: 9780124158054.

Baselice, Fabio, Giampaolo Ferraioli, and Aymen Shabou

2010 'Field map reconstruction in magnetic resonance imaging using Bayesian estimation', *Sensors (Basel, Switzerland)*, 10, 1, PMID: 22315539 PMCID: PMC3270840, pp. 266–279, ISSN: 1424-8220, DOI: 10.3390/s100100266.

Basser, P. J., J. Mattiello, and D. LeBihan

1994 'MR diffusion tensor spectroscopy and imaging', *Biophysical Journal*, 66, 1, pp. 259–267, ISSN: 0006-3495, DOI: 10.1016/S0006-3495(94)80775-1, http://www.sciencedirect.com/science/article/pii/S0006349594807751 (visited on 02/20/2014).

Beaulieu, Christian

2002 'The basis of anisotropic water diffusion in the nervous system - a technical review', *NMR in biomedicine*, 15, 7 (Dec. 2002), PMID: 12489094, pp. 435–455, ISSN: 0952-3480, DOI: 10.1002/nbm.782.

Behrens, T E J, M W Woolrich, M Jenkinson, H Johansen-Berg, R G Nunes, S Clare, P M Matthews, J M Brady, and S M Smith

2003 'Characterization and propagation of uncertainty in diffusion-weighted MR imaging', *Magnetic resonance in medicine: official journal of the Society of Magnetic Resonance in Medicine / Society of Magnetic Resonance in Medicine*, 50, 5 (Nov. 2003), PMID: 14587019, pp. 1077–1088, ISSN: 0740-3194, DOI: 10.1002/mrm.10609.

Behrens, T E J, H Johansen Berg, S Jbabdi, M F S Rushworth, and M W Woolrich

2007 'Probabilistic diffusion tractography with multiple fibre orientations: What can we gain?', *NeuroImage*, 34, 1, PMID: 17070705, pp. 144–155, ISSN: 1053-8119, DOI: 10.1016/j.neuroimage.2006.09.018.

Bello, Lorenzo, Anna Gambini, Antonella Castellano, Giorgio Carrabba, Francesco Acerbi, Enrica Fava, Carlo Giussani, Marcello Cadioli, Valeria Blasi, Alessandra Casarotti, Costanza Papagno, Arun K Gupta, Sergio Gaini, Giuseppe Scotti, and Andrea Falini

2008 'Motor and language DTI Fiber Tracking combined with intraoperative subcortical mapping for surgical removal of gliomas', *NeuroImage*, 39, 1, PMID: 17911032, pp. 369–382, ISSN: 1053-8119, DOI: 10.1016/j.neuroimage.2007.08.031.

Berman, Jeffrey I, Mitchel S Berger, Pratik Mukherjee, and Roland G Henry

2004 'Diffusion-tensor imaging-guided tracking of fibers of the pyramidal tract combined with intraoperative cortical stimulation mapping in patients with gliomas', *Journal of neurosurgery*, 101, 1 (July 2004), PMID: 15255253, pp. 66–72, ISSN: 0022-3085, DOI: 10.3171/jns.2004.101.1.0066.

Berman, Jeffrey I, Mitchel S Berger, Sung Won Chung, Srikantan S Nagarajan, and Roland G Henry

2007 'Accuracy of diffusion tensor magnetic resonance imaging tractography assessed using intraoperative subcortical stimulation mapping and magnetic source imaging', *Journal of neurosurgery*, 107, 3 (Sept. 2007), PMID: 17886545, pp. 488–494, ISSN: 0022-3085, DOI: 10.3171/JNS-07/09/0488.

Berman, Jeffrey I, SungWon Chung, Pratik Mukherjee, Christopher P Hess, Eric T Han, and Roland G Henry

2008 'Probabilistic streamline q-ball tractography using the residual bootstrap', *NeuroImage*, 39, 1, PMID: 17911030, pp. 215–222, ISSN: 1053-8119, DOI: 10.1016/j.neuroimage.2007.08.021.

Bertani, Giulio, Enrica Fava, Giuseppe Casaceli, Giorgio Carrabba, Alessandra Casarotti, Costanza Papagno, Antonella Castellano, Andrea Falini, Sergio M Gaini, and Lorenzo Bello

2009 'Intraoperative mapping and monitoring of brain functions for the resection of low-grade gliomas: technical considerations', *Neurosurgical focus*, 27, 4 (Oct. 2009), PMID: 19795953, E4, ISSN: 1092-0684, DOI: 10.3171/2009.8.FOCUS09137.

Blits, Kathleen C.

1999 'Aristotle: Form, function, and comparative anatomy', *The Anatomical Record*, 257, 2, 58–63, ISSN: 1097-0185, DOI: 10.1002/(SICI)1097-0185(19990415)257:2<58::AID-AR6>3.0.CO;2-I, http://onlinelibrary.wiley.com/doi/10.1002/(SICI)1097-0185(19990415)257:2<58::AID-AR6>3.0.CO;2-I/abstract (visited on 02/20/2014).

Bodammer, Nils, Jörn Kaufmann, Martin Kanowski, and Claus Tempelmann

2004 'Eddy current correction in diffusion-weighted imaging using pairs of images acquired with opposite diffusion gradient polarity', *Magnetic Resonance in Medicine*, 51, 1, 188–193, ISSN: 1522-2594, DOI: 10.1002/mrm.10690, http://onlinelibrary.wiley.com/doi/10.1002/mrm.10690/abstract (visited on 02/03/2014).

Castellano, Antonella, Lorenzo Bello, Caterina Michelozzi, Marcello Gallucci, Enrica Fava, Antonella Iadanza, Marco Riva, Giuseppe Casaceli, and Andrea Falini

2012 'Role of diffusion tensor magnetic resonance tractography in predicting the extent of resection in glioma surgery', *Neuro-oncology*, 14, 2 (Feb. 2012), PMID: 22015596 PMCID: PMC3266379, pp. 192–202, ISSN: 1523-5866, DOI: 10.1093/neuonc/nor188.

Catani, Marco and Dominic H Ffytche

2010 'New section: Cortex Clinical Neuroanatomy', *Cortex; a journal devoted to the study of the nervous system and behavior*, 46, 1, PMID: 19409542, p. 1, ISSN: 1973-8102, DOI: 10.1016/j.cortex.2009.03.009.

Catani, Marco and Dominic H ffytche

2010 'On 'the study of the nervous system and behaviour'', *Cortex; a journal devoted to the study of the nervous system and behavior*, 46, 1, PMID: 19524888, pp. 106–109, ISSN: 1973-8102, DOI: 10.1016/j.cortex.2009.03.012.

Catani, Marco and Marsel Mesulam

2008 'The arcuate fasciculus and the disconnection theme in language and aphasia: history and current state', *Cortex; a journal devoted to the study of the nervous system and behavior*, 44, 8 (Sept. 2008), PMID: 18614162 PMCID: PMC2740371, pp. 953–961, ISSN: 0010-9452, DOI: 10.1016/j.cortex.2008.04.002.

Catani, Marco and Michel Thiebaut de Schotten

2008 'A diffusion tensor imaging tractography atlas for virtual in vivo dissections', *Cortex; a journal devoted to the study of the nervous system and behavior*, 44, 8 (Sept. 2008), PMID: 18619589, pp. 1105–1132, ISSN: 0010-9452, DOI: 10.1016/j.cortex.2008.05.004.

Catani, Marco, Robert J Howard, Sinisa Pajevic, and Derek K Jones

2002 'Virtual in vivo interactive dissection of white matter fasciculi in the human brain', *NeuroImage*, 17, 1 (Sept. 2002), PMID: 12482069, pp. 77–94, ISSN: 1053-8119.

Catani, Marco, Derek K Jones, Rosario Donato, and Dominic H Ffytche

2003 'Occipito-temporal connections in the human brain', *Brain: a journal of neurology*, 126 (Pt 9Sept. 2003), PMID: 12821517, pp. 2093–2107, ISSN: 0006-8950, DOI: 10.1093/brain/awg203.

Catani, Marco, Derek K Jones, and Dominic H ffytche

2005 'Perisylvian language networks of the human brain', *Annals of neurology*, 57, 1, PMID: 15597383, pp. 8–16, ISSN: 0364-5134, DOI: 10.1002/ana.20319.

Catani, Marco, Flavio Dell'acqua, Alberto Bizzi, Stephanie J Forkel, Steve C Williams, Andrew Simmons, Declan G Murphy, and Michel Thiebaut de Schotten

2012a 'Beyond cortical localization in clinico-anatomical correlation', *Cortex; a journal devoted to the study of the nervous system and behavior*, 48, 10 (Dec. 2012), PMID: 22995574, pp. 1262–1287, ISSN: 1973-8102, DOI: 10.1016/j.cortex.2012.07.001.

Catani, Marco, Flavio Dell'acqua, Francesco Vergani, Farah Malik, Harry Hodge, Prasun Roy, Romain Valabregue, and Michel Thiebaut de Schotten

2012b 'Short frontal lobe connections of the human brain', *Cortex; a journal devoted to the study of the nervous system and behavior*, 48, 2 (Feb. 2012), PMID: 22209688, pp. 273–291, ISSN: 1973-8102, DOI: 10.1016/j.cortex.2011.12.001.

Chen, Xiaolei, Daniel Weigel, Oliver Ganslandt, Rudolf Fahlbusch, Michael Buchfelder, and Christopher Nimsky

2007 'Diffusion tensor-based fiber tracking and intraoperative neuronavigation for the resection of a brainstem cavernous angioma', *Surgical neurology*, 68, 3 (Sept. 2007), PMID: 17719968, 285–291; discussion 291, ISSN: 0090-3019, DOI: 10.1016/j.surneu.2007.05.005.

Chowdhury, Forhad, Mohammod Haque, Mainul Sarkar, Shamim Ara, and Mohammod Islam

2010 'White fiber dissection of brain; the internal capsule: a cadaveric study', *Turkish neurosurgery*, 20, 3 (July 2010), PMID: 20669103, pp. 314–322, ISSN: 1019-5149, DOI: 10.5137/1019-5149.JTN.3052-10.2.

Chuang, Nelson, Susumu Mori, Akira Yamamoto, Hangyi Jiang, Xin Ye, Xin Xu, Linda J Richards, Jeremy Nathans, Michael I Miller, Arthur W Toga, Richard L Sidman, and Jiangyang Zhang

2011 'An MRI-based atlas and database of the developing mouse brain', *NeuroImage*, 54, 1, PMID: 20656042 PMCID: PMC2962762, pp. 80–89, ISSN: 1095-9572, DOI: 10.1016/j.neuroimage.2010.07.043.

Ciccarelli, O, T E Behrens, D R Altmann, R W Orrell, R S Howard, H Johansen-Berg, D H Miller, P M Matthews, and A J Thompson

2006 'Probabilistic diffusion tractography: a potential tool to assess the rate of disease progression in amyotrophic lateral sclerosis', *Brain: a journal of neurology*, 129 (Pt 7July 2006), PMID: 16672290, pp. 1859–1871, ISSN: 1460-2156, DOI: 10.1093/brain/awl100.

Clark, Chris A, Thomas R Barrick, Mary M Murphy, and B Anthony Bell

2003 'White matter fiber tracking in patients with space-occupying lesions of the brain: a new technique for neurosurgical planning?', *NeuroImage*, 20, 3 (Nov. 2003), PMID: 14642471, pp. 1601–1608, ISSN: 1053-8119.

Close, Thomas G, Jacques-Donald Tournier, Fernando Calamante, Leigh A Johnston, Iven Mareels, and Alan Connelly

2009 'A software tool to generate simulated white matter structures for the assessment of fibre-tracking algorithms', *NeuroImage*, 47, 4 (Oct. 1, 2009), PMID: 19361565, pp. 1288–1300, ISSN: 1095-9572, DOI: 10.1016/j.neuroimage.2009.03.077.

Dale, A M, B Fischl, and M I Sereno

1999 'Cortical surface-based analysis. I. Segmentation and surface reconstruction', *NeuroImage*, 9, 2 (Feb. 1999), PMID: 9931268, pp. 179–194, ISSN: 1053-8119, DOI: 10.1006/nimg.1998.0395.

D'Andrea, Giancarlo, Albina Angelini, Andrea Romano, Antonio Di Lauro, Giovanni Sessa, Alessandro Bozzao, and Luigi Ferrante

2012 'Intraoperative DTI and brain mapping for surgery of neoplasm of the motor cortex and the corticospinal tract: our protocol and series in BrainSUITE', *Neurosurgical review*, 35, 3 (July 2012), PMID: 22370809, 401–412; discussion 412, ISSN: 1437-2320, DOI: 10.1007/s10143-012-0373-6.

Dargi, F, M A Oghabian, A Ahmadian, H Zadeh, M Zarei, and A Boroomand

2007 'Modified fast marching tractography algorithm and its ability to detect fibre crossing', *Conference proceedings: ... Annual International Conference of the IEEE Engineering in Medicine and Biology Society. IEEE Engineering in Medicine and Biology Society. Conference*, 2007, PMID: 18001954, pp. 319–322, ISSN: 1557-170X, DOI: 10.1109/IEMBS.2007.4352288.

Deletis, V and F Sala

2001 'The role of intraoperative neurophysiology in the protection or documentation of surgically induced injury to the spinal cord', *Annals of the New York Academy of Sciences*, 939 (June 2001), PMID: 11462765, pp. 137–144, ISSN: 0077-8923.

Deletis, Vedran and Francesco Sala

2008 'Intraoperative neurophysiological monitoring of the spinal cord during spinal cord and spine surgery: a review focus on the corticospinal tracts', *Clinical neurophysiology: official journal of the International Federation of Clinical Neurophysiology*, 119, 2 (Feb. 2008), PMID: 18053764, pp. 248–264, ISSN: 1388-2457, DOI: 10.1016/j.clinph.2007.09.135.

Descoteaux, Maxime, Rachid Deriche, Thomas R Knösche, and Alfred Anwander

2009 'Deterministic and probabilistic tractography based on complex fibre orientation distributions', *IEEE transactions on medical imaging*, 28, 2 (Feb. 2009), PMID: 19188114, pp. 269–286, ISSN: 1558-254X, DOI: 10.1109/TMI.2008.2004424.

Ebeling, U. and D. v Cramon

1992 'Topography of the uncinate fascicle and adjacent temporal fiber tracts', *Acta Neurochirurgica*, 115, 3 (Sept. 1, 1992), pp. 143–148, ISSN: 0001-6268, 0942-0940, DOI: 10.1007/BF01406373, http://link.springer.com/article/10.1007/BF01406373 (visited on 02/03/2014).

Ebeling, U and H J Reulen

1988 'Neurosurgical topography of the optic radiation in the temporal lobe', *Acta neurochirurgica*, 92, 1, PMID: 3407471, pp. 29–36, ISSN: 0001-6268.

Epelbaum, Stéphane, Philippe Pinel, Raphael Gaillard, Christine Delmaire, Muriel Perrin, Sophie Dupont, Stanislas Dehaene, and Laurent Cohen

2008 'Pure alexia as a disconnection syndrome: new diffusion imaging evidence for an old concept', *Cortex; a journal devoted to the study of the nervous system and behavior*, 44, 8 (Sept. 2008), PMID: 18586235, pp. 962–974, ISSN: 0010-9452, DOI: 10.1016/j.cortex.2008.05.003.

Fernandez-Miranda, Juan C, Sudhir Pathak, Johnathan Engh, Kevin Jarbo, Timothy Verstynen, Fang-Cheng Yeh, Yibao Wang, Arlan Mintz, Fernando Boada, Walter Schneider, and Robert Friedlander

2012 'High-definition fiber tractography of the human brain: neuroanatomical validation and neurosurgical applications', *Neurosurgery*, 71, 2 (Aug. 2012), PMID: 22513841, pp. 430–453, ISSN: 1524-4040, DOI: 10.1227/NEU.0b013e3182592faa.

Fountas, Kostas N and Eftychia Z Kapsalaki

2005 'Volumetric assessment of glioma removal by intraoperative high-field magnetic resonance imaging', *Neurosurgery*, 56, 5 (May 2005), PMID: 15912601, E1166; author reply E1166, ISSN: 1524-4040.

Friman, Ola, Gunnar Farnebäck, and Carl-Fredrik Westin

2006 'A Bayesian approach for stochastic white matter tractography', *IEEE transactions on medical imaging*, 25, 8 (Aug. 2006), PMID: 16894991, pp. 965–978, ISSN: 0278-0062.

Gerstner, Elizabeth R, Poe-Jou Chen, Patrick Y Wen, Rakesh K Jain, Tracy T Batchelor, and Gregory Sorensen

2010 'Infiltrative patterns of glioblastoma spread detected via diffusion MRI after treatment with cediranib', *Neuro-oncology*, 12, 5 (May 2010), PMID: 20406897 PMCID: PMC2940624, pp. 466–472, ISSN: 1523-5866, DOI: 10.1093/neuonc/nop051.

Golby, Alexandra J, Gordon Kindlmann, Isaiah Norton, Alexander Yarmarkovich, Steven Pieper, and Ron Kikinis

2011 'Interactive diffusion tensor tractography visualization for neurosurgical planning', *Neurosurgery*, 68, 2 (Feb. 2011), PMID: 21135713 PMCID: PMC3112275, pp. 496–505, ISSN: 1524-4040, DOI: 10.1227/NEU.0b013e3182061ebb.

González-Darder, José M, Pablo González-López, Fernando Talamantes, Vicent Quilis, Victoria Cortés, Guillermo García-March, and Pedro Roldán

2010 'Multimodal navigation in the functional microsurgical resection of intrinsic brain tumors located in eloquent motor areas: role of tractography', *Neurosurgical focus*, 28, 2 (Feb. 2010), PMID: 20121440, E5, ISSN: 1092-0684, DOI: 10.3171/2009.11.FOCUS09234.

Goodlett, Casey B, P Thomas Fletcher, John H Gilmore, and Guido Gerig

2009 'Group analysis of DTI fiber tract statistics with application to neurodevelopment', *NeuroImage*, 45, 1 (Mar. 2009), PMID: 19059345 PMCID: PMC2727755, S133–142, ISSN: 1095-9572, DOI: 10.1016/j.neuroimage.2008.10.060.

Hageman, Nathan S, Arthur W Toga, Katherine L Narr, and David W Shattuck

2009 'A diffusion tensor imaging tractography algorithm based on Navier-Stokes fluid mechanics', *IEEE transactions on medical imaging*, 28, 3 (Mar. 2009), PMID: 19244007 PMCID: PMC2770434, pp. 348–360, ISSN: 1558-254X, DOI: 10.1109/TMI.2008.2004403.

Hayashi, Yutaka, Masashi Kinoshita, Mitsutoshi Nakada, and Jun-ichiro Hamada

2012 'Correlation between language function and the left arcuate fasciculus detected by diffusion tensor imaging tractography after brain tumor surgery', *Journal of neurosurgery*, 117, 5 (Nov. 2012), PMID: 22937935, pp. 839–843, ISSN: 1933-0693, DOI: 10.3171/2012.8.JNS12348.

Henry, Roland G, Jeffrey I Berman, Srikantan S Nagarajan, Pratik Mukherjee, and Mitchel S Berger

2004 'Subcortical pathways serving cortical language sites: initial experience with diffusion tensor imaging fiber tracking combined with intraoperative language mapping', *NeuroImage*, 21, 2 (Feb. 2004), PMID: 14980564, pp. 616–622, ISSN: 1053-8119, DOI: 10.1016/j.neuroimage.2003.09.047.

Herweh, C, M Akbar, M Wengenroth, M Blatow, J Mair-Walther, N Rehbein, E Nennig, J P Schenk, S Heiland, and C Stippich

2009 'DTI of commissural fibers in patients with Chiari II-malformation', *NeuroImage*, 44, 2, PMID: 18849000, pp. 306–311, ISSN: 1095-9572, DOI: 10.1016/j.neuroimage.2008.09.006.

Hong, Ji Heon, Byung Yeon Choi, Chul Hoon Chang, Seong Ho Kim, Young Jin Jung, Woo Mok Byun, and Sung Ho Jang

2012 'Injuries of the cingulum and fornix after rupture of an anterior communicating artery aneurysm: a diffusion tensor tractography study', *Neurosurgery*, 70, 4 (Apr. 2012), PMID: 21937938, pp. 819–823, ISSN: 1524-4040, DOI: 10.1227/NEU.0b013e3182367124.

Huang, Hao, Jiangyang Zhang, Hangyi Jiang, Setsu Wakana, Lidia Poetscher, Michael I Miller, Peter C M van Zijl, Argye E Hillis, Robert Wytik, and Susumu Mori

2005 'DTI tractography based parcellation of white matter: application to the mid-sagittal morphology of corpus callosum', *NeuroImage*, 26, 1 (May 15, 2005), PMID: 15862219, pp. 195–205, ISSN: 1053-8119, DOI: 10.1016/j.neuroimage.2005.01.019.

Ishak, G E, A V Poliakov, S L Poliachik, R P Saneto, Jr Novotny E J, S McDaniel, J G Ojemann, D W W Shaw, and S D Friedman

2012 'Tract-based spatial statistical analysis of diffusion tensor imaging in pediatric patients with mitochondrial disease: widespread reduction in fractional anisotropy of white matter tracts', *AJNR. American journal of neuroradiology*, 33, 9 (Oct. 2012), PMID:

22499843, pp. 1726–1730, ISSN: 1936-959X, DOI: 10.3174/ajnr.A3045.

Jacobson, Stanley and Elliott M. Marcus

2011 *Neuroanatomy for the Neuroscientist*, Springer, 419 pp., ISBN: 9781441996534.

Jbabdi, Saad, Timothy E J Behrens, and Stephen M Smith

2010 'Crossing fibres in tract-based spatial statistics', *NeuroImage*, 49, 1, PMID: 19712743, pp. 249–256, ISSN: 1095-9572, DOI: 10.1016/j.neuroimage.2009.08.039.

Jellison, Brian J, Aaron S Field, Joshua Medow, Mariana Lazar, M Shariar Salamat, and Andrew L Alexander

2004 'Diffusion tensor imaging of cerebral white matter: a pictorial review of physics, fiber tract anatomy, and tumor imaging patterns', *AJNR. American journal of neuroradiology*, 25, 3 (Mar. 2004), PMID: 15037456, pp. 356–369, ISSN: 0195-6108.

Jenkins, Thomas, Olga Ciccarelli, Ahmed Toosy, Katherine Miszkiel, Claudia Wheeler-Kingshott, Daniel Altmann, Laura Mancini, Steve Jones, Gordon Plant, David Miller, and Alan Thompson

2010a 'Dissecting structure-function interactions in acute optic neuritis to investigate neuroplasticity', *Human brain mapping*, 31, 2 (Feb. 2010), PMID: 19662659, pp. 276–286, ISSN: 1097-0193, DOI: 10.1002/hbm.20863.

Jenkins, Thomas M, Ahmed T Toosy, Olga Ciccarelli, Katherine A Miszkiel, Claudia A Wheeler-Kingshott, Andrew P Henderson, Constantinos Kallis, Laura Mancini, Gordon T Plant, David H Miller, and Alan J Thompson

2010b 'Neuroplasticity predicts outcome of optic neuritis independent of tissue damage', *Annals of neurology*, 67, 1, PMID: 20186956, pp. 99–113, ISSN: 1531-8249, DOI: 10.1002/ana.21823.

Jenkinson, Mark

2003 'Fast, automated, N-dimensional phase-unwrapping algorithm', *Magnetic resonance in medicine: official journal of the Society of Magnetic Resonance in Medicine / Society of Magnetic Resonance in Medicine*, 49, 1, PMID: 12509838, pp. 193–197, ISSN: 0740-3194, DOI: 10.1002/mrm.10354.

Jones, Derek K

2010 *Diffusion MRI: theory, methods, and application*, Oxford University Press, Oxford; New York, ISBN: 9780195369779 0195369777.

Kamada, Kyousuke, Tomoki Todo, Yoshitaka Masutani, Shigeki Aoki, Kenji Ino, Tetsuya Takano, Takaaki Kirino, Nobutaka Kawahara, and Akio Morita

2005 'Combined use of tractography-integrated functional neuronavigation and direct fiber stimulation', *Journal of neurosurgery*, 102, 4 (Apr. 2005), PMID: 15871509, pp. 664–672, ISSN: 0022-3085, DOI: 10.3171/jns.2005.102.4.0664.

Kamada, Kyousuke, Tomoki Todo, Takahiro Ota, Kenji Ino, Yoshitaka Masutani, Shigeki Aoki, Fumiya Takeuchi, Kensuke Kawai, and Nobuhito Saito

2009 'The motor-evoked potential threshold evaluated by tractography and electrical stimulation', *Journal of neurosurgery*, 111, 4 (Oct. 2009), PMID: 19199462, pp. 785–795, ISSN: 1933-0693, DOI: 10.3171/2008.9.JNS08414.

Kaneko, Nobuyuki, Warren W Boling, Takaharu Shonai, Kazumi Ohmori, Yoshiaki Shiokawa, Hiroki Kurita, and Takanori Fukushima

2012 'Delineation of the safe zone in surgery of sylvian insular triangle: morphometric analysis and magnetic resonance imaging study', *Neurosurgery*, 70, 2 (June 2012), PMID: 21841521, 290–298; discussion 298–299, ISSN: 1524-4040, DOI: 10.1227/NEU.0b013e3182315112.

Kier, E Leon, Lawrence H Staib, Lawrence M Davis, and Richard A Bronen

2004 'MR imaging of the temporal stem: anatomic dissection tractography of the uncinate fasciculus, inferior occipitofrontal fasciculus, and Meyer's loop of the optic radiation', *AJNR. American journal of neuroradiology*, 25, 5 (May 2004), PMID: 15140705, pp. 677–691, ISSN: 0195-6108.

Kim, Yun-Hee, Dae-Shik Kim, Ji Heon Hong, Chang Hyun Park, Ning Hua, Kevin C Bickart, Woo Mok Byun, and Sung Ho Jang

2008 'Corticospinal tract location in internal capsule of human brain: diffusion tensor tractography and functional MRI study', *Neuroreport*, 19, 8 (May 28, 2008), PMID: 18463493, pp. 817–820, ISSN: 0959-4965, DOI: 10.1097/WNR.0b013e328300a086.

Kinoshita, Manabu, Kei Yamada, Naoya Hashimoto, Amami Kato, Shuichi Izumoto, Takahito Baba, Motohiko Maruno, Tsunehiko Nishimura, and Toshiki Yoshimine

2005 'Fiber-tracking does not accurately estimate size of fiber bundle in pathological condition: initial neurosurgical experience using neuronavigation and subcortical white matter stimulation', *NeuroImage*, 25, 2 (Apr. 1, 2005), PMID: 15784421, pp. 424–429, ISSN: 1053-8119, DOI: 10.1016/j.neuroimage.2004.07.076.

Kouwe, André J.W. van der, Thomas Benner, and Anders M. Dale

2006 'Real-time rigid body motion correction and shimming using cloverleaf navigators', *Magnetic Resonance in Medicine*, 56, 5, 1019–1032, ISSN: 1522-2594, DOI: 10.1002/mrm.21038, http://onlinelibrary.wiley.com/doi/10.1002/mrm.21038/abstract (visited on 02/03/2014).

L, Bello, Riva M, Casaceli G, and Fava E

2011 'Technological Advances in Glioma Surgery', *European Association of NeuroOncology Magazine*, 1, 1 (Aug. 30, 2011), pp. 13–19, http://www.kup.at/journals/abbildungen/gross/16265.html (visited on 02/20/2014).

Lagan&#224, M, M. Rovaris, A. Ceccarelli, C. Venturelli, S. Marini, and G. Baselli

2010 'DTI Parameter Optimisation for Acquisition at 1.5T: SNR Analysis and Clinical Application', *Computational Intelligence and Neuroscience*, 2010, ISSN: 1687-5265, DOI: 10.1155/2010/254032, http://www.hindawi.com/journals/cin/2010/254032/abs/ (visited on 02/18/2014).

Law, Meng, Stanley Yang, James S Babb, Edmond A Knopp, John G Golfinos, David Zagzag, and Glyn Johnson

2004 'Comparison of cerebral blood volume and vascular permeability from dynamic susceptibility contrast-enhanced perfusion MR imaging with glioma grade', *AJNR. American journal of neuroradiology*, 25, 5 (May 2004), PMID: 15140713, pp. 746–755, ISSN: 0195-6108.

Le Bihan, D, J F Mangin, C Poupon, C A Clark, S Pappata, N Molko, and H Chabriat

2001 'Diffusion tensor imaging: concepts and applications', *Journal of magnetic resonance imaging: JMRI*, 13, 4 (Apr. 2001), PMID: 11276097, pp. 534–546, ISSN: 1053-1807.

Le Bihan, Denis, Cyril Poupon, Alexis Amadon, and Franck Lethimonnier

2006 'Artifacts and pitfalls in diffusion MRI', *Journal of magnetic resonance imaging: JMRI*, 24, 3 (Sept. 2006), PMID: 16897692, pp. 478–488, ISSN: 1053-1807, DOI: 10.1002/jmri.20683.

Leclercq, Delphine, Hugues Duffau, Christine Delmaire, Laurent Capelle, Peggy Gatignol, Mathieu Ducros, Jacques Chiras, and Stéphane Lehéricy

2010 'Comparison of diffusion tensor imaging tractography of language tracts and intraoperative subcortical stimulations', *Journal of neurosurgery*, 112, 3 (Mar. 2010), PMID: 19747052, pp. 503–511, ISSN: 1933-0693, DOI: 10.3171/2009.8.JNS09558.

Lee, E J, K J Ahn, E K Lee, Y S Lee, and D B Kim

2013 'Potential role of advanced MRI techniques for the peritumoural region in differentiating glioblastoma multiforme and solitary metastatic lesions', *Clinical radiology*, 68, 12 (Dec. 2013), PMID: 23969153, e689–697, ISSN: 1365-229X, DOI: 10.1016/j.crad.2013.06.021.

Leemans, Alexander and Derek K. Jones

2009 'The B-matrix must be rotated when correcting for subject motion in DTI data', *Magnetic Resonance in Medicine*, 61, 6, 1336–1349, ISSN: 1522-2594, DOI: 10.1002/mrm.21890, http://onlinelibrary.wiley.com/doi/10.1002/mrm.21890/abstract (visited on 02/03/2014).

Lenfeldt, Niklas, Anne Larsson, Lars Nyberg, Richard Birgander, Anders Eklund, and Jan Malm

2011 'Diffusion tensor imaging reveals supplementary lesions to frontal white matter in idiopathic normal pressure hydrocephalus', *Neurosurgery*, 68, 6 (June 2011), PMID: 21336219, 1586–1593; discussion 1593, ISSN: 1524-4040, DOI: 10.1227/NEU.0b013e31820f3401.

Lepski, Guilherme, Jürgen Honegger, Marina Liebsch, Marília Grando Sória, Porn Narischat, Kristofer Fingerle Ramina, Thomas Nägele, Ulrike Ernemann, and Marcos Tatagiba

2012 'Safe resection of arteriovenous malformations in eloquent motor areas aided by functional imaging and intraoperative monitoring', *Neurosurgery*, 70, 2 (June 2012), PMID: 21946511, 276–288; discussion 288–289, ISSN: 1524-4040, DOI: 10.1227/NEU.0b013e318237aac5.

Liberman, Gilad, Yoram Louzoun, Orna Aizenstein, Deborah T Blumenthal, Felix Bokstein, Mika Palmon, Benjamin W Corn, and Dafna Ben Bashat

2013 'Automatic multi-modal MR tissue classification for the assessment of response to bevacizumab in patients with glioblastoma', *European journal of radiology*, 82, 2 (Feb. 2013), PMID: 23017192, e87–94, ISSN: 1872-7727, DOI: 10.1016/j.ejrad.2012.09.001.

Liu, Tianming

2011 'A few thoughts on brain ROIs', *Brain imaging and behavior*, 5, 3 (Sept. 2011), PMID: 21556745 PMCID: PMC3927780, pp. 189–202, ISSN: 1931-7565, DOI: 10.1007/s11682-011-9123-6.

Maesawa, Satoshi, Masazumi Fujii, Norimoto Nakahara, Tadashi Watanabe, Toshihiko Wakabayashi, and Jun Yoshida

2010 'Intraoperative tractography and motor evoked potential (MEP) monitoring in surgery for gliomas around the corticospinal tract', *World neurosurgery*, 74, 1 (July 2010), PMID: 21300007, pp. 153–161, ISSN: 1878-8750, DOI: 10.1016/j.wneu.2010.03.022.

Mandonnet, Emmanuel, Aurélien Nouet, Peggy Gatignol, Laurent Capelle, and Hugues Duffau

2007 'Does the left inferior longitudinal fasciculus play a role in language? A brain stimulation study', *Brain: a journal of neurology*, 130 (Pt 3Mar. 2007), PMID: 17264096, pp. 623–629, ISSN: 1460-2156, DOI: 10.1093/brain/awl361.

Manjón, José V, Pierrick Coupé, Antonio Buades, Vladimir Fonov, D Louis Collins, and Montserrat Robles

2010 'Non-local MRI upsampling', *Medical image analysis*, 14, 6 (Dec. 2010), PMID: 20566298, pp. 784–792, ISSN: 1361-8423, DOI: 10.1016/j.media.2010.05.010.

Martino, Juan, Christian Brogna, Santiago G Robles, Francesco Vergani, and Hugues Duffau

2010 'Anatomic dissection of the inferior fronto-occipital fasciculus revisited in the lights of brain stimulation data', *Cortex; a journal devoted to the study of the nervous system and behavior*, 46, 5 (May 2010), PMID: 19775684, pp. 691–699, ISSN: 1973-8102, DOI: 10.1016/j.cortex.2009.07.015.

Maruyama, Keisuke, Kyousuke Kamada, Masahiro Shin, Daisuke Itoh, Yoshitaka Masutani, Kenji Ino, Masao Tago, and Nobuhito Saito

2007 'Optic radiation tractography integrated into simulated treatment planning for Gamma Knife surgery', *Journal of neurosurgery*, 107, 4 (Oct. 2007), PMID: 17937214, pp. 721–726, ISSN: 0022-3085, DOI: 10.3171/JNS-07/10/0721.

Mayer, Dirk, Natalie M Zahr, Elfar Adalsteinsson, Brian Rutt, Edith V Sullivan, and Adolf Pfefferbaum

2007 'In vivo fiber tracking in the rat brain on a clinical 3T MRI system using a high strength insert gradient coil', *NeuroImage*, 35, 3 (Apr. 15, 2007), PMID: 17331742 PMCID: PMC1868575, pp. 1077–1085, ISSN: 1053-8119, DOI: 10.1016/j.neuroimage.2007.01.006.

Mesulam, Marsel

2005 'Imaging connectivity in the human cerebral cortex: the next frontier?', *Annals of neurology*, 57, 1, PMID: 15622538, pp. 5–7, ISSN: 0364-5134, DOI: 10.1002/ana.20368.

Mori, Susumu, Walter E Kaufmann, Christos Davatzikos, Bram Stieltjes, Laura Amodei, Kim Fredericksen, Godfrey D Pearlson, Elias R Melhem, Meiyappan Solaiyappan, Gerald V Raymond, Hugo W Moser, and Peter C M van Zijl

2002 'Imaging cortical association tracts in the human brain using diffusion-tensor-based axonal tracking', *Magnetic resonance in medicine: official journal of the Society of Magnetic Resonance in Medicine / Society of Magnetic Resonance in Medicine*, 47, 2 (Feb. 2002), PMID: 11810663, pp. 215–223, ISSN: 0740-3194.

Muacevic, A, E Uhl, H J Steiger, and H J Reulen

2000 'Accuracy and clinical applicability of a passive marker based frameless neuronavigation system', *Journal of clinical neuroscience: official journal of the Neurosurgical Society of Australasia*, 7, 5 (Sept. 2000), PMID: 10942662, pp. 414–418, ISSN: 0967-5868, DOI: 10.1054/jocn.1999.0226.

Mukherjee, P, S W Chung, J I Berman, C P Hess, and R G Henry

2008 'Diffusion tensor MR imaging and fiber tractography: technical considerations', *AJNR. American journal of neuroradiology*, 29, 5 (May 2008), PMID: 18339719, pp. 843–852, ISSN: 1936-959X, DOI: 10.3174/ajnr.A1052.

Niimi, Yasunari, Francesco Sala, Vedran Deletis, Avi Setton, Adauri Bueno de Camargo, and Alex Berenstein

2004 'Neurophysiologic monitoring and pharmacologic provocative testing for embolization of spinal cord arteriovenous malformations', *AJNR. American journal of neuroradiology*, 25, 7 (Aug. 2004), PMID: 15313696, pp. 1131–1138, ISSN: 0195-6108.

Nimsky, C, O Ganslandt, S Cerny, P Hastreiter, G Greiner, and R Fahlbusch

2000 'Quantification of, visualization of, and compensation for brain shift using intraoperative magnetic resonance imaging', *Neurosurgery*, 47, 5 (Nov. 2000), PMID: 11063099, 1070–1079; discussion 1079–1080, ISSN: 0148-396X.

Nimsky, C, O Ganslandt, H Kober, M Buchfelder, and R Fahlbusch

2001 'Intraoperative magnetic resonance imaging combined with neuronavigation: a new concept', *Neurosurgery*, 48, 5 (May 2001), PMID: 11334275, 1082–1089; discussion 1089–1091, ISSN: 0148-396X.

Nimsky, Christopher, Oliver Ganslandt, Peter Hastreiter, Ruopeng Wang, Thomas Benner, A Gregory Sorensen, and Rudolf Fahlbusch

2005 'Preoperative and intraoperative diffusion tensor imaging-based fiber tracking in glioma surgery', *Neurosurgery*, 56, 1, PMID: 15617595, 130–137; discussion 138, ISSN: 1524-4040.

Nimsky, Christopher, Oliver Ganslandt, Dorit Merhof, A Gregory Sorensen, and Rudolf Fahlbusch

2006 'Intraoperative visualization of the pyramidal tract by diffusion-tensor-imaging-based fiber tracking', *NeuroImage*, 30, 4 (May 1, 2006), PMID: 16364659, pp. 1219–1229, ISSN: 1053-8119, DOI: 10.1016/j.neuroimage.2005.11.001.

Nimsky, Christopher, Oliver Ganslandt, and Rudolf Fahlbusch

2007 'Implementation of fiber tract navigation', *Neurosurgery*, 61, 1 (July 2007), PMID: 18813159, 306–317; discussion 317–318, ISSN: 1524-4040, DOI: 10.1227/01.neu.0000279224.83998.7d.

Nucifora, Paolo G P, Ragini Verma, Seung-Koo Lee, and Elias R Melhem

2007 'Diffusion-tensor MR imaging and tractography: exploring brain microstructure and connectivity', *Radiology*, 245, 2 (Nov. 2007), PMID: 17940300, pp. 367–384, ISSN: 0033-8419, DOI: 10.1148/radiol.2452060445.

O'Donnell, Lauren J and Carl-Fredrik Westin

2011 'An introduction to diffusion tensor image analysis', *Neurosurgery clinics of North America*, 22, 2 (Apr. 2011), PMID: 21435570 PMCID: PMC3163395, pp. 185–196, viii, ISSN: 1558-1349, DOI: 10.1016/j.nec.2010.12.004.

O'Donnell, Lauren J, Carl-Fredrik Westin, and Alexandra J Golby

2009 'Tract-based morphometry for white matter group analysis', *NeuroImage*, 45, 3 (Apr. 15, 2009), PMID: 19154790 PMCID: PMC2768362, pp. 832–844, ISSN: 1095-9572, DOI: 10.1016/j.neuroimage.2008.12.023.

Pai, Darshan, Hamid Soltanian-Zadeh, and Jing Hua

2011 'Evaluation of fiber bundles across subjects through brain mapping and registration of diffusion tensor data', *NeuroImage*, 54 Suppl 1, PMID: 20547227, S165–175, ISSN: 1095-9572, DOI: 10.1016/j.neuroimage.2010.05.085.

Pallud, Johan, Luc Taillandier, Laurent Capelle, Denys Fontaine, Matthieu Peyre, François Ducray, Hugues Duffau, and Emmanuel Mandonnet

2012 'Quantitative morphological magnetic resonance imaging follow-up of low-grade glioma: a plea for systematic measurement of growth rates', *Neurosurgery*, 71, 3 (Sept. 2012), PMID: 22668885, 729–739; discussion 739–740, ISSN: 1524-4040, DOI: 10.1227/NEU.0b013e31826213de.

Parker, Geoff J M and Daniel C Alexander

2003 'Probabilistic Monte Carlo based mapping of cerebral connections utilising whole-brain crossing fibre information', *Information processing in medical imaging: proceedings of the ... conference*, 18 (July 2003), PMID: 15344498, pp. 684–695, ISSN: 1011-2499.

Parker, Geoffrey J M and Daniel C Alexander

2005 'Probabilistic anatomical connectivity derived from the microscopic persistent angular structure of cerebral tissue', *Philosophical transactions of the Royal Society of London. Series B, Biological sciences*, 360, 1457 (May 29, 2005), PMID: 16087434 PMCID: PMC1854923, pp. 893–902, ISSN: 0962-8436, DOI: 10.1098/rstb.2005.1639.

Pianykh, Oleg S

2011 *Digital imaging and communications in medicine (DICOM)*, Springer, Berlin; London, ISBN: 9783642108495 3642108490.

Pichler, Josef, Corinna Pachinger, Manuela Pelz, and Raimund Kleiser

2013 'MRI assessment of relapsed glioblastoma during treatment with bevacizumab: volumetric measurement of enhanced and FLAIR lesions for evaluation of response and progression–a pilot study', *European journal of radiology*, 82, 5 (May 2013), PMID: 23399039, e240–245, ISSN: 1872-7727, DOI: 10.1016/j.ejrad.2012.12.018.

Prabhu, Sujit S, Jaime Gasco, Sudhakar Tummala, Jefrey S Weinberg, and Ganesh Rao

2011 'Intraoperative magnetic resonance imaging-guided tractography with integrated monopolar subcortical functional mapping for resection of brain tumors. Clinical article', *Journal of neurosurgery*, 114, 3 (Mar. 2011), PMID: 20964594, pp. 719–726, ISSN: 1933-0693, DOI: 10.3171/2010.9.JNS10481.

Procaccio, F, A Polo, P Lanteri, and F Sala

2001 'Electrophysiologic monitoring in neurointensive care', *Current opinion in critical care*, 7, 2 (Apr. 2001), PMID: 11373514, pp. 74–80, ISSN: 1070-5295.

Pulvermüller, Friedemann

1999 'Words in the brain's language', *Behavioral and Brain Sciences*, 22, 2, pp. 253–279, DOI: 10.1017/S0140525X9900182X.

Qazi, Arish A, Alireza Radmanesh, Lauren O'Donnell, Gordon Kindlmann, Sharon Peled, Stephen Whalen, Carl-Fredrik Westin, and Alexandra J Golby

2009 'Resolving crossings in the corticospinal tract by two-tensor streamline tractography: Method and clinical assessment using fMRI', *NeuroImage*, 47 Suppl 2 (Aug. 2009), PMID: 18657622 PMCID: PMC2746909, T98–106, ISSN: 1095-9572, DOI: 10.1016/j.neuroimage.2008.06.034.

Rocca, M A, E Pagani, B Colombo, P Tortorella, A Falini, G Comi, and M Filippi

2008 'Selective diffusion changes of the visual pathways in patients with migraine: a 3-T tractography study', *Cephalalgia: an international journal of headache*, 28, 10 (Oct. 2008), PMID: 18644035, pp. 1061–1068, ISSN: 1468-2982, DOI: 10.1111/j.1468-2982.2008.01655.x.

Roessler, K, M Donat, R Lanzenberger, K Novak, A Geissler, A Gartus, A R Tahamtan, D Milakara, T Czech, M Barth, E Knosp, and R Beisteiner

2005 'Evaluation of preoperative high magnetic field motor functional MRI (3 Tesla) in glioma patients by navigated electrocortical stimulation and postoperative outcome', *Journal of neurology, neurosurgery, and psychiatry*, 76, 8 (Aug. 2005), PMID: 16024896 PMCID: PMC1739751, pp. 1152–1157, ISSN: 0022-3050, DOI: 10.1136/jnnp.2004.050286.

Rohde, G.k., A.s. Barnett, P.j. Basser, S. Marenco, and C. Pierpaoli

2004 'Comprehensive approach for correction of motion and distortion in diffusion-weighted MRI', *Magnetic Resonance in Medicine*, 51, 1, 103–114, ISSN: 1522-2594, DOI: 10.1002/mrm.10677, http://onlinelibrary.wiley.com/doi/10.1002/mrm.10677/abstract (visited on 02/03/2014).

S Pujol, V. Magnotta

2009 'Towards validation of DTI tractography: Statistical Analysis of the differences observed among tractography algorithms'.

Sala, F, M J Krzan, G Jallo, F J Epstein, and V Deletis

2000 'Prognostic value of motor evoked potentials elicited by multipulse magnetic stimulation in a surgically induced transitory lesion of the supplementary motor area: a case report', *Journal of neurology, neurosurgery, and psychiatry*, 69, 6 (Dec. 2000), PMID: 11080242 PMCID: PMC1737156, pp. 828–831, ISSN: 0022-3050.

Sala, F, P Manganotti, V Tramontano, A Bricolo, and M Gerosa

2007a 'Monitoring of motor pathways during brain stem surgery: what we have achieved and what we still miss?', *Neurophysiologie clinique = Clinical neurophysiology*, 37, 6 (Dec. 2007), PMID: 18083495, pp. 399–406, ISSN: 0987-7053, DOI: 10.1016/j.neucli.2007.09.013.

Sala, F, A Beltramello, and M Gerosa

2007b 'Neuroprotective role of neurophysiological monitoring during endovascular procedures in the brain and spinal cord', *Neurophysiologie clinique = Clinical neurophysiology*, 37, 6 (Dec. 2007), PMID: 18083497, pp. 415–421, ISSN: 0987-7053, DOI: 10.1016/j.neucli.2007.10.004.

Sala, Francesco

2010 'Intraoperative neurophysiology is here to stay', *Child's nervous system: ChNS: official journal of the International Society for Pediatric Neurosurgery*, 26, 4 (Apr. 2010), PMID: 20179948, pp. 413–417, ISSN: 1433-0350, DOI: 10.1007/s00381-010-1090-5.

Sala, Francesco, Matevz J Krzan, and Vedran Deletis

2002 'Intraoperative neurophysiological monitoring in pediatric neurosurgery: why, when, how?', *Child's nervous system: ChNS: official journal of the International Society for Pediatric Neurosurgery*, 18, 6 (July 2002), PMID: 12172930, pp. 264–287, ISSN: 0256-7040, DOI: 10.1007/s00381-002-0582-3.

Sala, Francesco, Giorgio Palandri, Elisabetta Basso, Paola Lanteri, Vedran Deletis, Franco Faccioli, and Albino Bricolo

2006 'Motor evoked potential monitoring improves outcome after surgery for intramedullary spinal cord tumors: a historical control study', *Neurosurgery*, 58, 6 (June 2006), PMID: 16723892, 1129–1143; discussion 1129–1143, ISSN: 1524-4040, DOI: 10.1227/01.NEU.0000215948.97195.58.

Sarlls, Joelle E and Carlo Pierpaoli

2009 'In vivo diffusion tensor imaging of the human optic chiasm at sub-millimeter resolution', *NeuroImage*, 47, 4 (Oct. 1, 2009), PMID: 19520170 PMCID: PMC2735123, pp. 1244–1251, ISSN: 1095-9572, DOI: 10.1016/j.neuroimage.2009.05.098.

Schultz, Thomas and Hans-Peter Seidel

2008 'Estimating crossing fibers: a tensor decomposition approach', *IEEE transactions on visualization and computer graphics*, 14, 6 (Dec. 2008), PMID: 18989020, pp. 1635–1642, ISSN: 1077-2626, DOI: 10.1109/TVCG.2008.128.

Sedrak, Mark, Alessandra Gorgulho, Andrew Frew, Eric Behnke, Antonio DeSalles, and Nader Pouratian

2011 'Diffusion tensor imaging and colored fractional anisotropy mapping of the ventralis intermedius nucleus of the thalamus', *Neurosurgery*, 69, 5 (Nov. 2011), PMID: 21697755, 1124–1129; discussion 1129–1130, ISSN: 1524-4040, DOI: 10.1227/NEU.0b013e3182296a42.

Seo, J P and S H Jang

2013 'Different characteristics of the corticospinal tract according to the cerebral origin: DTI study', *AJNR. American journal of neuroradiology*, 34, 7 (July 2013), PMID: 23370470, pp. 1359–1363, ISSN: 1936-959X, DOI: 10.3174/ajnr.A3389.

Sherbondy, Anthony J, Robert F Dougherty, Sandy Napel, and Brian A Wandell

2008 'Identifying the human optic radiation using diffusion imaging and fiber tractography', *Journal of vision*, 8, 10, PMID: 19146354 PMCID: PMC2759943, pp. 12.1–11, ISSN: 1534-7362, DOI: 10.1167/8.10.12.

Smith, Stephen M, Heidi Johansen-Berg, Mark Jenkinson, Daniel Rueckert, Thomas E Nichols, Karla L Miller, Matthew D Robson, Derek K Jones, Johannes C Klein, Andreas J Bartsch, and Timothy E J Behrens

2007 'Acquisition and voxelwise analysis of multi-subject diffusion data with tract-based spatial statistics', *Nature protocols*, 2, 3, PMID: 17406613, pp. 499–503, ISSN: 1750-2799, DOI: 10.1038/nprot.2007.45.

Smits, M, M W Vernooij, P A Wielopolski, A J P E Vincent, G C Houston, and A van der Lugt

2007 'Incorporating functional MR imaging into diffusion tensor tractography in the preoperative assessment of the corticospinal tract in patients with brain tumors', *AJNR. American journal of neuroradiology*, 28, 7 (Aug. 2007), PMID: 17698540, pp. 1354–1361, ISSN: 0195-6108, DOI: 10.3174/ajnr.A0538.

Soares, José M, Paulo Marques, Victor Alves, and Nuno Sousa

2013 'A hitchhiker's guide to diffusion tensor imaging', *Frontiers in neuroscience*, 7, PMID: 23486659 PMCID: PMC3594764, p. 31, ISSN: 1662-4548, DOI: 10.3389/fnins.2013.00031.

Sokki, Anilkumar Masalavada, Dhananjaya Ishwar Bhat, and Bhagavatula Indira Devi

2012 'Cortical reorganization following neurotization: a diffusion tensor imaging and functional magnetic resonance imaging study', *Neurosurgery*, 70, 5 (May 2012), PMID: 22513809, 1305–1311; discussion 1311, ISSN: 1524-4040, DOI: 10.1227/NEU.0b013e318241017d.

Stadlbauer, Andreas, Christopher Nimsky, Rolf Buslei, Erich Salomonowitz, Thilo Hammen, Michael Buchfelder, Ewald Moser, Antje Ernst-Stecken, and Oliver Ganslandt

2007 'Diffusion tensor imaging and optimized fiber tracking in glioma patients: Histopathologic evaluation of tumor-invaded white matter structures', *NeuroImage*, 34, 3 (Feb. 1, 2007), PMID: 17166744, pp. 949–956, ISSN: 1053-8119, DOI: 10.1016/j.neuroimage.2006.08.051.

Stadlbauer, Andreas, Thilo Hammen, Peter Grummich, Michael Buchfelder, Torsten Kuwert, Arnd Dörfler, Christopher Nimsky, and Oliver Ganslandt

2011 'Classification of peritumoral fiber tract alterations in gliomas using metabolic and structural neuroimaging', *Journal of nuclear medicine: official publication, Society of Nuclear Medicine*, 52, 8 (Aug. 2011), PMID: 21810590, pp. 1227–1234, ISSN: 1535-5667, DOI: 10.2967/jnumed.111.090597.

Stieglitz, Lennart H, Wolf O Lüdemann, Mario Giordano, Andreas Raabe, Rudolf Fahlbusch, and Madjid Samii

2011 'Optic radiation fiber tracking using anteriorly angulated diffusion tensor imaging: a tested algorithm for quick application', *Neurosurgery*, 68, 5 (May 2011), PMID: 21273926, pp. 1239–1251, ISSN: 1524-4040, DOI: 10.1227/NEU.0b013e31820b52e1.

Stikov, Nikola, Lee M Perry, Aviv Mezer, Elena Rykhlevskaia, Brian A Wandell, John M Pauly, and Robert F Dougherty

2011 'Bound pool fractions complement diffusion measures to describe white matter micro and macrostructure', *NeuroImage*, 54, 2, PMID: 20828622 PMCID: PMC2997845, pp. 1112–1121, ISSN: 1095-9572, DOI: 10.1016/j.neuroimage.2010.08.068.

Sunaert, Stefan

2006 'Presurgical planning for tumor resectioning', *Journal of Magnetic Resonance Imaging*, 23, 6, 887–905, ISSN: 1522-2586, DOI: 10.1002/jmri.20582, http://onlinelibrary.wiley.com/doi/10.1002/jmri.20582/abstract (visited on 02/20/2014).

Takahashi, Emi, Guangping Dai, Ruopeng Wang, Kenichi Ohki, Glenn D Rosen, Albert M Galaburda, P Ellen Grant, and Van J Wedeen

2010 'Development of cerebral fiber pathways in cats revealed by diffusion spectrum imaging', *NeuroImage*, 49, 2, PMID: 19747553 PMCID: PMC2789885, pp. 1231–1240, ISSN: 1095-9572, DOI: 10.1016/j.neuroimage.2009.09.002.

Tao, Xiao-feng, Zhong-qiu Wang, Wan-qing Gong, Qing-jun Jiang, and Zeng-ru Shi

2009 'A new study on diffusion tensor imaging of the whole visual pathway fiber bundle and clinical application', *Chinese medical journal*, 122, 2, PMID: 19187643, pp. 178–182, ISSN: 0366-6999.

Toga, Arthur W, Kristi A Clark, Paul M Thompson, David W Shattuck, and John Darrell Van Horn

2012 'Mapping the human connectome', *Neurosurgery*, 71, 1 (July 2012), PMID: 22705717 PMCID: PMC3555558, pp. 1–5, ISSN: 1524-4040, DOI: 10.1227/NEU.0b013e318258e9ff.

Tomycz, Nestor D and Robert M Friedlander

2011 'The experience of pain and the putamen: a new link found with functional MRI and diffusion tensor imaging', *Neurosurgery*, 69, 4 (Oct. 2011), PMID: 21900799, N12–13, ISSN: 1524-4040, DOI: 10.1227/01.neu.0000405590.47966.e8.

Tournier, J-Donald, Fernando Calamante, David G Gadian, and Alan Connelly

2004 'Direct estimation of the fiber orientation density function from diffusion-weighted MRI data using spherical deconvolution', *NeuroImage*, 23, 3 (Nov. 2004), PMID: 15528117, pp. 1176–1185, ISSN: 1053-8119, DOI: 10.1016/j.neuroimage.2004.07.037.

Tournier, J-Donald, Chun-Hung Yeh, Fernando Calamante, Kuan-Hung Cho, Alan Connelly, and Ching-Po Lin

2008 'Resolving crossing fibres using constrained spherical deconvolution: validation using diffusion-weighted imaging phantom data', *NeuroImage*, 42, 2 (Aug. 15, 2008), PMID: 18583153, pp. 617–625, ISSN: 1095-9572, DOI: 10.1016/j.neuroimage.2008.05.002.

Tournier, Jacques-Donald, Susumu Mori, and Alexander Leemans

2011 'Diffusion tensor imaging and beyond', *Magnetic resonance in medicine: official journal of the Society of Magnetic Resonance in Medicine / Society of Magnetic Resonance in Medicine*, 65, 6 (June 2011), PMID: 21469191 PMCID: PMC3366862, pp. 1532–1556, ISSN: 1522-2594, DOI: 10.1002/mrm.22924.

Ulmer, Stephan

2010 'Neuroanatomy and Cortical Landmarks', in *fMRI*, ed. by Stephan Ulmer and Olav Jansen, Springer Berlin Heidelberg, pp. 5–13, ISBN: 978-3-540-68131-1, 978-3-540-68132-8, http://link.springer.com/chapter/10.1007/978-3-540-68132-8_2 (visited on 02/20/2014).

Upadhyay, N and A D Waldman

2011 'Conventional MRI evaluation of gliomas', *The British journal of radiology*, 84 Spec No 2 (Dec. 2011), PMID: 22433821 PMCID: PMC3473894, S107–111, ISSN: 1748-880X, DOI: 10.1259/bjr/65711810.

Urbanski, M, M Thiebaut de Schotten, S Rodrigo, C Oppenheim, E Touzé, J-F Méder, K Moreau, C Loeper-Jeny, B Dubois, and P Bartolomeo

2011 'DTI-MR tractography of white matter damage in stroke patients with neglect', *Experimental brain research*, 208, 4 (Feb. 2011), PMID: 21113581, pp. 491–505, ISSN: 1432-1106, DOI: 10.1007/s00221-010-2496-8.

Wakana, Setsu, Hangyi Jiang, Lidia M Nagae-Poetscher, Peter C M van Zijl, and Susumu Mori

2004 'Fiber tract-based atlas of human white matter anatomy', *Radiology*, 230, 1, PMID: 14645885, pp. 77–87, ISSN: 0033-8419, DOI: 10.1148/radiol.2301021640.

Wang, Mei-Yun, Jing-Liang Cheng, Yan-Hong Han, Yong-Li Li, Jian-Ping Dai, and Da-Peng Shi

2012 'Measurement of tumor size in adult glioblastoma: classical cross-sectional criteria on 2D MRI or volumetric criteria on high resolution 3D MRI?', *European journal of radiology*, 81, 9 (Sept. 2012), PMID: 21652157, pp. 2370–2374, ISSN: 1872-7727, DOI: 10.1016/j.ejrad.2011.05.017.

Wang, Yi, Aditya Gupta, Zhexing Liu, Hui Zhang, Maria L Escolar, John H Gilmore, Sylvain Gouttard, Pierre Fillard, Eric Maltbie, Guido Gerig, and Martin Styner

2011 'DTI registration in atlas based fiber analysis of infantile Krabbe disease', *NeuroImage*, 55, 4 (Apr. 15, 2011), PMID: 21256236 PMCID: PMC3062693, pp. 1577–1586, ISSN: 1095-9572, DOI: 10.1016/j.neuroimage.2011.01.038.

Wen, Patrick Y, David R Macdonald, David A Reardon, Timothy F Cloughesy, A Gregory Sorensen, Evanthia Galanis, John Degroot, Wolfgang Wick, Mark R Gilbert, Andrew B Lassman, Christina Tsien, Tom Mikkelsen, Eric T Wong, Marc C Chamberlain, Roger Stupp, Kathleen R Lamborn, Michael A Vogelbaum, Martin J van den Bent, and Susan M Chang

2010 'Updated response assessment criteria for high-grade gliomas: response assessment in neuro-oncology working group', *Journal of clinical oncology: official journal of the American Society of Clinical Oncology*, 28, 11 (Apr. 10, 2010), PMID: 20231676, pp. 1963–1972, ISSN: 1527-7755, DOI: 10.1200/JCO.2009.26.3541.

Winston, Gavin P, Laura Mancini, Jason Stretton, Jonathan Ashmore, Mark R Symms, John S Duncan, and Tarek A Yousry

2011 'Diffusion tensor imaging tractography of the optic radiation for epilepsy surgical planning: a comparison of two methods', *Epilepsy research*, 97, 1 (Nov. 2011), PMID: 21885257 PMCID: PMC3223565, pp. 124–132, ISSN: 1872-6844, DOI: 10.1016/j.eplepsyres.2011.07.019.

Wright, Alan J, G Fellows, T J Byrnes, K S Opstad, D J O McIntyre, J R Griffiths, B A Bell, C A Clark, T R Barrick, and F A Howe

2009 'Pattern recognition of MRSI data shows regions of glioma growth that agree with DTI markers of brain tumor infiltration', *Magnetic resonance in medicine: official journal of the Society of Magnetic Resonance in Medicine / Society of Magnetic Resonance in Medicine*, 62, 6 (Dec. 2009), PMID: 19785020, pp. 1646–1651, ISSN: 1522-2594, DOI: 10.1002/mrm.22163.

Wu, Wentao, Laura Rigolo, Lauren J O'Donnell, Isaiah Norton, Sargent Shriver, and Alexandra J Golby

2012 'Visual pathway study using in vivo diffusion tensor imaging tractography to complement classic anatomy', *Neurosurgery*, 70, 1 (Mar. 2012), PMID: 21808220 PMCID: PMC3236807, 145–156; discussion 156, ISSN: 1524-4040, DOI: 10.1227/NEU.0b013e31822efcae.

Zhang, Degang, Lei Guo, Gang Li, Jingxin Nie, Fan Deng, Kaiming Li, Xintao Hu, Tuo Zhang, Xi Jiang, Dajiang Zhu, Qun Zhao, and Tianming Liu

2010 'Automatic cortical surface parcellation based on fiber density information', in *2010 IEEE International Symposium on Biomedical Imaging: From Nano to Macro*, 2010 IEEE International Symposium on Biomedical Imaging: From Nano to Macro, pp. 1133–1136, DOI: 10.1109/ISBI.2010.5490193.

Zhu, Hongtu, Linglong Kong, Runze Li, Martin Styner, Guido Gerig, Weili Lin, and John H Gilmore

2011 'FADTTS: functional analysis of diffusion tensor tract statistics', *NeuroImage*, 56, 3 (June 1, 2011), PMID: 21335092 PMCID: PMC3085665, pp. 1412–1425, ISSN: 1095-9572, DOI: 10.1016/j.neuroimage.2011.01.075.

Zolal, Amir, Aleš Hejčl, Petr Vachata, Robert Bartoš, Ivan Humhej, Alberto Malucelli, Martina Nováková, Karel Hrach, Milouš Derner, and Martin Sameš

2012 'The use of diffusion tensor images of the corticospinal tract in intrinsic brain tumor surgery: a comparison with direct subcortical stimulation', *Neurosurgery*, 71, 2 (Aug. 2012), PMID: 22534425, 331–340; discussion 340, ISSN: 1524-4040, DOI: 10.1227/NEU.0b013e31825b1c18.